NOTE TO USERS

This reproduction is the best copy available.

UMI®

University of Alberta

The Synthesis of *iso*-Polydiacetylenes with Donor and/or Acceptor Substitution and Investigation of their Optical Properties.

by

©

SORIN CATALIN CIULEI

A thesis submitted to the Faculty of Graduate Studies and Research in partial
fulfillment of the requirements for the degree of Master of Science

Department of Chemistry

Edmonton, Alberta
Spring, 2002

National Library
of Canada

Acquisitions and
Bibliographic Services

395 Wellington Street
Ottawa ON K1A 0N4
Canada

Bibliothèque nationale
du Canada

Acquisitions et
services bibliographiques

395, rue Wellington
Ottawa ON K1A 0N4
Canada

Your file Votre référence

Our file Notre référence

The author has granted a non-exclusive licence allowing the National Library of Canada to reproduce, loan, distribute or sell copies of this thesis in microform, paper or electronic formats.

The author retains ownership of the copyright in this thesis. Neither the thesis nor substantial extracts from it may be printed or otherwise reproduced without the author's permission.

L'auteur a accordé une licence non exclusive permettant à la Bibliothèque nationale du Canada de reproduire, prêter, distribuer ou vendre des copies de cette thèse sous la forme de microfiche/film, de reproduction sur papier ou sur format électronique.

L'auteur conserve la propriété du droit d'auteur qui protège cette thèse. Ni la thèse ni des extraits substantiels de celle-ci ne doivent être imprimés ou autrement reproduits sans son autorisation.

0-612-69696-0

Canada

University of Alberta

Library Release Form

Name of Author: Sorin Catalin Ciulei
Title of Thesis: The Synthesis of *iso*-Polydiacetylenes with Donor and/or Acceptor Substitution and Investigation of their Optical Properties
Degree: Master of Science
Year this Degree Granted: 2002

Permission is hereby granted to the University of Alberta to reproduce single copies of this thesis and to lend or sell such copies for private, scholarly, or scientific research purposes only.

The author reserves all other publication and other rights in association with the copyright in the thesis, and except as hereinbefore provided, neither the thesis nor any substantial portion thereof may be printed or otherwise reproduced in any material form whatever without the author's prior written permission.

C. Ciuli

Sorin Catalin Ciulei
#201, 10625-83 Ave
Edmonton, AB, T6E 2E3
CANADA

April 11, 2002

University of Alberta

Faculty of Graduate Studies and Research

The undersigned certify that they have read, and recommend to the Faculty of Graduate Studies and Research for acceptance, a thesis entitled **The Synthesis of iso-Polydiacetylenes with Donor and/or Acceptor Substitution and Investigation of their Optical Properties** submitted by Sorin Catalin Ciulei in partial fulfillment of the requirement for the degree of **Master of Science**.

Dr. Rik. R. Tykwinski, Supervisor

D. L. J. Clive

Dr. Derrick L. J. Clive

Ray DeCorby

Dr. Ray DeCorby

April 05, 2002

Abstract

The synthesis and characterization of a series of novel cross-conjugated donor, acceptor, and donor-acceptor substituted *iso*-polydiacetylene oligomers have been reported in this thesis. Employing palladium catalyzed cross-coupling reactions, in which $PdCl_2(PPh_3)_2$ is used as a catalyst and CuI as a co-catalyst, the D-A cross-conjugated oligomers **118a**, **122**, and **126** that possess two methyl substituents have been synthesized in an iterative approach. For a thorough structure-property relationship study, D-A monomers having cyclohexyl **130** or two phenyl groups **140** have been also synthesized. The structural properties of these oligomers have been characterized by IR, ^1H and ^{13}C-NMR spectroscopies, high-resolution MS spectrometry and differential scanning calorimetry (DSC). The π-electronic communication, as a result of contributions from donor, acceptor, or donor-acceptor functionalization of these cross-conjugated systems has been investigated *via* UV-Vis spectroscopy.

Acknowledgements

I would like to express my sincerest gratitude to my supervisor, Professor Rik R. Tykwinski, for his advice, encouragement, support during my graduate program, and his assistance in the preparation of this thesis.

Thanks to all the staff in the Special Services (IR, NMR, MS, and Microanalysis) Division, in the general office, storeroom, machine shop, and glass shop.

I am thankful to all my research group members: K. Campbell, J. Cho, S. Eisler, and Y. Zhao for providing me with some starting materials and helping me editing this thesis.

Thanks to Dr. Ecaterina Merica, my previous superviser from Technical University of Iasi, Romania, for encouranging and helping me to study abroad. I also want to thank my wife, Mihaela, my parents and other relatives for their constant support and understanding.

Table of Contents

I. Introduction

1. Background 1

A. Linearly-conjugated oligomers 1

A.1 Polyenes 3

A.2 Thiophenes 9

A.3 Stilbene Analogues 18

A.4 Fluorene Derivatives 22

A.5 Acetylenic Derivatives 24

A.6 Ionic and zwitterionic derivatives 27

B. Transparency-Nonlinearity Trade-Off 27

B.1 Polyphenyls 28

B.2 Silanes 30

B.3 Imines and Hydrazones 33

B.4 Tolanes and Diaryl-1,2-Acetylenes 34

B.5 Spiro-compounds 36

C. Cross-conjugated Oligomers 37

2. Research Goals 51

II. Results and Discussion

A. Isopropylidene Series 53

1. Monomer Synthesis 53

2. Dimer Synthesis 64

3. Trimer Synthesis 68

B. Cyclohexylidene Series 73

C. Diphenyl Series 79

D. Stability 86

E. Solvent Dependency 87

III. Conclusions 91

IV. Experimental Section 93

V. References 113

VI. Appendix 121

List of Tables

Page

Table 1 Selected Physical Data for D/A *iso*-PDAs 87

Table 2 Absorption Characteristics of monomer **116** 89

Table 3 Absorption Characteristics of monomer **118** 90

Table 4 Crystallographic Experimental Details for **116** 121

Table 5 Selected Interatomic Distances (Å) for **116** 123

Table 6 Selected Interatomic Angles (deg) for **116** 124

Table 7 Torsional Angles (deg) for **116** 125

Table 8 Least-Squares Planes for **116** 127

Table 9 Crystallographic Experimental Details for **117** 128

Table 10 Selected Interatomic Distances (Å) for **117** 129

Table 11 Selected Interatomic Angles (deg) for **117** 130

Table 12 Torsional Angles (deg) for **117** 130

Table 13 Least-Squares Planes for **117** 131

Table 14 Crystallographic Experimental Details for **129** 132

Table 15 Selected Interatomic Distances (Å) for **129** 133

Table 16. Selected Interatomic Angles (deg) for **129** 134

Table 17. Torsional Angles (deg) for **129** 134

Table 18. Least-Squares Planes for **129** 135

List of Figures

Page

Fig. 1.1 Chemical structures of some polyacetylene derivatives 3

Fig. 1.2 Structures of the D-A substituted polyenes studied by Mukamel 4

Fig. 1.3 Structural formulae of the series of push-pull diphenylpolyenes investigated by Blanchard-Desce 5

Fig. 1.4 Donor-acceptor polyenes displaying very large nonlinearities 8

Fig. 1.5 Aromatic and quinoid forms of thiophene oligomers 9

Fig. 1.6 Molecular structure of octithiophene and some substituted quaterthiophene 10

Fig. 1.7 Structures of some D-A substituted thiophenes studied by Hutchings 11

Fig. 1.8 Thiophene/thiazole-aryl analogues of D-A stilbenes 16

Fig 1.9 Selected "matched" thiazole, thiophene and pyrrole analogues of D-A stilbenes 17

Fig 1.10 Molecular structures of stilbene, benzylideneaniline and azobenzene derivatives 18

Fig. 1.11 Monosubstituted benzenes and stilbenes studied by Cheng 19

Fig. 1.12 Structure of para-disubstituted benzenes and stilbenes studied by Cheng 20

Fig. 1.13 Other nitrostilbenes studied by Cheng 21
Fig. 1.14 Structures of 4,4'-disubstituted biphenyls and fluorenes 23
Fig. 1.15 Diphenylacetylenes studied by Stiegman and co-workers 24
Fig. 1.16 D-A zig-zag chromophores synthesized and studied by Nicoud 25
Fig. 1.17 Progression of polymeric backbones from polyacetylene to carbyne 26
Fig. 1.18 Stilbazolium salts and zwitterionic derivatives as efficient NLO materials 27
Fig. 1.19 Structures of some D-A polyphenyls 28
Fig. 1.20 Structural formulae of some octupolar molecules 29
Fig. 1.21 Structural formulae of some methylsilane derivatives studied by Zyss 31
Fig. 1.22 Structure of silane derivatives studied by Zyss 32
Fig. 1.23 Some D-A organosilicon compounds studied by Mignani 33
Fig. 1.24 Structure of D-A hydrazone derivatives 34
Fig. 1.25 Structure of D-A tolans 35
Fig. 1.26 Structure of 1,2-diaryl-acetylenes 35
Fig. 1.27 Molecular structures of (a) 1,1'-diamino-4,4'-dinitro-5,5'-spirobicyclopentadiene and (b) 2,2'-diamino-7,7'-dinitro-9,9'-spirobifluorene 36
Fig. 1.28 Molecular structures of some heterocyclic spiro-compounds 37
Fig. 1.29 Examples of cross-conjugated molecules 38
Fig. 1.30 Oxygen- and nitrogen-containing cross-conjugated compounds 38
Fig. 1.31 Cross-conjugated hydrocarbons reviewed by Hopf 39
Fig. 1.32 Structural formulae of chalcones and related compounds 40

Fig. 1.33 Molecular structures of cross-conjugated compounds studied by Brédas 41

Fig. 1.34 Chemical structures of some TEE derivatives studied by Diederich 42

Fig. 1.35 Schematic representation of possible conjugation pathways in D-A substituted TEEs 43

Fig. 1.36 Geminally bis-arylated TEEs **65-69**, and tetrakis-arylated TEEs **70-72** studied by Tykwinski 44

Fig 1.37 Geminally bis-arylated **74-77** and tris-arylated **78-81** TEEs studied by Tykwinski 44

Fig. 1.38 Additional TEEs studied by Tykwinski 45

Fig. 1.39 Bis-arylated *trans*-enediynes **96-97** and dimers **98-101** studied by Tykwinski 46

Fig. 1.40 The chemical structures of *iso*-PDA oligomers studied by Tykwinski 49

Fig. 1.41 Some high temperature polyimides and highly thermally stable chromophores for preparation of electro-optic polymers 50

Fig. 1.42 N- and S-cross-conjugated D-A oligomers 51

Fig. 1.43 Proposed cross-conjugated oligomers 52

Fig. 2.1 ORTEP drawing (20% probability level) of **116**, conformation A 56

Fig. 2.2 ORTEP drawing (20% probability level) of **116**, conformation B 57

Fig. 2.3 Interaction between the nonbonding p orbital of a nitrogen atom and a sp^2 hybrid orbital 59

Fig. 2.4 ORTEP drawing (20% probability level) of **117** 61

Fig. 2.5 UV-Vis absorption spectra of monomers **116, 117** and **118a** 64

Fig. 2.6 UV-Vis absorption spectra of dimers **120-122** 68

Fig. 2.7 UV-Vis absorption spectra of trimers **124 – 126** 72

Fig. 2.8 ORTEP drawing (20% probability level) of **129** 77

Fig. 2.9 UV-Vis absorption spectra of monomers **129** and **130** 79

Fig. 2.10 UV-Vis absorption spectra of monomers **138, 139,** and **140** 85

Fig. 2.11 UV-Vis absorption spectra comparing the effect of vinylidene substitution. 86

Fig. 2.12 UV-Vis absorption spectra of donor-substituted monomer **116** in various solvents 88

Fig. 2.13 UV-Vis absorption spectra of donor-acceptor-substituted monomer **118a** in various solvents 89

Fig. 6.1 ^{1}H and ^{13}C NMR spectra of compound **116** 137

Fig. 6.2 ^{1}H and ^{13}C NMR spectra of compound **117** 138

Fig. 6.3 ^{1}H and ^{13}C NMR spectra of compound **118a** 139

Fig. 6.4 ^{1}H and ^{13}C NMR spectra of compound **118b** 140

Fig. 6.5 ^{1}H and ^{13}C NMR spectra of compound **119** 141

Fig. 6.6 ^{1}H and ^{13}C NMR spectra of compound **120** 142

Fig. 6.7 ^{1}H and ^{13}C NMR spectra of compound **121** 143

Fig. 6.8 ^{1}H and ^{13}C NMR spectra of compound **122** 144

Fig. 6.9 ^{1}H and ^{13}C NMR spectra of compound **123** 145

Fig. 6.10 ^{1}H and ^{13}C NMR spectra of compound **124** 146

Fig. 6.11 ^{1}H and ^{13}C NMR spectra of compound **125** 147

Fig. 6.12 ^{1}H and ^{13}C NMR spectra of compound **126** 148

Fig. 6.13 ^{1}H and ^{13}C NMR spectra of compound **128** 149

Fig. 6.14 ^{1}H and ^{13}C NMR spectra of compound **129** 150

Fig. 6.15 ^{1}H and ^{13}C NMR spectra of compound **130** 151

Fig. 6.16 ^{1}H and ^{13}C NMR spectra of compound **138** 152

Fig. 6.17 ^{1}H and ^{13}C NMR spectra of compound **139** 153

Fig. 6.18 ^{1}H and ^{13}C NMR spectra of compound **140** 154

List of Symbols, Nomenclature and Abbreviations

A	Acceptor
Å	Angstrom
AM1	Austin Model 1
APT	Attached Proton Test
Aq	Aqueous
Bu	Butyl
ca.	Approximately
cm	Centimeter
CT	Charge Transfer
d	Doublet
D	Donor
D/A	Donor or Acceptor
D-A	Donor and Acceptor
Dec.	Decomposition Point
DEE	Diethynyl ethene
DMF	Dimethylformamide
DSC	Differential Scanning Calorimetry
DTT	Dithienothiophene

EFISH	Electric-Field-Induced Second-Harmonic Generation
e.g.	For Example
EOAM	Electrooptical Absorption Measurement
equiv	Equivalent
esu	Electrostatic Units
et al.	And Others
g	Grams
gem	Geminal
h	Hour(s)
Hex	Hexyl
HOMO	Highest Occupied Molecular Orbital
HRMS	High Resolution Mass Spectrometry
Hz	Hertz
i	Iso
ICT	Intramolecular Charge Transfer
IR	Infrared
λ_{max}	Lowest Energy Wavelength of Maximal Absorption
LUMO	Lowest Unoccupied Molecular Orbital
m	Multiplet
Me	Methyl

mg	Milligrams
MHz	Megahertz
mL	Milliliter
mmol	Millimole
mol	Mole
MOPAC	Molecular Orbital Package
Mp	Melting Point
MS	Mass Spectrometry
m/z	Mass-to-Charge Ratio
nm	Nanometer
NMR	Nuclear Magnetic Resonance
NLO	Nonlinear Optical
ORTEP	Oak Ridge Thermal Ellipsoid Plot
PA	Polyacetylene
PDA	Polydiacetylene
PDPA	Polydiphenylacetylene
Ph	Phenyl
PNA	*para*-Nitroaniline
PPA	Polyphenylacetylene
ppm	Parts Per Million

PPV	Polyphenylenevinylene
Pr	Propyl
PTA	Polytriacetylene
rt	Room Temperature
s	Singlet
SHG	Second-Harmonic Generation
t	Triplet
TBAF	Tetrabutylammonium Fluoride
TEE	Tetraethynyl ethene
TES	Triethylsilyl
THF	Tetrahydrofuran
THG	Third-Harmonic Generation
TIPS	Triisopropylsilyl
TLC	Thin Layer Chromatography
TMS	Trimethylsilyl
UV	Ultraviolet
Vis	Visible
ZINDO	Zerner Intermediate Neglect of Differential Overlap
μ_e	Dipole Moment in the Excited-State
μ_g	Dipole Moment in the Ground-State

I. INTRODUCTION

1. Background

A. Linearly-conjugated oligomers

The delocalized and polarizable π-electron system found in conjugated organic molecules dictates many of the properties necessary for the use of organic materials in nonlinear optical (NLO) applications.[1] Nonlinear optics is concerned with the interaction of one or more electromagnetic radiation fields with matter to produce a new field that differs in phase, frequency, polarization or direction from the initial field(s).[2] The alternating electric field of light, $\vec{E}$, imparts a polarization on the charged particles in the material. In an optically nonlinear material, the resulting polarization $\vec{P}$ is represented by a power series expansion of the form:

$$\vec{P} = \varepsilon_0(\chi^{(1)}\,\vec{E} + \chi^{(2)}\,\vec{E}\,\vec{E} + \chi^{(3)}\,\vec{E}\,\vec{E}\,\vec{E} + \ldots)$$

where ε_0 is the dielectric constant and the $\chi^{(n)}$ are electric susceptibilities of n-th order. In materials composed of molecules, the contributions of the induced molecular dipoles are similar:

$$\vec{P} = \alpha\vec{E} + 1/2!\beta\,\vec{E}\,\vec{E} + 1/3!\gamma\,\vec{E}\,\vec{E}\,\vec{E} + \ldots$$

where α, β and γ are first, second and third-order polarizabilities.

The quantities β and γ are also known as the molecular first and second hyperpolarizability, respectively. Urea and *p*-nitroaniline (PNA), the organic compounds used quite often as references, have β values of 2.3 x 10^{-30} esu[3] and 34.5 x 10^{-30} esu,[4] respectively

Traditionally, inorganic crystals have been investigated as materials with commercially relevant NLO properties. However, these materials are often expensive and difficult to process. As an alternative, organic compounds, which offer many advantages over their inorganic counterparts, have been explored. The ease of synthetic adjustment and processing, faster nonlinear response times, lower costs, and the possibility of tuning the properties of a material by altering its chemical structure have enticed chemists to study organic conjugated oligomers and polymers. In the quest for improved nonlinear optical materials, structure-function analyses have been conducted on molecular, oligomeric and polymeric systems. A common motif for these studies involves a direct comparison of conjugated systems of sequentially increasing lengths, the so-called oligomer approach.[1e] The optical properties of these systems are further manipulated via attachment of π-electron donor and acceptor groups. These structure-property relationships have been described for numerous linearly conjugated systems such as, among many others, polyenes, thiophenes, stilbenes, azobenzenes, and their derivatives.[5] It has been recognized that nonlinear optical activity of oligomers is related to the type of conjugated π-electron bridge. A difference in hyperpolarizability has been determined when oligomers bearing the same

D-A pair and the same conjugation length had different bridges, such as polyene, phenylene or thiophene.

A.1 Polyenes

One of the simplest conjugated systems is a one-dimensional conjugated polymer: polyacetylene (PA). Although it was found that polyacetylene has interesting NLO properties,[6] it cannot be easily used in optical applications because it exhibits poor stability and processability. Therefore, there have been various efforts to improve this situation. Unlike polyacetylene, substituted polyacetylenes, such as polyphenylacetylene (PPA, **Fig. 1.1**), dissolve in various organic solvents, are thermally stable and, by introducing bulky substituents on the phenyl groups, their optical properties can be controlled. The third-order nonlinear susceptibilities $\chi^{(3)}$ of polyacetylenes (PA) with different substituents have been calculated and reported.[5g] A red shift of λ_{max} (where λ_{max} is defined as the lowest energy wavelength of maximal absorption in the UV-Vis spectrum) and an increase of $\chi^{(3)}$ values have been observed with an increase in π-system length: from trans–rich polyphenylacetylene PPA to trans-polydiphenylacetylene PDPA and polynaphthylacetylene PNA (**Fig. 1.1**).

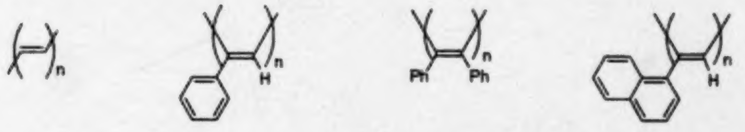

trans-PA trans PPA trans-PDPA trans-PNA

Fig. 1.1 Chemical structures of some polyacetylene derivatives.

Adding an electron-donating group and an electron-withdrawing group also enhances the second order NLO response.[5d,7] Nowadays, researchers attempt to understand the mechanism that leads to dramatic changes in optical polarizabilities *via* changes in the chain length and/or donor/acceptor strength as well as the limiting factors of these enhancements. Mukamel and co-workers[7b] studied the influence of the length of donor/acceptor polyene bridges with respect to the second-order polarizability, β **(Fig. 1.2)**.

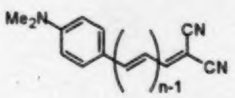

n= 5, 10, 15, 20, 30, 40

Fig. 1.2 Structures of the D-A substituted polyenes studied by Mukamel.[7b]

The results of this research suggested that the influence of the donor group was limited to within the first few adjacent double bonds, and the same was true for the acceptor. Therefore, for longer molecules, the effects of the donor and acceptor are totally decoupled (no charge transfer CT) and additive (β value of the D-A molecule is equal to the sum of β values of a molecule with only donor, D, and a molecule with only acceptor, A).

Blanchard-Desce and co-workers studied several soluble push-pull phenylpolyenes and diphenylpolyenes of various length.[5d,5h,8] Alkyl (cyclic and acyclic) substituents were grafted on the donor moiety in order to increase the solubility **(Fig 1.3)**.

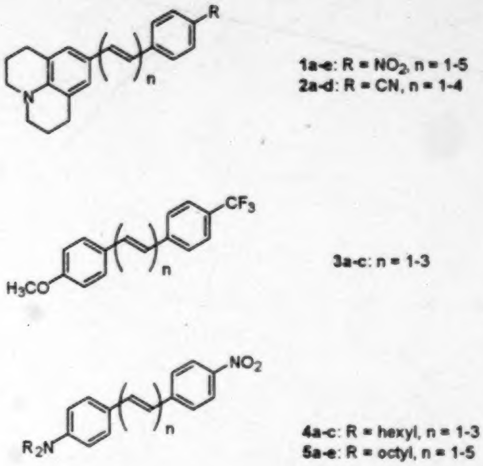
R
n
1a-e: R = NO_2, n = 1-5
2a-d: R = CN, n = 1-4
CF_3
H_3CO
n
3a-c: n = 1-3
NO_2
R_2N
n
4a-c: R = hexyl, n = 1-3
5a-e: R = octyl, n = 1-5

Fig. 1.3 Structural formulae of the series of push-pull diphenylpolyenes investigated by Blanchard-Desce.[5d]

Two alternative routes were used to prepare these series of push-pull diphenylpolyenes (**Scheme 1.1**).[5d] The first route was based on a Wittig condensation of a phosphonium salt bearing the donor moiety with polyenals having the acceptor end group. The second route relied on a Wittig-Horner-Emmons condensation of a phosphonate bearing the acceptor moiety with polyenal derivatives having the donor end group. This Horner modification was preferred to the classical Wittig reaction because both the reagents were deactivated by electronic effects, and a more reactive reagent was needed.

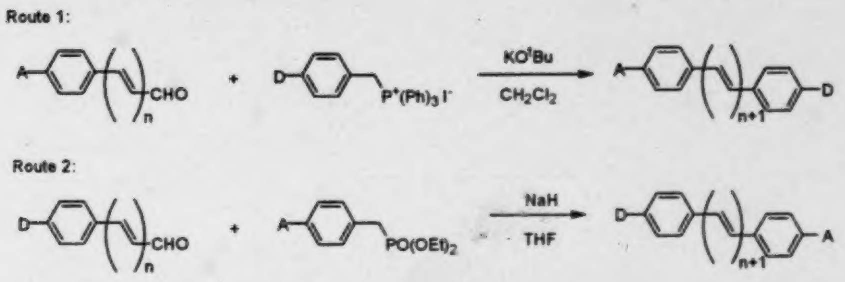

Scheme 1.1 Synthetic methodology used for the preparation of push-pull diphenylpolyenes.[5d]

To explore the extent of π-electron delocalization, ^{1}H NMR spectroscopic studies were performed. As coupling constants between adjacent vinylic protons are dependent on the corresponding carbon-carbon bond order, these studies gave an indication of bond length alternation in solution. The study of J_{HH} values indicated a pronounced bond order alternation along the polyenic chain. An oscillation of J_{HH} values along the polyenic chains going from the donor end to the acceptor end was noted: larger values ($13.7 < {}^3J_{HH} < 16.4$ Hz) corresponding to carbon-carbon bonds with dominant *trans* double bond character (${}^3J_{HH} \sim 16.5$ Hz) alternated with smaller values ($9.7 < {}^3J_{HH} < 11.2$ Hz) corresponding to carbon-carbon bonds with dominant anticoplanar single bond character (${}^3J_{HH} \sim 10$ Hz). It was noticed that the alternation had a tendency to lessen toward the middle of the polyenic chain, in particular for elongated derivatives. As a conclusion, from the study of coupling constants it was noted that stronger donor-acceptor pairs led to slightly less pronounced bond alternation (smaller J_{HH}). The electronic absorption spectra for **1 – 5** were recorded and compared. It was found that all push-pull diphenylpolyenes display positive solvatochromism; a bathochromic shift and broadening of the absorption band was observed with increasing solvent polarity. EOAM (electrooptical absorption measurements) and EFISH (electric-field-induced second-harmonic generation) experiments showed that stronger donor-acceptor pairs and longer polyenic chain led to larger first and second hyperpolarizabilities.

EFISH measurement of first hyperpolarizabilities β for a related series of donor-acceptor polyenes[9] indicated that compounds with acceptors that could gain aromaticity in the excited state, such as **6 – 10 (Fig. 1.4)**, had much larger β values than diphenylpolyenes, such as **5**.

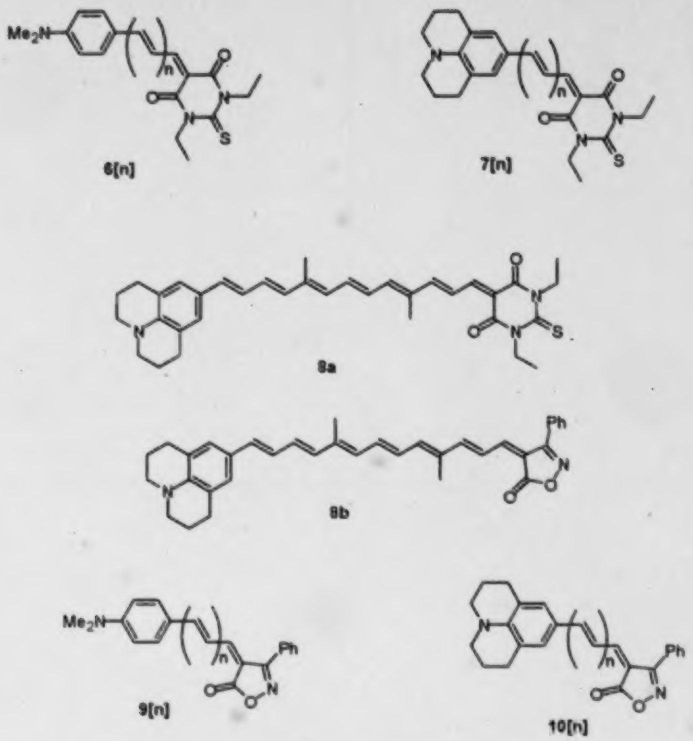

Fig. 1.4 Donor-acceptor polyenes displaying very large nonlinearities.[9]

A π-electron delocalization length study indicated that higher β values were obtained for longer delocalization paths (e.g. 2169 x 10^{-30} esu for **7[3]** *vs.* 87 x 10^{-30} esu for **7[0]**). It has been demonstrated that D-A-substituted carotenoids could display large second order nonlinearities.[10] Exceptionally high β values were obtained when *N,N'*-diethylthiobarbituric acid and 3-phenyl-5-isoxazolone were used as acceptors: $\mu\beta$ = 34770 x 10^{-48} esu for **8a**, $\mu\beta$ = 28500 x 10^{-48} esu, and β = 1781 x 10^{-30} esu for **8b**. X-ray determinations on **10[2]** and **10[3]** provided evidence for the decrease in bond length alternation. It was found that the difference in length between adjacent C-C bonds increased upon going from the acceptor to the donor. This observation was viewed as a result of the acceptor "pulling" on the π electrons more strongly than the donor is "pushing" them.

A.2 Thiophenes

Another extensively studied group of conjugated molecules are the thiophene oligomers and related compounds (**Fig 1.5**). Oligothiophenes have been known to be very efficient relays of π-electronic communication, almost comparable to polyenes.

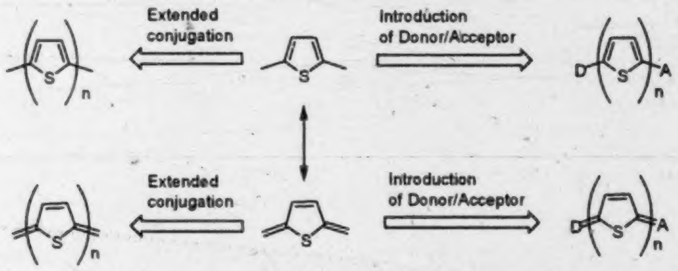
Extended conjugation
Introduction of Donor/Acceptor
S
n
D
A
Extended conjugation
Introduction of Donor/Acceptor

Fig. 1.5 Aromatic and quinoid forms of thiophene oligomers.

A number of theoretical and experimental studies on thiophene-containing chromophores have been carried out, and they have shown that polythiophenes are stable, easily synthesizeable and very processable compounds, showing high first hyperpolarizability β.[5b,11]

In second order NLO materials, charge transfer from donor to acceptor through an aromatic or heteroaromatic ring disturbs the aromaticity of the bridge. It is known that as the aromatic delocalization decreases, the energy required to polarize the molecule also decreases. This ultimately gives a reduced bond-length alternation across the π-conjugated bridge. Molecular orbital calculations of the first hyperpolarizability β for a series of D-A-substituted benzene, thiophene, furan and pyrrole oligomers indicated that the thiophenes were the most NLO active, whereas the benzene oligomers were the least active.[12] Octithiophene (**8T**) shown in **Fig. 1.6** was found to be the longest non-substituted oligomer of thiophene that can be synthesized and isolated as a pure crystalline compound. The molecule is fully planar, resulting in a high electron delocalization, based on field-effect mobility (μ_{FET}) measurements, up to three times higher than that of sexithiophene **6T**.[5g]

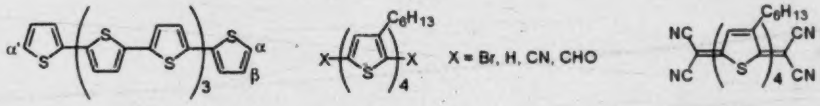

8T **11a** **11b**

Fig. 1.6 Molecular structure of octithiophene and some substituted quaterthiophene.

Alkyl substitution on all thiophene rings, in the β position, produced a blue shift of λ_{max} due to the twisted structures induced by the alkylation in the repeating units. Introduction of α,α'-end-capping electro-active groups in β-substituted quaterthiophene **11a** and **11b** produced red shifts in the electronic absorptions in the order of Br < CN < CHO < $C(CN)_2$ (**Fig. 1.6**).[5g]

Hutchings and co-workers[5a] studied the properties of molecules **12** to **18** (**Fig. 1.7**).

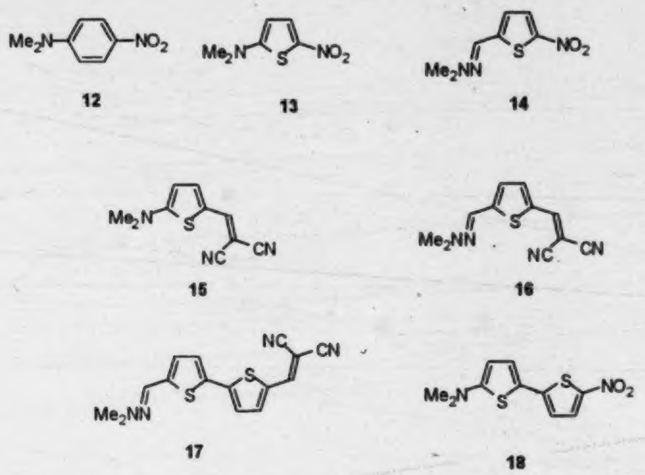
Me$_2$N
NO$_2$
12
13
14
15
16
17
18
S
Me$_2$NN
NC
CN

Fig. 1.7 Structures of some D-A substituted thiophenes studied by Hutchings.[5a]

Substitution of bromo-derivatives with dimethylamine or 1,1-dimethyl hydrazine yielded **13**, **14** and **18**. The thiophenes containing both the hydrazo and dicyanovinyl were synthesized as in **Scheme 1.2**.

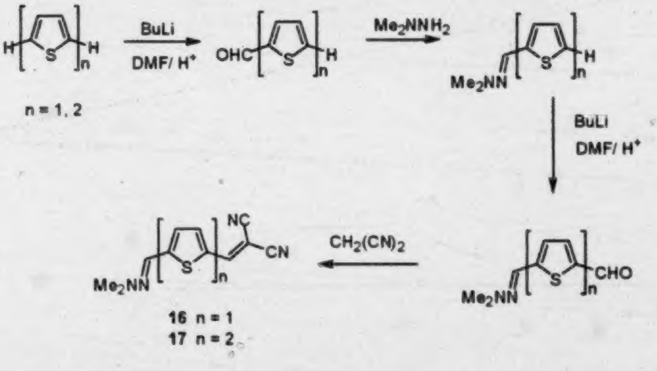
BuLi
DMF/ H$^+$
Me$_2$NNH$_2$
n = 1, 2
OHC
CHO
Me$_2$NN
CH$_2$(CN)$_2$
NC
CN
16 n = 1
17 n = 2

Scheme 1.2 The synthesis methods of **16** and **17**.

The main structure-property relationships deduced from these results were:

(i) thiophene provided a more efficient electron delocalization than benzene;

(ii) the increase was even greater for bithiophene compared with biphenyl;

(iii) increasing the conjugation pathlength by a second thiophene group in **17**, compared with monothiophene **16**, gave a further increase in the first order hyperpolarizability β; (iv) β value for dimethylhydrazono substitution was twice that of dimethylamino in a comparable molecule;

(v) dicyanovinyl was a more effective electron acceptor group than nitro.

A large number of thiophene derivatives were synthesized in two steps and studied by Kirsch *et al.*.[13] β-Chloroacroleins **20** were easily accessible from the substituted acetophenones **19** by the Vilsmeier-Haack reaction (**Scheme 1.3**). The second step was a one-pot synthesis to the desired arylthiophenes. Sodium sulfide was allowed to react with **20**, followed by condensation with the corresponding benzyl bromide.

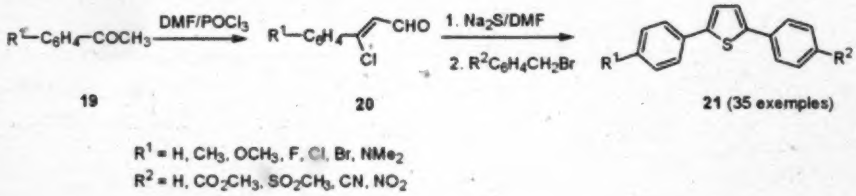

Scheme 1.3 The synthesis of some unsymmetrical diarylthiophenes.[13]

Study of the series of compounds **21** by UV-Vis spectroscopy showed that a red-shift in λ_{max} occurred when stronger donor ($F < Cl < Br < H < CH_3 <$

$OCH_3 < NMe_2$) or acceptor groups ($H < CO_2CH_3 < SO_2CH_3 < CN < NO_2$) were involved.

Blanchard-Desce and co-workers[14] reported the synthesis of NLO chromophores containing a fused terthiophene, namely dithienothiophene (DTT), as an electron relay. Formylation of DTT, followed by a Wittig reaction, yielded **22**, which, by condensation with malononitrile and 1,3-diethyl-2-thiobarbituric acid produced **23** and **24** respectively (**Scheme 1.4**).

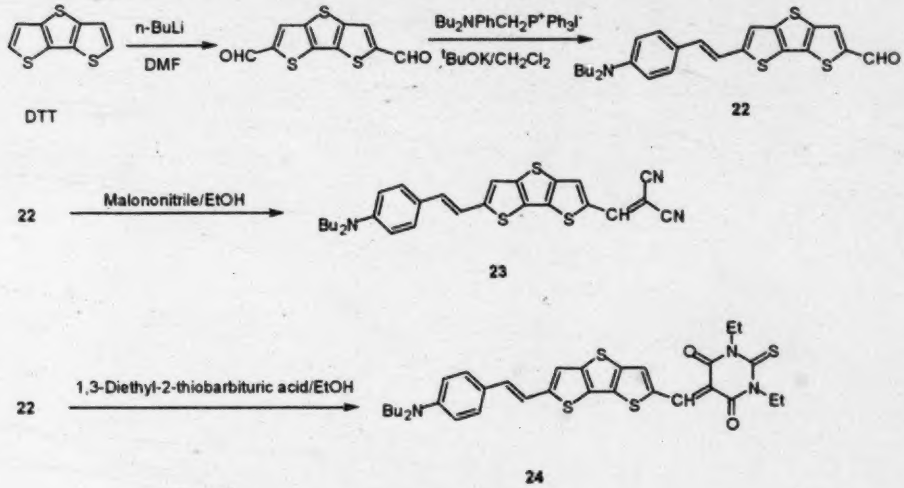
DTT
n-BuLi
DMF
OHC
CHO
$Bu_2NPhCH_2P^+Ph_3I^-$
$^tBuOK/CH_2Cl_2$
Bu_2N
22
Malononitrile/EtOH
CN
CH
23
1,3-Diethyl-2-thiobarbituric acid/EtOH
Et
N
S
O
24

Scheme 1.4 Synthesis of DTT-based chromophores.[14]

By studying the electronic behaviour of these chromophores it was found that **23** and **24** show a different tendency than **22**; their λ_{max} values exhibits a red-shift with an increase of solvent polarity up to a certain polarity limit (dioxane, CH_2Cl_2, acetone, DMF). A further increase in solvent polarity (MeCN) reverses this trend. This behavior had also been observed for some

D-A-substituted polyenes.[15,16] The cause of this inverted solvatochromism was explained by a larger ground-state polarization relative to the polyenic counterpart. That is to say that DTT-based push-pull chromophores had a comparatively larger contribution of the zwitterionic form in their ground-state structures. This characteristic also affects the magnitude of β, which varies with the dipole moment (ground-state polarization) and bond alternation. Compound **24** showed a high β value in CH_2Cl_2, but a negative one (explained by a negative $\Delta\mu = \mu_e\text{-}\mu_g$) in DMF, suggesting that the zwitterionic contribution to the ground state became predominant in highly polar solvents.

Calculated data for donor-heteroaromatic-acceptor chromophores have shown that electron-rich heterocycles weakly withdraw electron density from the donor and strongly donated electron density to the acceptor.[17] Stilbene NLO chromophores and heterocyclic analogues containing one thiophene or thiazole rings were analyzed using the ZINDO (sum-over-states) formalism (**Fig. 1.8**). Experimental and calculation data for compounds containing five-membered aromatic rings with two heteroatoms, such as thiazole, oxazole and imidazole showed that they increased the first hyperpolarizability significantly when replacing the benzene rings in **25**.[18] It was found that thiazole derivatives display larger first hyperpolarizabilities, β, than their aryl and thienyl analogues, and the magnitude of the increase depended on the regiochemistry of the thiazole substitution.[18] Also, the tricyanovinyl-substituted chromophores showed higher first hyperpolarizabilities than their dicyanovinyl analogues. Replacement of the aryl ring adjacent to the donor with a thiazole ring yielded only a small increase in first hyperpolarizability, and the orientation of the thiazole ring did not have a substantial effect (**26** *vs.* **33-34**). By contrast, when the thiazole ring was adjacent to the acceptor, a large increase in the hyperpolarizability was observed, depending on its regiochemistry. When the dipole of the thiazol moiety enhanced the molecular dipole, as in **29** and **30**, the first hyperpolarizability is maximized, and this situation is called a "matched" case. Conversely, **27** and **28** are called "mismatched".

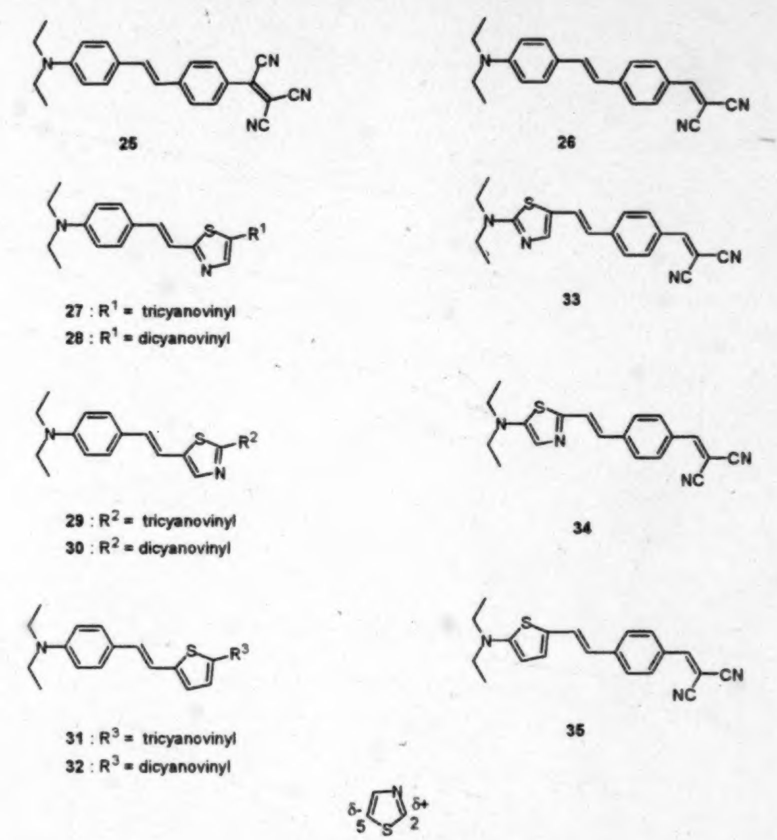
25
26
27 : R^1 = tricyanovinyl
28 : R^1 = dicyanovinyl
33
29 : R^2 = tricyanovinyl
30 : R^2 = dicyanovinyl
34
31 : R^3 = tricyanovinyl
32 : R^3 = dicyanovinyl
35
δ-
δ+
5
2

Fig. 1.8 Thiophene/thiazole-aryl analogues of D-A stilbenes investigated in references 18a-b.

Calculations performed for molecules obtained by replacing both aryl rings with thiophene, thiazole or pyrrole (**Fig. 1.9**) showed that: (i) bis-thiophene, thiophene-thiazole, and bis-thiazole chromophores displayed larger first hyperpolarizabilities than their stilbene analogues, (ii) the magnitude of the increase in hyperpolarizability depended on the regiochemistry of the thiazole substitution, (iii) the hyperpolarizabilities of "matched-matched" bis-thiazole chromophores (e.g., **36**) were higher than those of "matched" thiophene-thiazole derivatives (e.g., **37**), which exceeded those of bis-thiophene analogues, and (iv) pyrrole-thiazole chromophores (e.g., **38**) displayed the largest first order hyperpolarizability β.[18a-b]

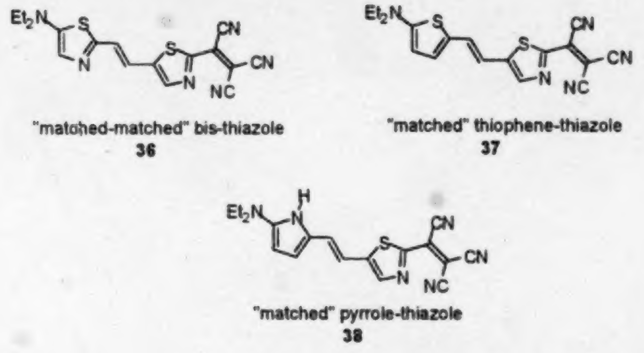

"matched-matched" bis-thiazole
36

"matched" thiophene-thiazole
37

"matched" pyrrole-thiazole
38

Fig 1.9 Selected "matched" thiazole, thiophene and pyrrole analogues of D-A stilbenes investigated in references 18a-b.

ZINDO calculation showed that both C2 and C5 carbons of pyrrole (see **Fig. 1.8** for numbering) were electron-deficient. Therefore, pyrrole weakly withdrew electron density from the donor and also added electron density to the bridge. When it was in conjugation with a "matched" thiazole molecule, as in structure **38**, a very large first hyperpolarizability was observed (307 x 10^{-30} esu) compared with the stilbene analogue (35 x 10^{-30} esu). Thus, the computations suggested that the incorporation of heteroatomic rings, with careful consideration of electronic factors, could allow for significant enhancement of molecular NLO properties.

A.3 Stilbene Analogues

Having long electron delocalization pathways and planar structures, stilbene derivatives have been investigated for their NLO properties. Van Walree *et al.*[19] studied the electronic properties of *N,N*-dimethylamino and/or nitro substituted stilbenes (C=C bridge), benzylideneanilines (C=N and N=C bridges) and azobenzenes (N=N bridges) using EFISH, UV spectroscopy, and PPP/SCF calculations (**Fig. 1.10**).

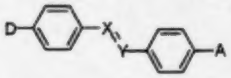

D = H, NMe$_2$; A = H, NO$_2$
X=Y = C=C, N=C, C=N, N=N

Fig 1.10 Molecular structures of stilbene, benzylideneaniline and azobenzene derivatives.

This study reported that first hyperpolarizabilitiy β of the ethylene and azo bridged D/A compounds are of comparable magnitude, whereas substitution of one carbon atom by a nitrogen reduces the NLO activity. A substantially lower β value was calculated for the benzylideneaniline having the partially negative charged nitrogen atom linked to the donor moiety.

A thorough investigation of stilbenes using solution-phase dc electric EFISH and third-harmonic generation (THG) experiments was done by Cheng *et al.*[20] Monosubstituted (**Fig. 1.11**) and disubstituted (**Fig. 1.12**) benzenes and stilbenes were studied. A wide range of electron-donating and withdrawing substituents was examined.

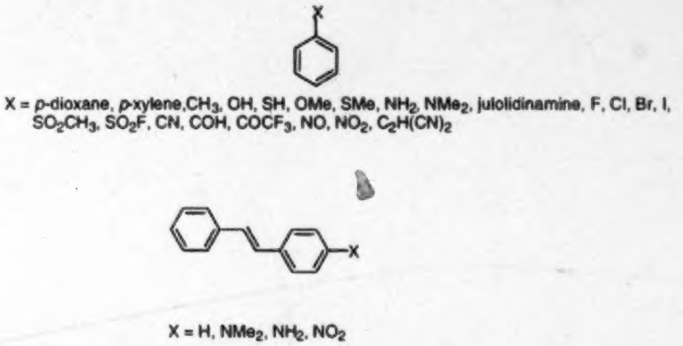
X
X = p-dioxane, p-xylene,CH$_3$, OH, SH, OMe, SMe, NH$_2$, NMe$_2$, julolidinamine, F, Cl, Br, I, SO$_2$CH$_3$, SO$_2$F, CN, COH, COCF$_3$, NO, NO$_2$, C$_2$H(CN)$_2$
X
X = H, NMe$_2$, NH$_2$, NO$_2$

Fig. 1.11 Monosubstituted benzenes and stilbenes studied by Cheng.[20]

For the monosubstituted benzene derivatives, it was found that, with the exception of *N,N*-dimethylaniline and julolidinamine, donors were ineffective in inducing charge and polarizability asymmetry (based on small permanent molecular dipole moments, μ, and first hyperpolarizabilities, β, values). Acceptor groups were more effective, but the substantially higher dipole moments of the acceptor-substituted benzenes did not produce a greater polarization of the benzene π system since the acceptor group dipoles are substantial. The first and second hyperpolarizabilities and molecular dipole moments μ were much higher in monosubstituted stilbenes than in monosubstituted benzenes. Therefore, the conjugation length played an important role in the molecular nonlinear optical polarizability. The cooperative effects of donor and acceptor groups were investigated by studying para-disubstituted benzene and 4,4'-disubstituted stilbene derivatives (**Fig. 1.12**).

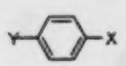

para-disubstituted benzenes

X	Y
SO_2Me	OH
CN	Me, Cl, Br, OPh, OMe, SMe, NH_2, NMe_2
CHO	Me, OPh, OMe, SMe, NMe_2
i-$SO_2C_3F_7$	OMe
$COCF_3$	OMe, OPh, NMe_2
NO	NMe_2
NO_2	Me, Br, OH, OPh, OMe, SMe, N_2H_3, NH_2, NMe_2, CN, CHO
$CHC(CN)_2$	OMe, NMe_2, julolidineamine
$C_2(CN)_3$	NH_2, NMe_2, julolidineamine

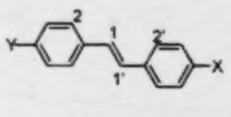

4,4'-disubstituted stilbenes

X	Y
$SO_2C_5H_{11}$	OHex-OH
$SO_2C_6F_{13}$	OMe
$COCF_3$	OMe
CN	OH, OMe, NMe_2
NO_2	H, Me, Br, OH, OPh, OMe, SMe, NH_2, NMe_2, julolidinamine, COOMe, CHO
Br	OMe

Fig. 1.12 Structure of para-disubstituted benzenes and stilbenes studied by Cheng.[20]

Comparing the monosubstituted and disubstituted compounds, a significant increase in μ and β values due to the charge-transfer (CT) interactions between the donor and acceptor groups was observed in the disubstituted benzenes and stilbenes. Between the D-A-substituted benzenes and stilbenes with the same substituents, typical enhancements of 6-8 times were noted for β. Small enhancements, less than 0.5D, were seen for μ in stilbenes. Therefore, increasing the local dipole separation did not result in a significant increase in the total dipole moment. This was viewed as an indication of the small fraction of electron donation to the acceptor in the ground state. But, as a result of the extended conjugation, the electronic absorption energy bands were about 50-60 nm red-shifted in comparison to those of the benzene derivatives. For a given acceptor, the nitro group for instance, the relative effectiveness of various donors was established, giving the approximate series: Me < Br < OH < OPh < SMe < N_2H_3 < NH_2 < NMe_2 < julolidineamine in increasing order.

The 2-, 3-, and 4-disubstituted nitro stilbenes were also studied. It was found that 2-, 3-, and 4-donor substitution gave comparable β values, and 4'-nitro substitution gave significantly higher β values than 2'- or 3'-nitro substitution (**Fig. 1.13**). This was explained by the effective alignment of molecular dipoles with CT axes and by the fact that the group dipole moments of the donors were much smaller than that of the nitro acceptor. As a result, the substitution pattern of the donor had only minor effect on the overall molecular dipole directions.

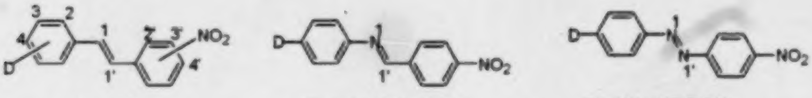

D = OMe, Br
Nitro disubstituted stilbene

D = H, Me, OMe, Br
1-Aza-substituted nitrostilbene

D = NH2, NEtEtOH
1,1'-Azo-substituted nitrostilbene

Fig. 1.13 Other nitrostilbenes studied by Cheng.[20]

The effects of heteroatom and electron-donating or electron-withdrawing side-group substitutions in D-A nitrostilbenes were studied. Contrary to the study reported by Jenneskens and co-workers,[19] 1- and/or 1'-aza or azo-substitution (**Fig. 1.13**) decreased β values by at least 25%. The effect of side group substitution on the donor moiety gave no advantage over the unsubstituted compound, except 2,4-dimethoxy-4'-nitrostilbene that showed a 20% increase of the second hyperpolarizability value *vs.* 4-methoxy-4'-nitrostilbene. On the other hand, 4-methoxy-2',4'-dinitrostilbene showed a 25% decrease in β *vs.* 4-methoxy-4'-nitrostilbene. Interpretation of this data indicated that an acceptor group has large dipole moments in comparison to a donor group. Therefore, multiple acceptor substituents led to a deviation between the molecular dipole axis and the molecular long axis containing dominant hyperpolarizability components. This ultimately resulted in lower optical nonlinearities. Conversely, due to their low group dipole moments, multiple donors could be used to enhance optical nonlinearity. A study on diphenylpolyenes showed that as the bridge length in stilbenes increased (i.e., polyenes), the β values increased.[5e]

A.4 Fluorene Derivatives

An interesting structure-property relationship concerns the dependence of the first hyperpolarizability on conjugation planarity. It is known that a nonplanar geometry gives a diminution of orbital overlap. To determine how orbital overlap influences the second order nonlinearities, Cheng *et al.*[5e] studied D-A interactions in 4,4'-disubstituted biphenyls and fluorenes (**Fig. 1.14**).

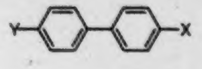

X = H, CN, $COCH_3$, $SO_2C_6H_{12}OH$, NO_2
Y = H, Br, OH, OMe, NH_2, NMe_2

Disubstituted Biphenyls

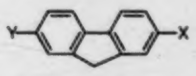

X = H, CN, NO_2
Y = H, Br, OMe, NMe_2

Disubstituted Fluorenes

Fig. 1.14 Structures of 4,4'-disubstituted biphenyls and fluorenes investigated in reference 5e.

It was found that the D-A biphenyls had lower β values than their fluorene analogues due to torsion along the phenyl-phenyl bond. But the differences in β were small (e.g., 9.2 x 10^{-30} esu for NO_2-biphenyl-OMe *vs.* 11 x 10^{-30} esu for NO_2-fluorene-OMe) suggesting a weak dependence on torsion for small angles. It is known that the torsional angle for biphenyl is 30° in solution, and 40° in the vapor phase.[5e] As the donor and acceptor strength increased, the β values for the biphenyl and the fluorine derivatives converged (e.g., 50 x 10^{-30} esu for NO_2-biphenyl-NMe_2 vs 55 x 10^{-30} esu for NO_2-fluorene-NMe_2). Therefore, strong donor and acceptor substituents likely produced more planar biphenyl derivatives. The torsional angle decreased from 27° for H-biphenyl-NO_2 to 18° for NMe_2-biphenyl-NO_2, as deduced from spectroscopic and hyperpolarizability data.

A.5 Acetylenic Derivatives

Series of donor-acceptor acetylene oligomers, in which changes in both the conjugation length and the donor-acceptor strength were made, were synthesized and studied by Stiegman and co-workers (**Fig. 1.15**).[21,5e]

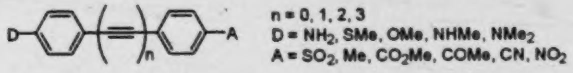
D
A
n
n = 0, 1, 2, 3
D = NH₂, SMe, OMe, NHMe, NMe₂
A = SO₂, Me, CO₂Me, COMe, CN, NO₂

Fig. 1.15 Diphenylacetylenes studied by Stiegman and co-workers.[21]

Very interesting observations emerged from the analysis of this series of molecules. Methylation of the amine group to methylamine and dimethylamine increased the D-A interaction and, subsequently, the β value. However, the increase in hyperpolarizability was significant only for strong acceptors; a nitro group producing an increase in β from 24 x 10^{-30} esu (for the amino group) to 46 x 10^{-30} esu (for the dimethylamino group). A weaker acceptor produced a modest increase in β: from 20 x 10^{-30} esu (for the amino group) to 29 x 10^{-30} esu (for the dimethylamino group) when the cyano acceptor was used. Another observation was related to conjugation length effects. The previous sections included oligomers that showed an increase of NLO properties with extension of the conjugation path. The studies conducted by Stiegman revealed a rather surprising conclusion for diphenylacetylenes: an increase in the conjugation length produced a decrease in second order NLO efficiency. For example, the reported values relative to urea for amino-nitro donor-acceptor pair were: 3 (n = 0), 0.2 (n = 1), 0.05 (n = 2), 0.03 (n = 3). Comparison of the dipole moment change, from the ground state to the excited state, for different D-A strengths showed a large variation. Weak D-A oligomers had large dipole moment changes, whereas stronger pairs showed smaller changes. Furthermore, as the conjugation length increased, the dipole moment change decreased – a trend that was counterintuitive. In comparison to D-A benzenes and stilbenes,[3e] acetylene derivatives had higher β values than benzenes (about two times) and lower values than stilbenes derivatives (by about one-half).

Nicoud and Wong[22] synthesized a new class of highly hyperpolarizable 1,2-disubstituted π-conjugated system, also called zig-zag chromophores (**Fig. 1.16**).

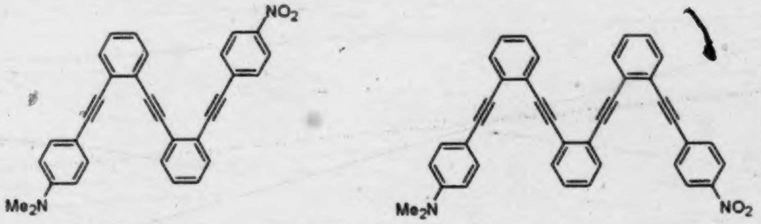

39 **40**

Fig. 1.16 D-A zig-zag chromophores synthesized and studied by Nicoud.[22]

Palladium coupling reactions were used to synthesize dimer **39** and trimer **40**. AM1 semi-empirical calculations provided β values for **39** and **40**. The vectorial projection of static β along the permanent dipole moment, $\beta_\mu(0)$ were calculated (25.6×10^{-30} esu for **39** and 12.4×10^{-30} esu for **40**) and compared to $\beta(0)$ for PNA (5.4×10^{-30} esu). A shift of λ_{max} to longer wavelength with the incorporation of a donor (dimethylamino) and an acceptor (nitro) group into the phenyl-ethynyl backbone was noted: about 40 nm for **39** and 70 nm for **40**, versus the unsubstituted derivatives.

For many years, polyacetylenes (PA) and polydiacetylenes (PDA) (**Fig. 1.17**) were the only known single-strand conjugated oligomers with a non-aromatic all-carbon backbone. However, Diederich and co-workers[23,24] succeeded in the preparation of oligomers with a polytriacetylene (PTA) backbone (see section C. Cross-conjugated oligomers).

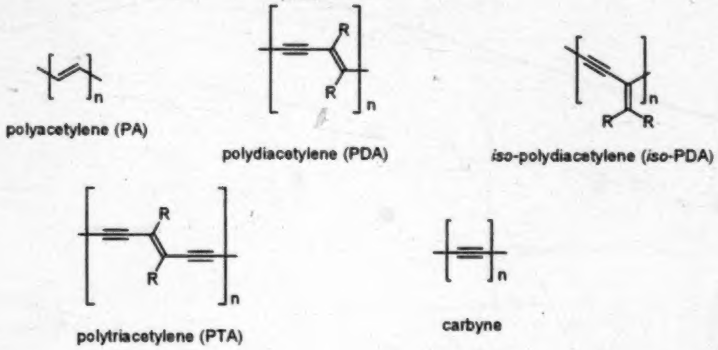

Fig. 1.17 Progression of polymeric backbones from polyacetylene to carbyne.

An experimental study done by Martin et al.[25] on disubstituted PTAs led to a few conclusions: (1) an increase in the conjugation length resulted in larger values of second hyperpolarizability; (2) D-D- and A-A–substituted PTAs showed an increase in second hyperpolarizability by up to 14 times when compared with Me_3Si-protected PTAs; (3) changing from D-D- or A-A-substitution to acentric D-A-substituted PTAs resulted in a two-fold increase in γ.

A.6 Ionic and zwitterionic derivatives

The use of ionic extremities in the hyperpolarizable molecules produced molecules with very high first and second hyperpolarizability.[5b,26,27] Cationic acceptors were found to be more efficient than the neutral ones (**Fig. 1.18**).

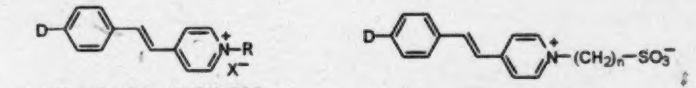

$D = NMe_2$, $R = CH_3$, $X = CH_3OSO_3$
$D = NMe_2$, $R = CH_3$, $X = TsO$

Stilbazolium salts

$D = MeS$, $C_{10}H_{21}S$
$n = 2, 3, 4$

Zwitterionic stilbazolium derivatives

41

Fig. 1.18 Stilbazolium salts and zwitterionic derivatives as efficient NLO materials.[27]

A very high SHG efficiency was measured for **41** (n = 3, D = MeS): 370 times that of urea.

B. Transparency-Nonlinearity Trade-Off

The previous studies have continually shown that as the nonlinear optical responses (β, γ) of linearly conjugated organic chromophores are enhanced via increasing the length of the π-system, a concurrent decease in transparency in the UV-Vis electronic absorption is encountered. A transparency-efficiency trade-off is thus established. Efforts to circumvent this trade-off have explored the development of NLO chromophores with non-traditional motifs for conjugation and donor-acceptor interactions, including two- and three dimensional, spiro- and homo-conjugation, as well as the σ-π-interactions found in silanes.

B.1 Polyphenyls

Polyphenyls were found to be interesting candidates towards the improvement of the nonlinearity-transparency trade-off. Theoretical[28] and experimental[29] studies have evidenced a large enhancement of β (in the range of 150 x 10^{-30} esu, for the nitroderivative with n = 4) when increasing the number n of phenyl rings. **(Fig. 1.19)**

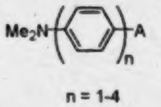

42: A = CN
43: A = NO_2

Fig. 1.19 Structures of some D-A polyphenyls.

All of the CN-substituted molecules displayed a λ_{max} lower than 360 nm, showing an interesting compromise in terms of the nonlinearity-transparency trade-off. In fact, the improved transparency of polyphenyls in the blue or UV range was partially accounted for by the limitation of the ICT between the donor and the acceptor group, due to the important torsion angle. Stronger acceptors, like NO_2, showed red-shifted λ_{max}, the molecules being planar as discussed previously in section A.4. Comparison of **42** and **43**, showed smaller β values for cyano compounds. Small differences were noted for n = 1-2, but substantially larger for n = 3-4 (β = 100 x 10^{-30} esu *vs.* β = 155 x 10^{-30} esu for **42** and **43**, respectively, with n = 4). With respect to chromophore lengths, NLO efficiency for shorter oligomers was small (n = 3 - 4) but still 20 times the value of urea for the D-A byphenyl.

Octupolar molecules (molecules with threefold rotational symmetry) also offer an interesting alternative to this issue. It has been known since the pioneering work of Zyss and coworkers[30] that non-centrosymmetrical, non-dipolar molecular frameworks (such as octupolar molecules) can exhibit a non-zero β value. Most studies have been dedicated to two-dimensional octupolar molecules (eg. 1,3,5-triamino-2,4,6-trinitrobenzene).[31] In contrast, only a few 3D octupolar molecules (mostly organometallic derivatives) have been investigated.[32,26c] Blanchard-Desce *et al.*[33] studied orthogonalized biphenyl derivatives.(**Fig. 1.20**)

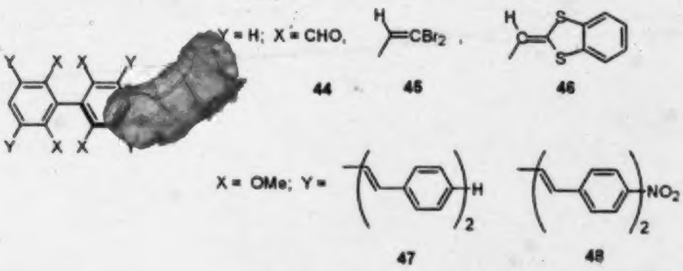

Fig. 1.20 Structural formulae of some octupolar molecules investigated in reference 33.

The molecular design of these chromophores was based upon a central biphenyl moiety, where the two phenyl units were kept perpendicular due to steric repulsion between ortho-substituents. Electron-withdrawing or electron-donating substituents were chosen on the four *ortho* positions of the phenyl rings for **44**, **45** and **46**. Charge transfer was observed from the substituents to the phenyl rings or vice versa. Both **44** and **45** displayed comparable β values with p-nitroaniline, PNA, (as calculated by harmonic light scattering, HLS) but a much larger transparency range was maintained. A better β value was observed for **46**, 4 times larger than that for PNA, while still retaining full transparency in the visibile range. These promising results were followed by the study of a second generation of octupolar biphenyls, with electron-donating methoxy groups in the four *ortho* positions (to maintain orthogonality between the two rings) and elongated conjugated rods at the four *meta* position. Either electronically neutral (**47**) or electron-withdrawing groups (**48**) were taken in consideration to investigate the potential increase in nonlinearity due to multidimensional charge transfer (CT). Comparison of molecules **47** and **48** demonstrated that multidimensional intramolecular CT (from the core to the periphery of the molecule) played a significant role. Octupolar molecule **48** exhibited a β value nine times larger than that of **47**, a value similar to that found for **44**, while still displaying transparency in the visible range.

B.2 Silanes

Another method used to maintain the transparency has been the replacement of carbon with sp^3 hybridized heteroatoms of the third row of the periodic table. These atoms could be placed either at the end of conjugation path (and used as electroactive substituents) or between two fully conjugated moieties, such as phenyl rings. Not only is a σ bond electron isolating compared to a π bond, but the overlap of the external $3s$ and $3p$ orbitals of the heteroatom with the $2s$ and $2p$ orbitals of the carbon atom is relatively poor. These characteristics could give a blue-shift for λ_{max}. On the other hand, the $3s$ and $3p$ orbitals of the heteroatom are more polarizable than the $2s$ and $2p$ orbitals of carbon, giving therefore a significant nonlinear response.

Sulfur-containing systems have been studied, and they showed good transparency-nonlinearity trade-off.[34] However, the silicon derivatives have been more widely studied.[11h, 35] The specific interest in silicon as compared to sulfur is focused on the higher degree of connectivity (4 instead of 2) to adjacent moieties. The trimethylsilyl (TMS) group has been used as an electroactive substituent and as a part of the conjugation path in the studies performed by Zyss and coworkers (**Fig. 1.21**).[36]

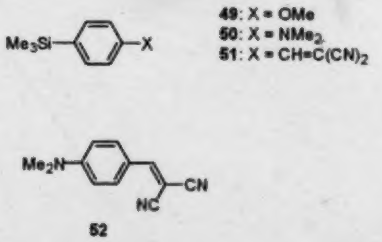

49: X = OMe
50: X = NMe_2
51: X = CH=C(CN)$_2$

52

Fig. 1.21 Structural formulae of some methylsilane derivatives studied by Zyss.[36]

When used as an electroactive substituent, it was found that the trimethylsilanyl group interacted weakly with donor groups (static hyperpolarizability $\beta(0) = 0.3 \times 10^{-30}$ esu for **49**, $\beta(0) = 4 \times 10^{-30}$ esu for **50** but more strongly (approximately as a methoxy group) with acceptors ($\beta(0) = 9 \times 10^{-30}$ esu for **51**). A large blue shift was observed for **51** (λ_{max} = 322 nm) as compared with **52** (λ_{max} = 440 nm, $\beta(0) = 16 \times 10^{-30}$ esu).

The Si atom has also been tested as an electron bridge, connecting separate phenyl rings. An increase in $\beta(0)$ (from 11×10^{-30}esu and 16×10^{-30}esu for n = 1 and n = 2, respectively, to 26×10^{-30}esu for n = 6) and λ_{max} (from 320 nm and 334 nm for n = 1 and n = 2, respectively, to 385 nm for n = 6) was observed with increasing n (**Fig. 1.22**).

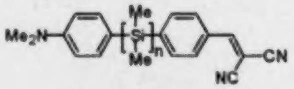

n = 1, 2, 6

Fig. 1.22 Structure of silane derivatives studied by Zyss.[36]

This σ electron delocalization over the Si-Si chain showed the ability of silicon-based molecules to bring a better optimization of the transparency-efficiency trade-off.

The same conclusions were reached by Mignani *et al.*[37] who synthesized and studied several organosilicon compounds (**Fig. 1.23**). They also found that TMS group was more effective as an electron-releasing group. When Si atom was used as part of the conjugation path, it was found that **54** displayed larger hyperpolarizability than **53**, and that **55** and **56** showed a small increase in hyperpolarizability comparing with **53**.

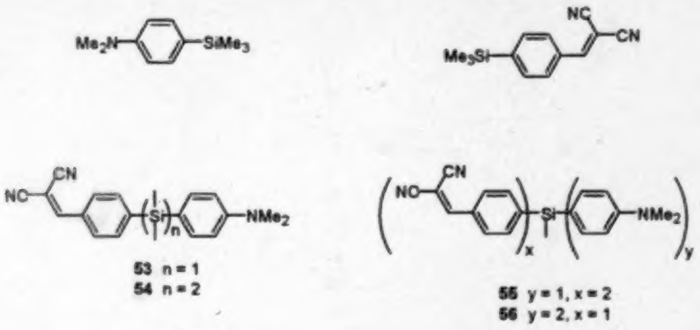

Fig. 1.23 Some D-A organosilicon compounds studied by Mignani.[37]

B.3 Imines and Hydrazones

As discussed in section **A.3**, benzylideneanilines, the aza analogs of stilbene (**Fig. 1.10**), displayed lower hyperpolarizability than the corresponding stilbenes. Nevertheless, their low λ_{max} make them interesting molecules to study. Calculations made by Toray Industries Research Laboratories[38] showed that the position of the imine nitrogen atom induced a dramatic change in the ICT absorption. Higher β and λ_{max} (but not much higher than 400 nm) values were noticed when the nitrogen atom was closer to the donor and the carbon atom was closer to the acceptor.

Similar to imines, hydrazones (obtained by coupling a substituted hydrazine to a carbonyl functionality) bring an additional filled *p* orbital into the conjugation system. Here again, as for imines, two kinds of D-A derivatives are possible, leading to derivatives of type **57** and **58** (**Fig. 1.24**).[36]

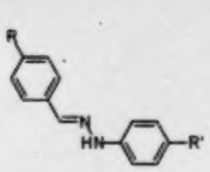

57 R = donor, R' = acceptor

58 R = acceptor, R' = donor

Fig. 1.24 Structure of D-A hydrazone derivatives studied in reference 36.

For compounds of type **57**, it was found that the presence of an additional acceptor group, in *meta* position with respect to R', significantly improved the nonlinearity of the molecule.[36] To the contrary, on the electron donating side, one or two additional donor groups in *ortho* position with respect to R weakened the nonlinear response of the molecule. Having maximum absorption wavelengths around 400 nm, the hydrazones studied displayed good transparency-nonlinearity trade-off.

B.4 Tolans and Diaryl-1,2-Acetylenes

The π electron system present in the carbon-carbon triple bond can also be part of the conjugation path in donor-acceptor NLO chromophores as presented in section **A.5**. The advantage of the tolan molecule (diphenyl-1,2-acetylene) is that the acetylenic bond induces a hypsochromic (blue) shift when compared to similar molecules bearing a double bond. A series of "push-pull" tolanes (**Fig. 1.25**) have been synthesized and studied for their NLO properties by different research groups.[36] Contrary to biaryl or stilbene analogs, no steric interaction between *ortho*-hydrogens is present in tolans, and the two aromatic rings can lie in the same plane. Calculations of the molecular structure and heat of formation using an AM1 semi-empirical method indicated that the energy between an all-planar geometry and an orthogonal geometry of the aryl rings was less than 0.3 kcal/mol. As a result all the conformers can exist at room temperature. Calculations by a Finite Field MNDP method showed that when the two rings were orthogonal, CT was still present, the first hyperpolarizability being a half of the maximum obtained for all-planar conformation. Therefore, there is always a significant hyperpolarizability irrespective of the conformation of the push-pull tolans.

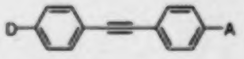

D = OMe, NMe_2, SMe, Me, Br, NH_2
A = NO_2, CN, COOMe, COMe, SO_2Me

Fig. 1.25 Structure of D-A tolans investigated in reference 36.

The β values determined by the EFISH technique revealed that the methylthio (MeS) groups led to a noticeable increase of β value without significant loss of transparency in comparison with the methoxy (OMe) group. The bromo substituent, although electronegative, could give a relatively large β value and good transparency when opposed to a strong acceptor group, such as cyano or nitro.

In order to investigate a possible tuning of the linear and nonlinear optical properties of donor-acceptor tolan analogs, four push-pull 1,2-diaryl-acetylenes, where the aryl ring was a pyridyl or a phenyl ring, were studied (**Fig. 1.26**).

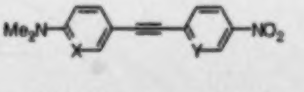

X = C, N
Y = C, N

Fig. 1.26 Structure of 1,2-diaryl-acetylenes investigated in reference 36.

A blue-shift of λ_{max} was observed for all the compounds, when the pyridyl ring was bearing the donor group, but a surprising red-shift was noticed when the pyridyl ring was bearing the acceptor group. It was concluded that the nitro-pyridyl ring was a stronger acceptor than a nitro-phenyl group. β values for these compounds were lower than in tolans, however, making them less interesting as NLO materials.

B.5 Spiro-compounds

Spiroconjugated molecules have been proposed as basic units in molecular materials with unusual nonlinear properties.[39] Ab initio calculations done by Luo *et al.*[40] and experimental studies performed by Kim *et al.*[41] showed that symmetrical spiro-compounds (**Fig. 1.27**) displayed dramatically increased hyperpolarizability in comparison with the monomer units.

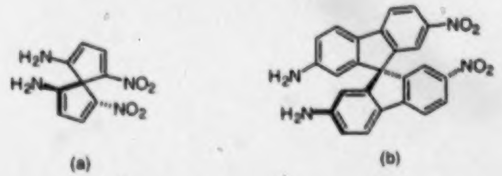

Fig. 1.27 Molecular structures of (a) 1,1'-diamino-4,4'-dinitro-5,5'-spirobicyclopentadiene and (b) 2,2'-diamino-7,7'-dinitro-9,9'-spirobifluorene.

Low absorption (λ_{max} is around 400 nm) and high first hyperpolarizabilities make these symmetrical spiro-compounds useful in the design of a new class of NLO materials. Heterocyclic spiro-compounds have also been studied. These investigations revealed that only symmetrical spiro-compounds displayed CT.[42,43] Only weak or no interactions occurred between the two π moieties of unsymmetrical spiro-compounds (**Fig. 1.28**).[44]

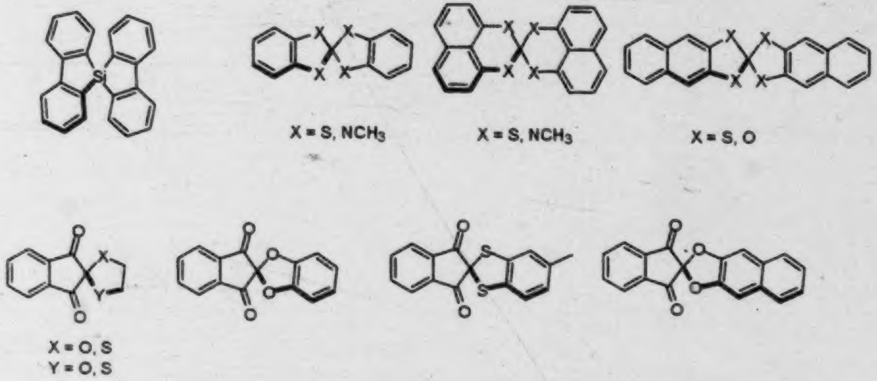

Fig. 1.28 Molecular structures of some heterocyclic spiro-compounds.

C. Cross-conjugated Oligomers

Another group of conjugated compounds displaying good transparency/ nonlinearity trade-off is cross-conjugated oligomers. Cross-conjugation represents an alternative mode of moderated π-electronic communication that has, to date, been largely ignored. Although they are very common in organic chemistry, cross-conjugated compounds (**Fig. 1.29**) cannot be found very often in the undergraduate or graduate textbooks. The main reason is that there are few examples of structurally related series of cross-conjugated chromophores suitable for a detailed analysis and, therefore, their electron distribution and properties are not well known. As a consequence, an understanding of the effects of D-A interactions for cross-conjugated molecules is currently unavailable.

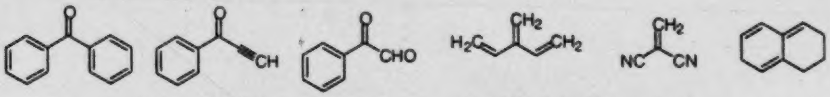

Fig. 1.29 Examples of cross-conjugated molecules.

Cross-conjugated compounds are defined as systems possessing three unsaturated groups, two of which, although conjugated to a third unsaturated center are not conjugated to each other.[45] Each unsaturated center possesses 2n π electrons, where n is a integer. The lone pair of electrons of a singly bonded nitrogen or oxygen atom is considered an unsaturated center, and the compounds from **Fig. 1.30** are considered cross-conjugated.

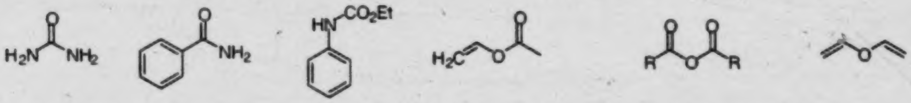

Fig. 1.30 Oxygen- and nitrogen-containing cross-conjugated compounds.

A thorough review on cross-conjugated compounds was made by Hopf.[46] Methods of formation of dendralenes, fulvenes, fulvalenes, zero-bridge annulenes (pentalene, azulene, heptalene), and [n]radialenes were covered **(Fig.1.31)**.

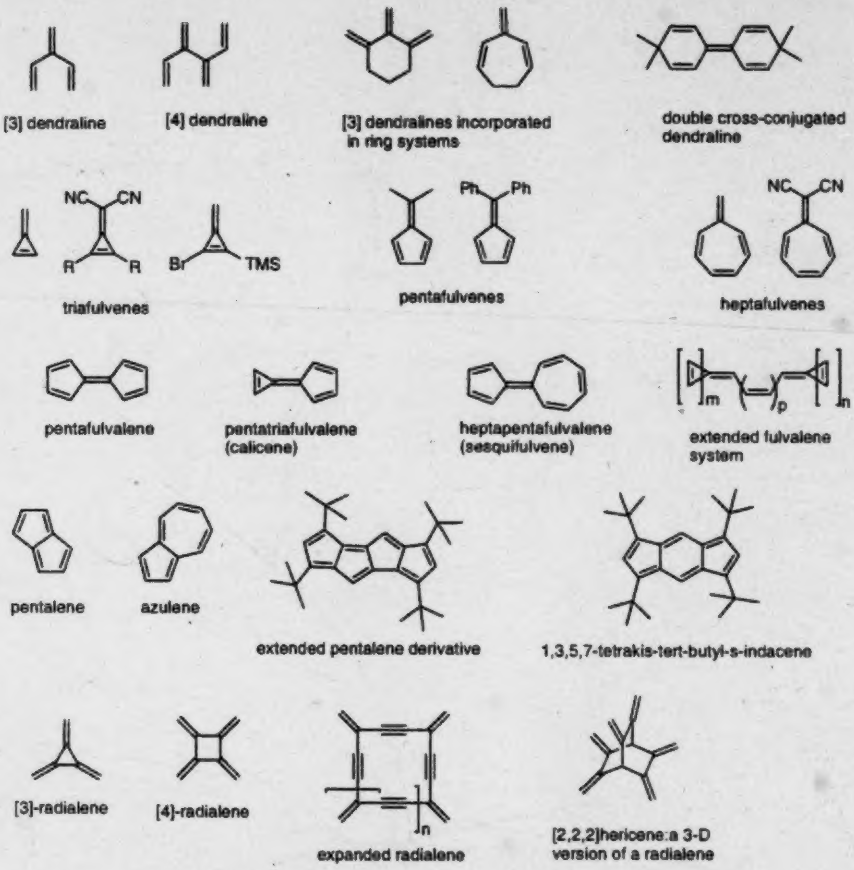
[3] dendraline
[4] dendraline
[3] dendralines incorporated in ring systems
double cross-conjugated dendraline
NC
CN
R
R
Br
TMS
triafulvenes
Ph
Ph
pentafulvenes
NC
CN
heptafulvenes
pentafulvalene
pentatriafulvalene (calicene)
heptapentafulvalene (sesquifulvene)
m
p
n
extended fulvalene system
pentalene
azulene
extended pentalene derivative
1,3,5,7-tetrakis-tert-butyl-s-indacene
[3]-radialene
[4]-radialene
n
expanded radialene
[2,2,2]hericene:a 3-D version of a radialene

Fig. 1.31 Cross-conjugated hydrocarbons reviewed by Hopf.[46]

More important for electrooptical applications are the donor and/or acceptor substituted cross-conjugated compounds, which could have high nonlinear optical activities as well as wide transparency windows.

Chalcones and related compounds (**Fig. 1.32**) are cross-conjugated chromophores displaying large SHG signals and high energy absorption.

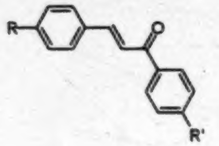

	R	R'	
59a	Donor	Acceptor	
59b	Acceptor	Donor	
59c	Me_2N	CN	(DACC)
59d	Br	OCH_3	(BMC)
59e	OCH_3	OEt	(MEC)

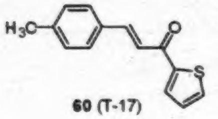

60 (T-17)

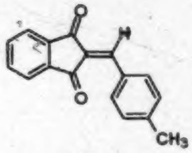

61

Fig. 1.32 Structural formulae of some chalcones and related compounds investigated in references 27 and 36.

Measurements made by EFISH technique showed that chalcones were more efficient when the acceptor group was placed on the benzoyl (Ph-CO-) group, like in **59a** vs. **59b**.[27,36] Studies made in Japan showed that the addition of powerful acceptor groups, such as NO_2 or CN, was unnecessary, the withdrawing effect of the carbonyl function being sufficient.[36] D-A compound **59c** showed very high SHG signal intensity (150 x urea)[27] whereas **59d**, **59e**, and **60** presented substantially lower signals. Of special interest is 1-(2-thienyl)-3-(4-tolyl)propene-1-one (**60**) which showed a SHG signal intensity of 15 x urea and had a high blue-light region transparency with a cut-off wavelength of 390 nm, whereas **59c** had a cut-off at 595 nm. Another interesting product is **61**. It showed a SHG signal intensity of 15 x urea and a cut-off at 412 nm.

Bredas and co-workers[47] studied several cross-conjugated chromophores having carbonyl group as a spacer **(Fig.1.33)**.

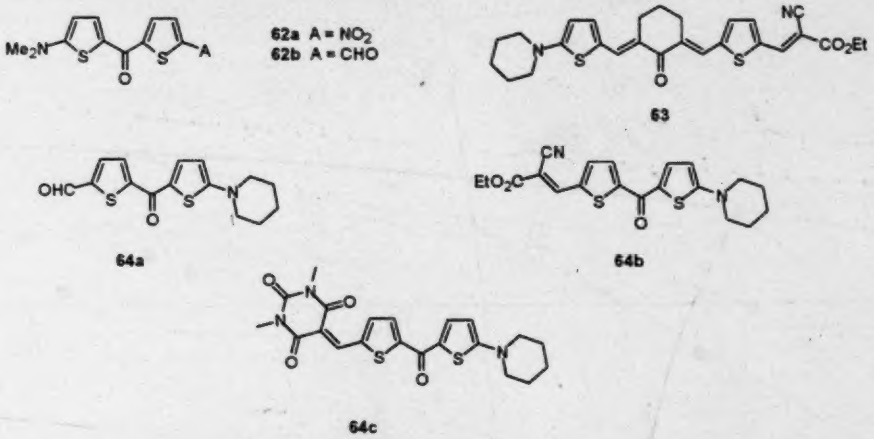

Fig. 1.33 Molecular structures of cross-conjugated compounds studied by Brédas.[47]

It was observed that all studied compounds showed positive solvatochromism (red-shift) when the polarity of the solvent was increased from cyclohexane to toluene and to DMSO. Comparison of **64a-c** spectra showed a red shift of λ_{max} with increasing of the acceptor strength. Also an increase of β was found when the strength of the acceptor was increased. Experimental calculation of β for **64b** (about 20 x PNA) and **63** (about 70 x PNA) confirmed an increase of the first hyperpolarizability with respect to an increased π-conjugated path length. Therefore, good electron delocalization (influenced by the strength of the acceptor) through the cross-conjugated center was observed.

Derivatives of tetraethynylethene (TEE) are an interesting class of conjugated molecules. Following the first preparation of the parent tetraethynylethene **TEE** in 1991,[48] synthetic routes to derivatives with any desired substitution and protection pattern have been performed by Diederich and coworkers (**Fig. 1. 34**).[49,24b]

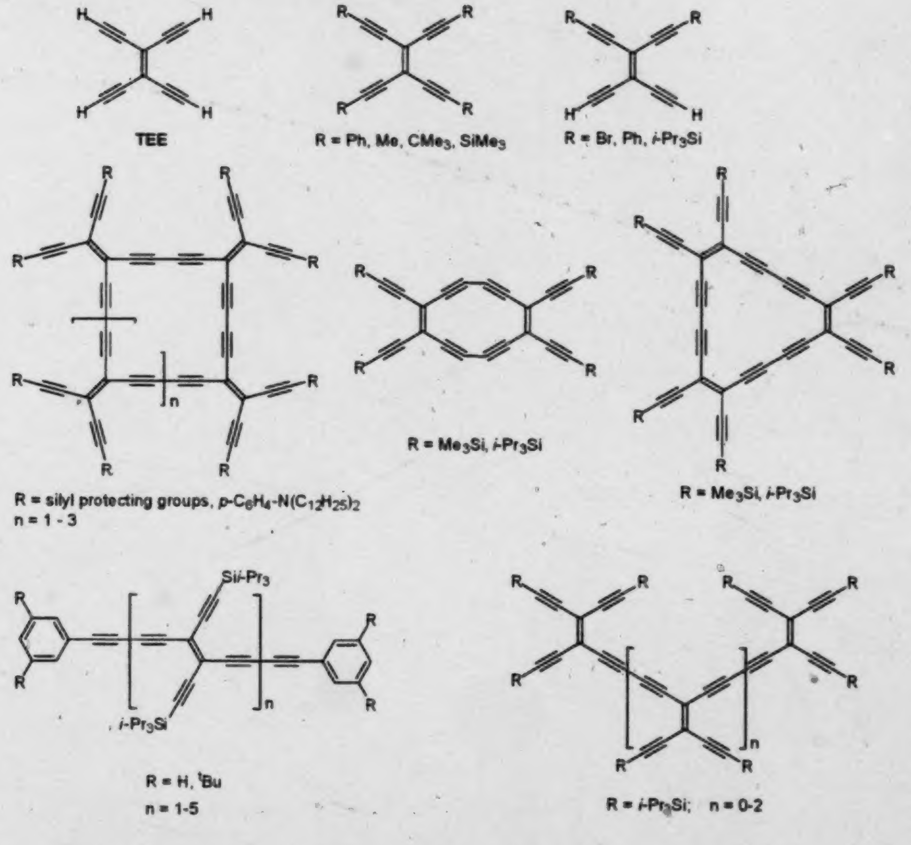
TEE
R = Ph, Me, CMe3, SiMe3
R = Br, Ph, i-Pr3Si
R = silyl protecting groups, p-C6H4-N(C12H25)2
n = 1 - 3
R = Me3Si, i-Pr3Si
R = Me3Si, i-Pr3Si
Si i-Pr3
i-Pr3Si
R = H, tBu
n = 1-5
R = i-Pr3Si; n = 0-2

Fig. 1.34 Chemical structures of some TEE derivatives studied by Diederich.[49]

To enhace the appeal of TEEs as materials for electronics and photonics, the synthesis of D and/or A-substituted derivatives was accomplished by

Diederich and co-workers[50,24b] By varying the attachment of *p*-donor, and *p*-acceptor substituted phenyl rings to the planar TEE chromophore, different D-A conjugation paths were generated (**Fig. 1.35**).

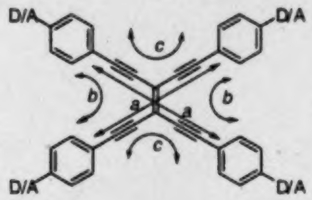

Fig. 1.35 Schematic representation of possible conjugation pathways in D-A substituted TEEs.

Trans- and *cis*-orientation of the substituents provided one-dimensional linear conjugation (paths *a* and *b*), geminal substitution afforded one-dimensional cross-conjugation (path *c*), and substitution at all four terminal alkynes gave full, two-dimensional D-A conjugation through a combination of four linear (*a* and *b*) and two cross-conjugated paths (*c*). The Sonogashira reaction was used for the cross-coupling of aryl or vinyl halides with terminal alkynes to afford D-A compounds.[51] Some of the bis- and tetrakis-arylated TEEs synthesized by Diederich and co-workers are shown in **Fig. 1.36**.

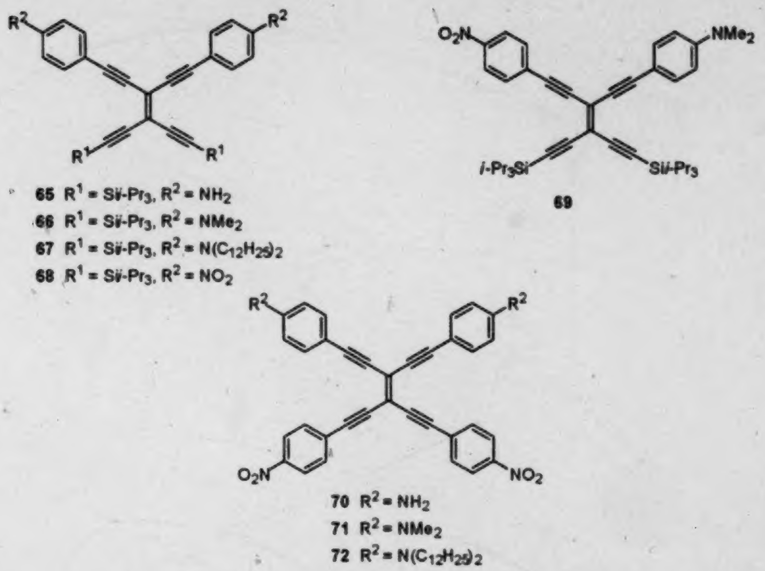

65 $R^1 = Si$-i-Pr_3, $R^2 = NH_2$
66 $R^1 = Si$-i-Pr_3, $R^2 = NMe_2$
67 $R^1 = Si$-i-Pr_3, $R^2 = N(C_{12}H_{25})_2$
68 $R^1 = Si$-i-Pr_3, $R^2 = NO_2$

69

70 $R^2 = NH_2$
71 $R^2 = NMe_2$
72 $R^2 = N(C_{12}H_{25})_2$

Fig. 1.36 Geminally bis-arylated TEEs **65-69**, and tetrakis-arylated TEEs **70-72** studied by Diederich.[50]

The differentially silyl-protected dibromide **73** was coupled with different donor and acceptors to give the bis-, tris- or tetrakis-arylated TEEs **74-81** **(Fig 1.37)**.

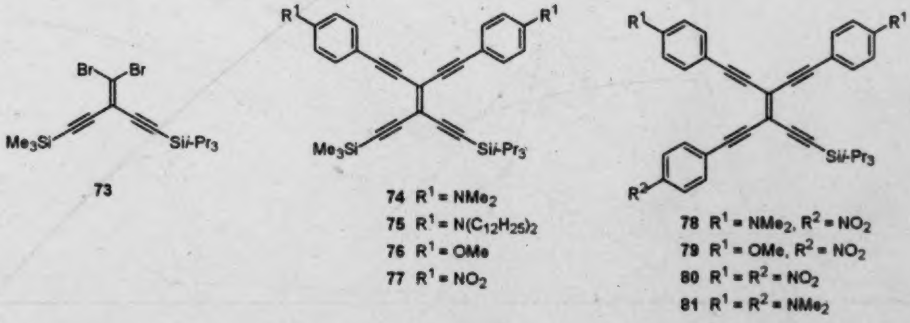

73

74 $R^1 = NMe_2$
75 $R^1 = N(C_{12}H_{25})_2$
76 $R^1 = OMe$
77 $R^1 = NO_2$

78 $R^1 = NMe_2$, $R^2 = NO_2$
79 $R^1 = OMe$, $R^2 = NO_2$
80 $R^1 = R^2 = NO_2$
81 $R^1 = R^2 = NMe_2$

Fig 1.37 Geminally bis-arylated **74-77** and tris-arylated **78-81** TEEs studied by Diederich.[50]

Many other mono-, bis-, and tetrakis- arylated TEEs were synthesized using the same Sonogashira cross-coupling techniques (**Fig. 1.38**).

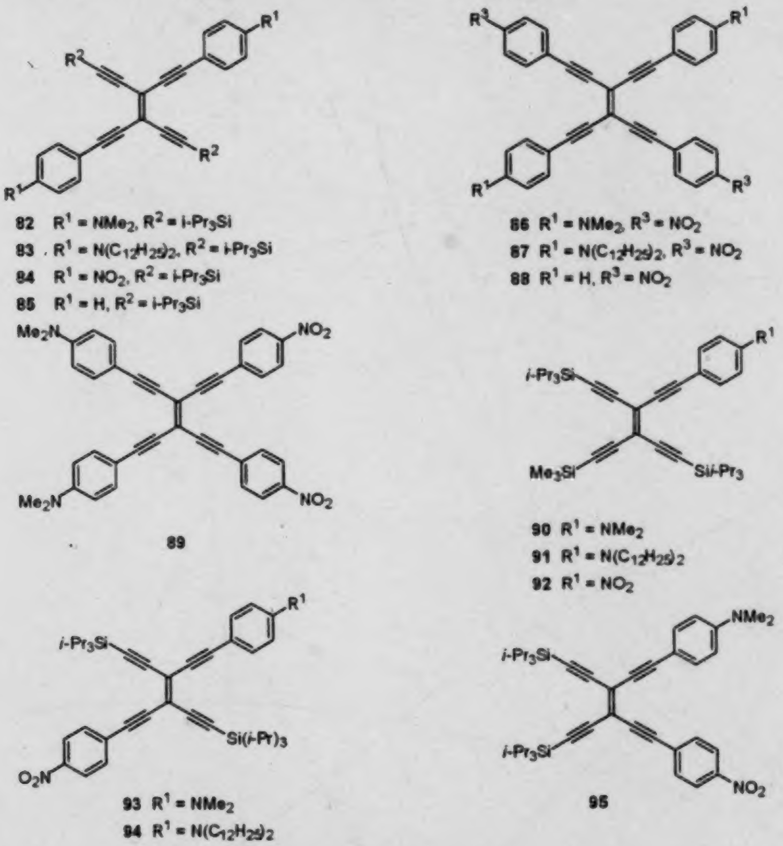
R1
R2
R2
R1
82 R1 = NMe2, R2 = i-Pr3Si
83 R1 = N(C12H25)2, R2 = i-Pr3Si
84 R1 = NO2, R2 = i-Pr3Si
85 R1 = H, R2 = i-Pr3Si
R3
R1
R1
R3
86 R1 = NMe2, R3 = NO2
87 R1 = N(C12H25)2, R3 = NO2
88 R1 = H, R3 = NO2
Me2N
NO2
Me2N
NO2
89
R1
i-Pr3Si
Me3Si
Si-i-Pr3
90 R1 = NMe2
91 R1 = N(C12H25)2
92 R1 = NO2
R1
i-Pr3Si
Si(i-Pr)3
O2N
93 R1 = NMe2
94 R1 = N(C12H25)2
NMe2
i-Pr3Si
i-Pr3Si
NO2
95

Fig. 1.38 Additional TEEs studied by Diederich.[50]

For a thorough investigation of the electronic effects, *trans*-enediynes **96** and 97, and dimers **98-101** were also synthesized (**Fig. 1.39**).

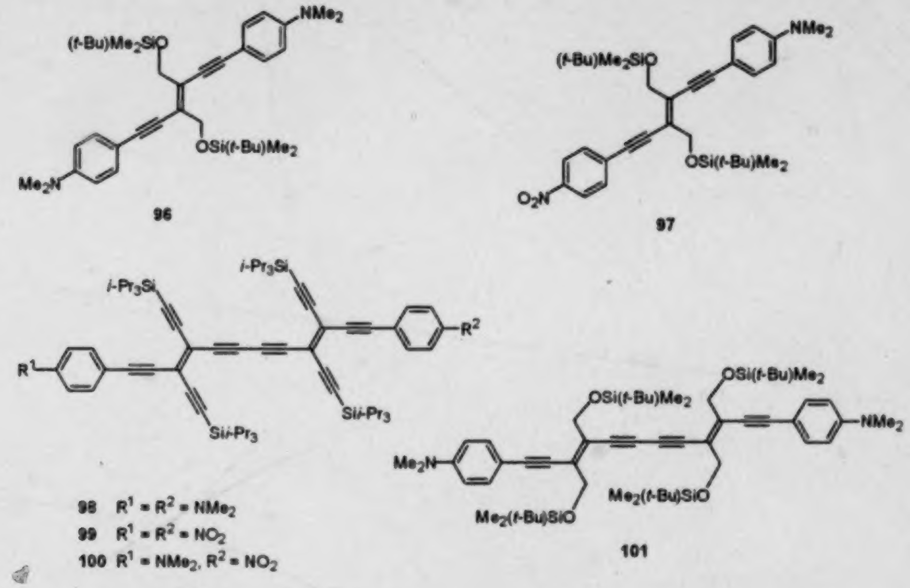

Fig. 1.39 Bis-arylated *trans*-enediynes **96-97** and dimers **98-101** studied by Diederich.[50]

The UV-Vis spectra of the arylated TEEs provided a great deal of information about their electronic structures. It was found that all D-A-substituted molecules exhibited broad absorption bands at lower energy (with end-absorption extending beyond 550 nm) than their donor- or acceptor-substituted corresponding molecules. Charge delocalization along linear conjugation paths in cis- (**95**, λ_{max} = 471 nm) and trans-D-A substituted molecules (**93**, λ_{max} = 468 nm) was more effective than along cross-conjugation paths in the corresponding geminally substituted derivatives (**69**, λ_{max} = 447 nm). The same observation was noted for donor- and acceptor-bis-substituted TEEs: **82** (λ_{max} = 459 nm) *vs.* **66** (λ_{max} = 428 nm) and **84** (λ_{max} = 403 nm) *vs.* **68** (λ_{max} = 388 nm), respectively. The N-substitution in the donor group strongly influenced the position of the intramolecular CT band, the strongest donor-substituted compound having bathochromic shifted absorption when compared to the other ones (λ_{max} **[72]** = 511 nm > λ_{max} **[71]** = 486 nm > λ_{max} **[70]** = 471 nm). Protonation of the $R_2NC_6H_4$ group in D-A TEEs resulted in the complete disappearance of the CT band The pendant $R_3Si\text{-}C\equiv C$ groups had a substantial participation in the overall π-electron delocalization. For example, λ_{max} of **101** was 70 nm higher in energy than λ_{max} of **98**. The bis-acceptor derivatives **68** and **84** had a nearly solvent independent spectra, whereas the bis-donor molecules **66** and **82** showed a slightly positive solvatochromism. It was also found that the tris-arylated derivatives **78** and **81** exhibited a much stronger solvatochromism than the bis-arylated counterparts; a comparison with the tetrakis-arylated derivatives was not done because of their limited solubility in apolar solvents.

The first and second hyperpolarizabilities for some of these compounds were measured with the EFISH[52] and THG (third-harmonic generation)[53] methods. A high β value was found for the *trans*-D-A-substituted **93**, almost twice the sum of β values for the D-substituted **90** and A-substituted **92**. Although a higher β value was calculated (using MOPAC software package) for the dimer **100**, a slightly twisted CT axis due to solvent-chromophore interactions made the measured β to be similar to that of monomer **93** ($400 \times 10^{-40} m^4/V$). A low β ($88 \times 10^{-40} m^4/V$) value was found for the cross-conjugated D-A TEE **69**, indicating a less efficient cross conjugation between donor and acceptor. The measured value for **95** (*cis* configuration), was about three times smaller then the one for **93** (*trans* configuration). A very high β value (almost 530 x $10^{-40}m^4/V$) was found for the tetrasubstituted TEE **71**, which shows two D-A linearly conjugation paths. THG experiments provided the second hyperpolarizability γ for the series of D and/or A-substituted 1,2-diethynylethenes (DEEs) and TEEs.[53] It was found that the chromophores with two-dimensionally conjugated TEE framework generally displayed increased γ values in comparison to one-dimensionally conjugated DEEs. A substantial increase in optical nonlinearities in both the DEEs and TEEs series was observed upon increasing the length of the conjugated framework. It was also observed that strong electron donor substituents such as *N,N*-dialkylamino groups led to larger γ than did electron acceptors, such as nitro groups, and that replacing mildly electron-donors (methoxy) with strongly ones (*N,N*-dialkylamino) afforded up to 6-fold increases in γ. The influence of *cis*-, *trans*-, and *gem*-(geminal) substitution for bis-functionalized TEE and DEE molecules was also studied: γ values decreased in the order *tran* > *cis* >> *gem*.

Tykwinski and co-workers synthesized the first series of *iso*-polydiacetylenes (*iso*-PDAs) **102-108** **(Fig. 1.40)**.[54,55]

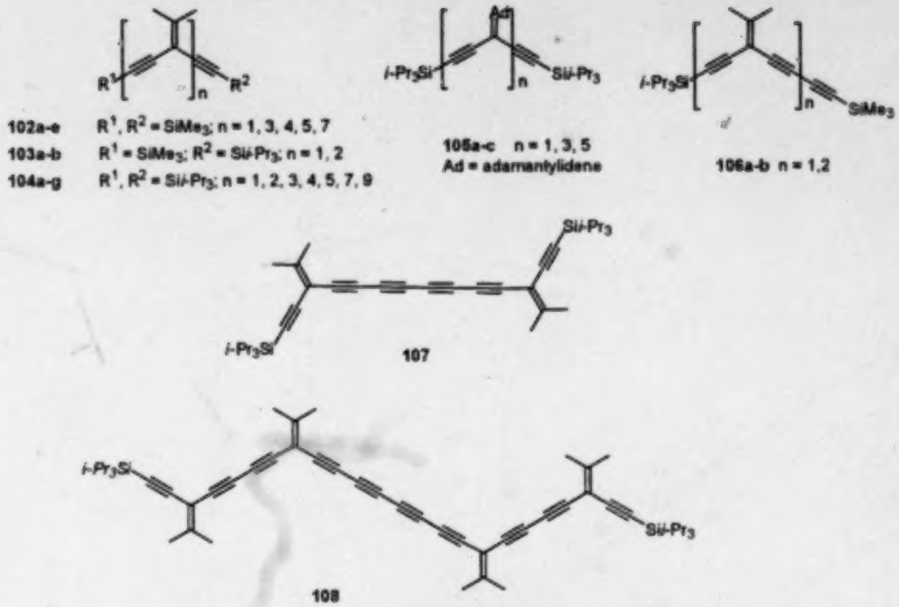
R1
R2
n
102a-e R1, R2 = SiMe3; n = 1, 3, 4, 5, 7
103a-b R1 = SiMe3; R2 = Si-i-Pr3; n = 1, 2
104a-g R1, R2 = Si-i-Pr3; n = 1, 2, 3, 4, 5, 7, 9
Ad
i-Pr3Si
Si-i-Pr3
105a-c n = 1, 3, 5
Ad = adamantylidene
SiMe3
106a-b n = 1,2
107
108

Fig. 1.40 The chemical structures of *iso*-PDA oligomers studied by Tykwinski.[54,55]

The investigation of electronic properties showed an increase in the molar absorption and bathochromic shift as the number of enyne monomer units increased for the series **104a-g**.[54] Therefore π-electron communication was present along the cross-conjugated framework. Pendant functionality change from isopropylidene to adamantylidene had only a small effect on the molar absorptivity and overall shape of the UV-Vis spectra. The lower energy cut-offs for the adamantlyidene trimer **105b** and pentamer **105c** are red-shifted by about 10 nm versus those of analogous isopropylidene derivatives **104c** and **104e**. A totally different result was obtained from the analysis of the UV-Vis spectra of **107** and **108**.[55] The longer conjugated path in **108** (*vs.*

107) did not produce a bathochromic shift. Therefore a minimal contribution from cross-conjugation was deduced from the spectra of these compounds.

Cross-conjugated NLO chromophores with large molecular nonlinearities and high thermal and chemical stabilities have been investigated for application in high speed electro-optic modulation and switching (**Fig. 1.41**). These chromophores were dopped into polyimides and tested by Kenney *et al.*[56]

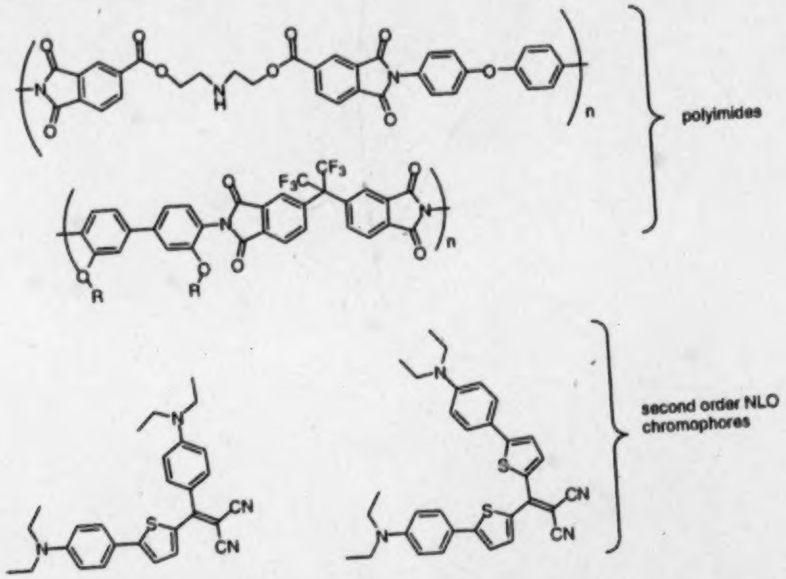

Fig. 1.41 Some high temperature polyimides and highly thermally stable chromophores for preparation of electro-optic polymers.

Cross-conjugated molecules consisting of an unsaturated center with a lone pair of electrons have also been investigated. These molecules showed high optical nonlinearities and a good transparency-nonlinearity trade-off (**Fig. 1.42**).[57]

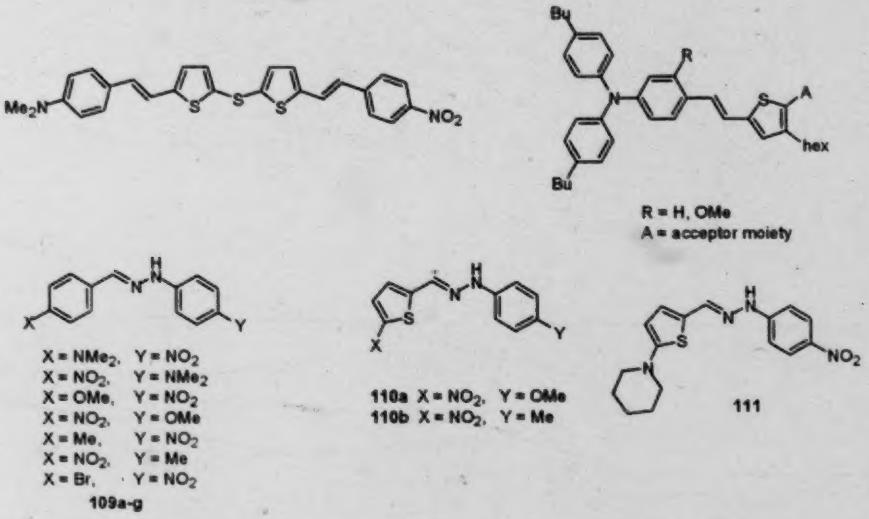
Me$_2$N
S
S
S
NO$_2$
Bu
R
N
S
A
hex
Bu
R = H, OMe
A = acceptor moiety
H
N
N
X
Y
X = NMe$_2$, Y = NO$_2$
X = NO$_2$, Y = NMe$_2$
X = OMe, Y = NO$_2$
X = NO$_2$, Y = OMe
X = Me, Y = NO$_2$
X = NO$_2$, Y = Me
X = Br, Y = NO$_2$
109a-g
H
N
N
S
X
Y
110a X = NO$_2$, Y = OMe
110b X = NO$_2$, Y = Me
H
N
N
S
N
NO$_2$
111

Fig. 1.42 N- and S-cross-conjugated D-A oligomers.[57]

The highest β values were measured by EFISH for **109a** (200 x 10^{-40} m^4/V), **110a** (220 x 10^{-40} m^4/V) and **111** (220 x 10^{-40} m^4/V). SHG measurements for **109 – 111** showed high efficiency, from a few times to two orders of magnitude larger than that of urea.

2. Research Goals

Our interest in constructing cross-conjugated oligomers arises from curiosity about their unique and quite unexplored mode of π-electron delocalization. According to previous studies on cross-conjugated *iso*-polydiacetylenes (*iso*-PDAs), reduced π-electron communication along the polymer framework has been observed relative to the analogous linearly conjugated materials. As discussed in this introduction, donor and acceptor-substituted oligomers have been found to have large first hyperpolarizabilities and may have application to optical devices, such as frequency doublers and electrooptical modulators. In order to understand structure-property relationships, as well as develop materials with novel electronic and optical properties, we focused our investigation of cross-conjugated systems toward end-capping the *iso*-PDA structure with donor and acceptor groups (**Fig. 1.43**).

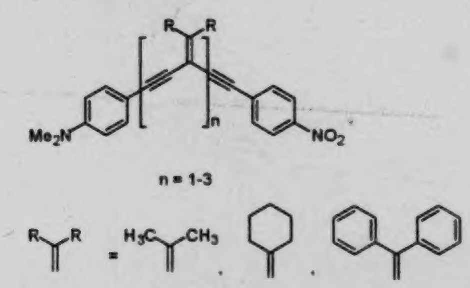

Fig. 1.43 Proposed cross-conjugated oligomers.

p-Nitrobenzene and *p*-*N*,*N*-dimethylaniline groups were chosen as the acceptor and donor, respectively. The Sonogashira coupling reaction was used to attach the donor and acceptor groups to the oligomers. The oligomers were characterized via ^{1}H and ^{13}C NMR and IR spectroscopy, HRMS spectrometry and differential scanning calorimetry (DSC). Their electronic absorption spectra were investigated in order to understand their π-electronic properties.

II. RESULTS AND DISCUSSION

A. Isopropylidene Series

1. Monomer Synthesis

Synthesis of the desired series of cross-conjugated *iso*-PDA chromophores began from isobutyryl chloride **112** (**Scheme 2.1**). Reaction of bis(trimethylsilyl)acetylene with the acyl halide **112** under Friedel-Crafts conditions gave the ketone **113**, which was then reacted with triflic anhydride in the presence of a base.[58] Both 2,6-lutidine and 2,6-di-*t*-butyl-4-methylpyridine were considered for the triflation reaction. Experimentally, it was found that the more hindered base gave a higher yield for this reaction (70% compared with 50% for lutidine). The product, 1-(trimethylsilylethynyl)-2-dimethyl-vinyl triflate **114**, was coupled with triisopropylsilylacetylene to give the differentially protected starting material **115** as the basis for the series of chromophores (**Scheme 2.1**).[54a]

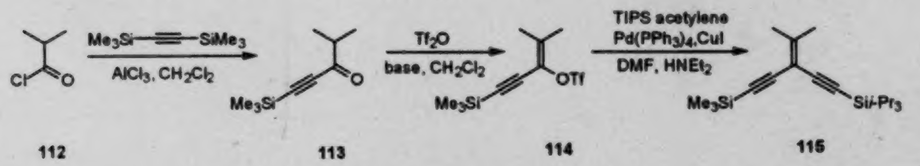
Me3Si—≡—SiMe3
AlCl3, CH2Cl2
Tf2O
base, CH2Cl2
TIPS acetylene
Pd(PPh3)4,CuI
DMF, HNEt2
Cl
O
Me3Si
O
Me3Si
OTf
Me3Si
Si*i*-Pr3
112
113
114
115

Scheme 2.1 The synthetic route to the starting material **115**.

Protodesilylation of **115** with K_2CO_3 in wet MeOH/THF (5:1) effected removal of the trimethylsilyl (TMS) moiety, while leaving the more robust triisopropylsilyl (TIPS) protecting group intact (**Eq. 2.1**). This monodesilylated derivative was carried on directly, following work-up, to a Pd-catalyzed cross-coupling reaction with *p*-iodo-*N*,*N*-dimethylaniline[59] to afford the donor-substituted monomer **116** in 63% yield as a yellow solid.

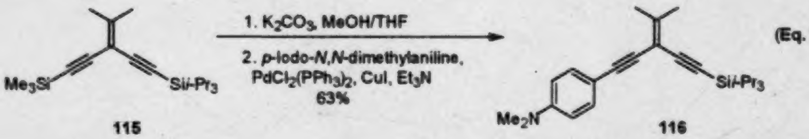
Me$_3$Si
Si*i*-Pr$_3$
1. K$_2$CO$_3$, MeOH/THF
2. *p*-iodo-*N*,*N*-dimethylaniline, PdCl$_2$(PPh$_3$)$_2$, CuI, Et$_3$N
63%
Me$_2$N
Si*i*-Pr$_3$

115 **116** (Eq. 2.1)

The resulting low yield was due in part to the formation of the homocoupled byproduct (~16% yield) as well as purification difficulties resulting from the fact that both the final product and *p*-iodo-*N*,*N*-dimethylaniline have similar retention factors. Purification on a silica gel column gave only one sixth of the pure product expected, the rest coming together with *p*-iodo-*N*,*N*-dimethylaniline. Therefore a silica gel-H column was tried. The smaller size of the particles was expected to give a better packing of the column, decreasing the diffusion. Although most of the product could be isolated pure *via* this technique, product contamination with *p*-iodo-*N*,*N*-dimethylaniline remained problematic.

Confirmation of the structure of monomer **116** is based on analysis of the spectroscopic data. The ^{1}H NMR spectrum shows a singlet at δ 1.09 (triisopropylsilyl group). The four methyl groups appear as three singlets; the peaks at δ 2.059 and δ 2.063 assigned to dimethylvinylidene group and the other singlet at δ 2.95 assigned to dimethylaniline group. For simplicity, the coupling constants of the aryl protons for the *p*-*N*,*N*-dimethylaminophenyl moiety have been reported as pseudo first-order, even though they are second-order spin systems. The two aromatic protons closer to the acetylene group are deshielded and show up at δ 7.31 (d, J = 9.0 Hz, 2H). The other two are shielded and their signal appears at δ 6.61 (d, J = 9.0 Hz, 2H). The ^{13}C NMR spectrum supports this assignment. The deshielded aromatic carbon atoms, α and γ to the N atom, appear at δ 150 and δ 132.5, respectively. The shielded carbon atoms appear upfield at δ 111.9 (β to N) and δ 110.7. For olefins, it is known that alkyl substituents increase δ of the adjacent carbon atom and decrease δ of the other carbon in the vinyl compounds; acetylene substituents have an opposite effect.[60] In monomer **116**, the synergetic effect of the two ethynyl bonds and the two geminal methyl groups polarizes the vinylidene bond. Therefore the signal of the =$\underline{C}Me_2$ carbon can be seen at δ 152.8. The other sp^2 carbon and the acetylene carbon atoms have signals between δ 84 and δ 105. The TIPS group gives two signals, at δ 11.4 and δ 18.7. The alkylidene methyl groups give signals at δ 22.8 and δ 22.7. The two methyl groups from the donor moiety give one signal at δ 40.3. The IR spectrum shows the triple bonds (2202 and 2150 cm^{-1}) and the aromatic ring/double bonds (1607 and 1520 cm^{-1}). The mass spectrum confirms the assigned structure.

The X-Ray crystallographic data shows two different crystallographic structures for monomer **116**. Although the dimethylaniline group is in conjugation with the acetylene group adjacent to it, in the ground state it can still rotate around the intervening single bond. The best conjugation would occur when the aromatic ring is in the same plane with C(3), C(6), C(7) and C(8) or perpendicular to it, **(Fig 2.1)**. The structural data indicates that one solid state conformer has a dihedral angle between the aromatic ring and the plane composed of C(3), C(6), C(7) and C(8) of 71.56°, conformation A, **(Fig 2.1)** whereas the other one has a dihedral angle of 10.5°, conformation B (**Fig. 2.2**). The bulky TIPS group has also a slightly different orientation.

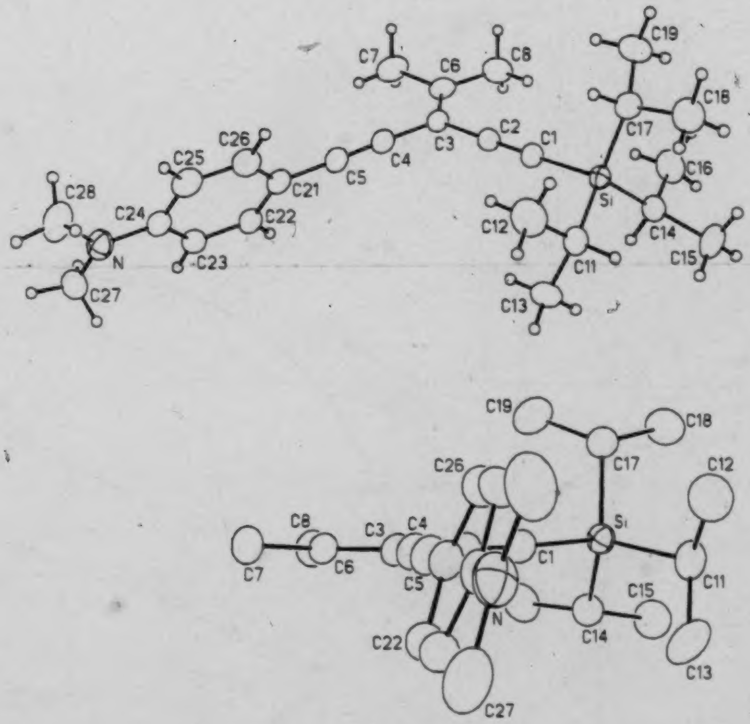
C7
C6
C8
C19
C18
C17
C26
C3
C2
C1
C25
C4
C21
C5
C16
C28
C24
Si
C22
C12
C14
N
C23
C11
C15
C27
C13
C19
C18
C26
C17
C12
C8
C4
C3
Si
C1
C7
C6
C5
C11
C15
N
C22
C14
C13
C27

Fig. 2.1 ORTEP drawing (20% probability level) of **116**, conformation A. Selected bond lengths (Å) and angles (°): N-C(24) 1.367(4), C(21)-C(5) 1.433(4), C(5)-C(4) 1.193(4), C(4)-C(3) 1.442(4), C(3)-C(6) 1.335(4), C(2)-C(1) 1.200(3); C(24)-N-C(27) 120.6(3), C(26)-C(21)-C(5) 122.8(3), C(2)-C(3)-C(4) 114.6(3), Si-C(1)-C(2) 177.6(3), C(1)-Si-C(14) 106.96(13).

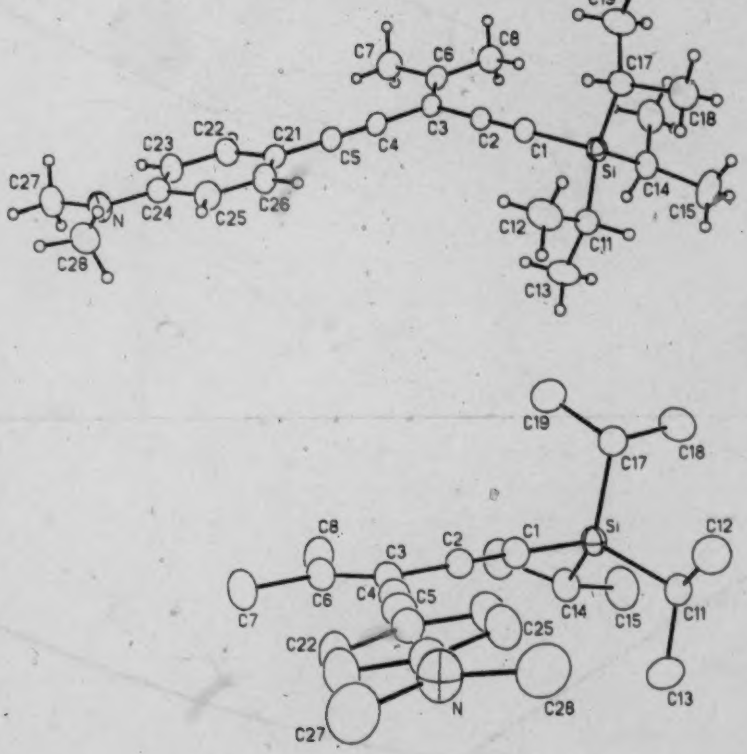
C19
C7
C6
C8
C17
C22
C21
C23
C3
C18
C4
C2
C5
C1
Si
C27
C24
C26
C14
N
C25
C12
C15
C11
C28
C13
C19
C18
C17
C8
C1
Si
C12
C3
C2
C4
C5
C6
C7
C14
C15
C11
C25
C22
N
C28
C13
C27

Fig. 2.2 ORTEP drawing (20% probability level) of **116**, conformation B. Selected bond lengths (Å) and angles (°): N-C(24) 1.370(4), C(21)-C(5) 1.434(4), C(5)-C(4) 1.182(4), C(4)-C(3) 1.444(4), C(3)-C(6) 1.339(4), C(2)-C(1) 1.200(3); C(24)-N-C(27) 121.5(3), C(26)-C(21)-C(5) 121.5(3), C(2)-C(3)-C(4) 116.5(3), Si-C(1)-C(2) 175.7(3), C(1)-Si-C(14) 106.04(13).

It is known that *i*-Pr$_3$Si is a weakly donating group whereas dimethylaniline group is a strong donor.[37] A stronger donor could result in the elongation of a conjugated acetylenic bond and shortening of a single bond. This is not confirmed for **116** by the X-ray data. The triple bond on the TIPS branch is 1.200 Å, just a little longer than the triple bond on the dimethylaniline branch, which is 1.193 Å for conformer A, and 1.182 Å for conformer B. These differences, however, are not considered significant.

An analogous sequence of protodesilylation and cross-coupling of deprotected **115** with *p*-iodonitrobenzene gave acceptor-substituted monomer **117** in 82% yield **(Eq. 2.2)**.

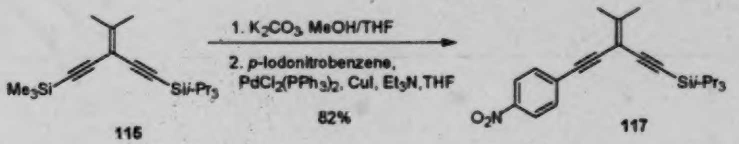

(Eq. 2.2)

Although some homocoupling product was again observed (16% yield), the yield for this coupling was higher than the previous one because the product was more easily purified from the reaction mixture. Characterization of monomer **117** rests on analysis of its spectra.

The ^{1}H NMR spectrum confirms the presence of a TIPS group (δ 1.1), one isopropylidene group (δ 2.10 and δ 2.11) and four aromatic protons. These aromatic protons are deshielded by the presence of the strongly electron withdrawing NO$_2$ group. Therefore, they show up at δ 7.54 and δ 8.16 as two doublets. Because the structure of **117** is similar to that of **116**, their ^{13}C NMR spectra are quite similar. The only significant differences are the absence of the resonance of dimethylamino methyl groups near 40 ppm and the deshielded aromatic carbon attached to the acetylene bond in **117**. This is expected because the nitro group shifts this carbon resonance to 130.6 ppm. The dimethylamino group from monomer **116** shifts it upfield to 110.7 ppm. Also, the sp^2 carbon atom attached to the geminal methyl groups is deshielded as a result of the linear conjugation induced by the nitro group, and it resonates at 157 ppm, *versus* 152.8 ppm in the electron rich **116**. The IR spectrum shows the presence of triple (2206 and 2148 cm^{-1}) and double/aromatic bonds (1592 and 1520 cm^{-1}) as well as of NO_2 group (1343 cm^{-1}). The high resolution mass spectrum shows a molecular ion peak at *m/z* 381, the molecular mass of **117**. The base peak is present at *m/z* 338, assigned to fragment $[M - i\text{-}Pr]^+$.

Empirically, the more *s* character a hybrid orbital has, the stronger are the bonds it forms. The nitrogen is hybridized sp^3 (25% *s* character) in amines and sp^2 (33.3% *s*) in nitro compounds (**Fig. 2.3**). Therefore a C-N bond should be stronger in the nitro derivatives when compared with amines.

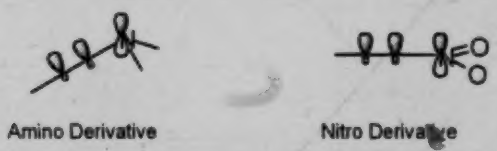

Fig. 2.3 Interaction between the nonbonding p orbital of a nitrogen atom and a sp^2 hybrid orbital.

The crystallographic data of **116** and **117** do not confirm this assumption. The bond between N atom and the aromatic ring is longer by 0.1 Å in **117** than in **116**. Therefore, we deduced that the degree of overlapping and the linear conjugation decreases in **117** *vs.* **116**. Shorter ethenyl bonds (C(3)–C(4): 1.339 and 1.335 Å) are found in **116** than in **117** (C(3)–C(4): 1.362 Å), suggesting a better electron delocalization in **116** (**Fig. 2.4**).

The dihedral angle between the planes of nitro group and benzene ring is 20.3°. Therefore, the aromatic ring is twisted from the plan of conjugation. The dihedral angle between C(3), C(4), C(5), C(6) and the ring is 10.44°, similar to that as found in one of the conformers of **116**. Although **117** has a donor-acceptor structure, TIPS being a weak donor, there is little apparent difference between the degree of conjugation in **116** and **117**. The triple bonds are about the same length: 1.211 Å (1.200 Å in **116**) on the TIPS branch and 1.196 Å (1.193 Å in structure A and 1.182 Å in structure B of **116**) on the other branch.

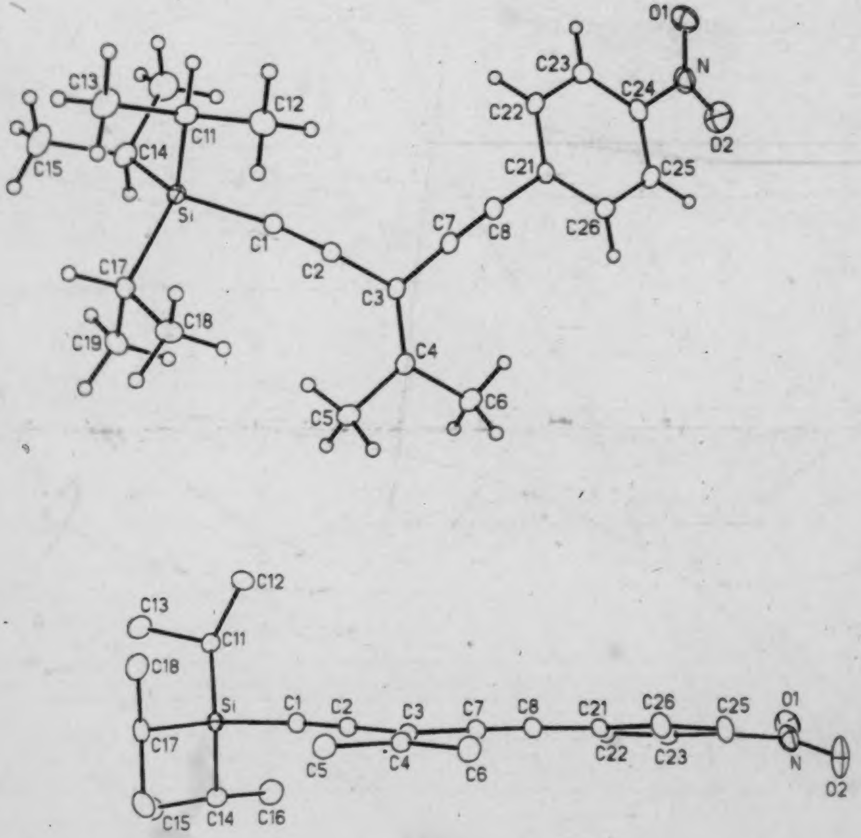
O1
N
O2
C23
C24
C22
C21
C25
C26
C7
C8
C13
C11
C12
C14
C15
Si
C1
C2
C3
C17
C18
C19
C4
C5
C6
C12
C13
C11
C18
Si
C1
C2
C3
C7
C8
C21
C26
C25
O1
C17
C4
C5
C6
C22
C23
N
O2
C15
C14
C16

Fig. 2.4 ORTEP drawing (20% probability level) of **117**. Selected bond lengths (Å) and angles (°): N-C(24) 1.471(3), C(21)-C(8) 1.439(2), C(8)-C(7) 1.196(2), C(7)-C(3) 1.439(2), C(3)-C(4) 1.362(2), C(2)-C(1) 1.211(2); C(24)-N-O(1) 118.0(2), C(26)-C(21)-C(8) 120.14(16), C(2)-C(3)-C(7) 117.80(14), Si-C(1)-C(2) 171.88(14), C(1)-Si-C(14) 107.30(8).

As the precursor to D-A monomer **118a**, we chose to use donor-substituted **116** with the expectation that the cross-coupling of **116** with electron-deficient *p*-iodonitrobenzene would be easier than the coupling of **117** with *p*-iodo-*N,N*-dimethylaniline. Thus, treating a THF solution of **116** with a slight excess of tetrabutylammonium fluoride (TBAF) effected removal of the TIPS moiety, and cross-coupling with *p*-iodonitrobenzene provided D-A-substituted monomer **118a** as an orange solid in 70% yield and the homocoupling byproduct **118b** in 10% yield (**Eq. 2.3**).

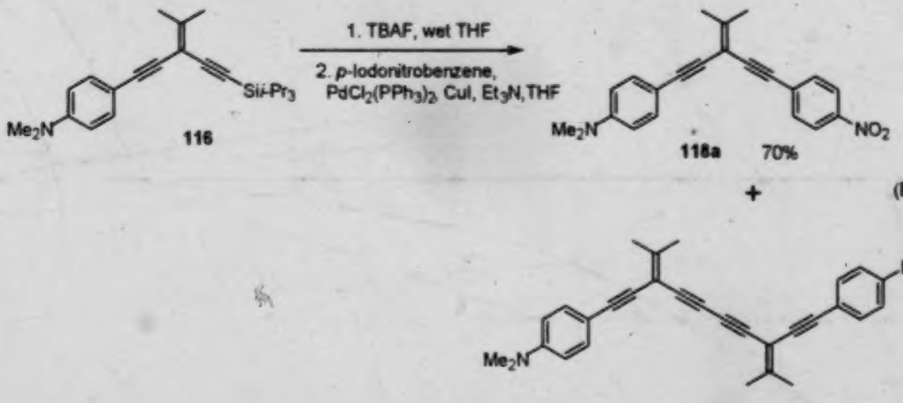

116

118a 70%

118b 10%

(**Eq. 2.3**)

The modest yield was due again to purification difficulties and synthesis of the homocoupling byproduct. Even after silica gel-H flash chromatography some product remained contaminated with 4-iodo-*N,N*-dimethylaniline.

Characterization of monomer **118a** was done based on comparison of its spectra with the spectra of monomers **116** and **117**. The NMR and IR spectra of **118a** look like a combination of spectra of **116** and **117**. As previously observed, the sp^2 carbon atom bound to the two geminal methyl groups resonates at 152.8 ppm in **116** and at 157 ppm in **117**. When both donor and acceptor groups are attached, an intermediate resonance is observed at 154.9 ppm. The structural assignment of **118a** is supported by HRMS analysis, which shows a molecular ion base peak at *m/z* 344, giving the molecular formula of **118a**: $C_{22}H_{20}N_2O_2$.

Characterization of homocoupling product **118b** was based on analysis of its spectra to the spectra of starting material **116**. The ^{1}H NMR spectrum shows, as expected, two doublets for the aromatic protons at 7.32 and 6.61 ppm, one singlet at 2.95 ppm for two dimethylamino, and two singlets at 2.09 and 2.08 ppm for the isopropylidene groups. Comparing the ^{13}C NMR spectrum of **118b** with that of **116**, one can easily see their resemblance, **118b** being a symmetrical molecule. The IR spectrum shows the presence of double and triple bonds in the molecule at 2202 and 2133 cm^{-1}, and 1609 and 1585 cm^{-1} respectively. The mass spectrum shows a molecular ion peak at *m/z* 444 corresponding to molecular mass of **118b**.

Comparing the UV-Vis spectra of **116**, **117**, and **118a**, one can see that the UV-Vis absorption of **118a** is extended more towards lower energy, suggesting a cross-conjugation interaction between the donor and the acceptor (**Fig. 2.5**). As a result of donor-acceptor substitution, monomer **118a** is clearly a more highly colored orange solid in comparison to donor (**116**) and acceptor (**117**) monomers, which are yellow solids. In the absence of cross-conjugated D–A interactions across the alkylidene spacer, one expects the spectrum of **118a** to merely be a composite of its parts, *i.e.* **116** and **117**. The difference between the more colored **118a**, versus **116** and **117**, is found in the lower energy region of the spectrum that extends out beyond 450 nm for **118a**. The UV-Vis characteristics of **116**, **117** and **118a** are similar to those observed for tetraethynylethene derivatives with cross-conjugated D/A substitution.[50b] Their behavior, however, dramatically contrasts that of similar linearly conjugated chromophores, which show significant bathochromic shifts upon D-A substitution.[3d-e,53]

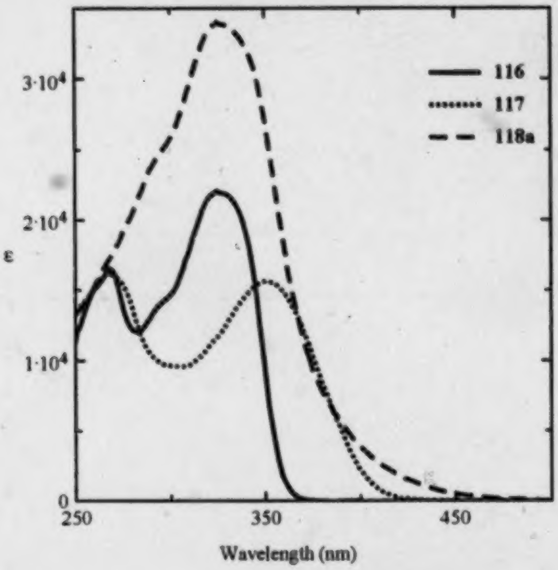

Fig. 2.5 UV-Vis absorption spectra of monomers **116**, **117** and **118a**.

2. Dimer Synthesis

The assembly of longer D/A oligomers began with the common building block **115**. Following desilylation of **115** with K_2CO_3, cross-coupling with vinyl triflate **114** utilizing $Pd(PPh_3)_4$/CuI and Et_2NH in DMF gave *iso*-PDA dimer **119** (**Eq. 2.4**).[54a]

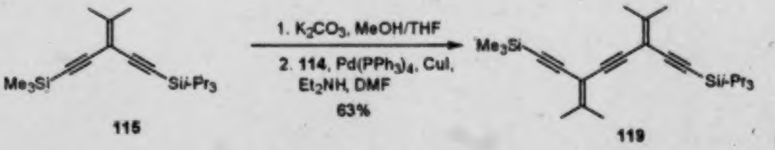
Me3Si
Si*i*-Pr3
115
1. K2CO3, MeOH/THF
2. 114, Pd(PPh3)4, CuI, Et2NH, DMF
63%
Me3Si
Si*i*-Pr3
119

(Eq. 2.4)

The ^{1}H NMR spectrum for **119** shows the methyl signals of the two isopropylidene groups centered at 2 ppm and those of the TMS (0.17 ppm) and TIPS (1.07 ppm) groups. Because of electron delocalization, the isopropylidene sp^2 carbon signals can be found downfield at δ 154.4 and δ 153.7 in the ^{13}C NMR spectrum. All the others sp^2 and sp^3 carbons have resonance frequencies between δ 88 and δ 104. The four isopropylidene methyl carbons can be found at δ 22.5 and δ 22.7. The TIPS group gives two signals, one at δ 11.3 and the other at δ 18.6, as found in the previous structures. The TMS group gives one signal at δ 0.5, as expected. The presence of ethenyl and ethynyl functionality is confirmed *via* analysis of IR spectrum. A strong absorption at 2149 cm^{-1} is an indication of ethynyl groups presence in the molecule. The ethenyl stretching vibration should be a weak peak at 1690-1650 cm^{-1} that is often absent (as it is in this case).[61] The TMS group gives a strong vibration at 842 cm^{-1} and a medium one at 1249 cm^{-1}. The confirmation of the assigned structure is also provided by MS analysis, which shows a molecular ion base peak at *m/z* 410.

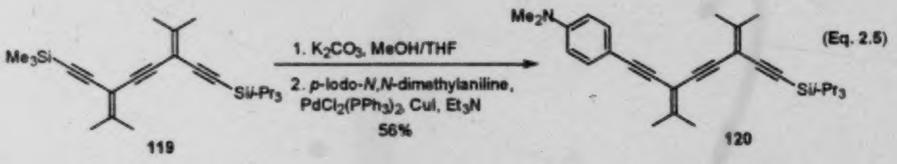

Selective removal of the TMS moiety of **119**, followed by cross-coupling of the relatively unstable intermediate with *p*-iodo-*N,N*-dimethylaniline gave **120** in 56% yield **(eq. 2.5)**

The low yield was due to the formation of the homocoupled byproduct present in 32% yield. As well, a portion of the product could not be recovered from the reaction mixture because of similar retention factors of **120** and *p*-iodo-*N,N*-dimethylaniline.

Characterization of dimer **120** was based on analysis of its spectra relative to the spectra of monomer **116** and starting materials. The NMR spectra of dimer **120** are similar to those of the monomer **116**. The presence of four resonances centered at 2 ppm in the ^{1}H NMR spectrum and four resonances at 22.6-22.8 ppm in the ^{13}C NMR spectra suggest the presence of the isopropylidene methyls. Four resonances at 153.6, 151.5, 102.3 and 102.0 ppm show the presence of two deshielded and two shielded sp^2 carbons of the olefins. Two additional resonances at 88 – 89 ppm confirms the presence of an additional triple bond in **120** relative to **116**. The IR spectra of **120** and **116** are also very similar, due to analogous functionality. The mass spectrum also supports the structure assignment with the expected signal at *m/z* 457.

Selective removal of the TMS moiety of **119**, followed by cross-coupling of the relatively unstable intermediate with *p*-iodonitrobenzene gave **121** (**Eq. 2.6**).

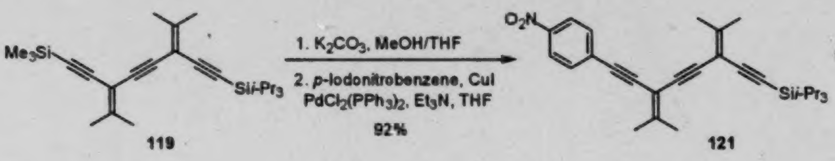

(Eq. 2.6)

Characterization of dimer **121** was based on analysis of its spectra in comparison to the spectra of monomer **117** and the starting materials. The ^{1}H NMR spectrum shows, as expected, two doublets for the aromatic protons at 8.16 and 7.54 ppm, four singlets centered at 2 ppm for four isopropylidene methyl groups, and a singlet at 1.07 ppm for the TIPS moiety. Comparing the ^{13}C NMR spectrum of **121** with that of **119**, one can see the presence of aromatic carbons at 132.0 ppm (*ortho* to NO$_2$), 123.6 ppm (*meta* to NO$_2$), 146.8 ppm (*para* to NO$_2$) and 130.6 ppm (adjacent to NO$_2$). The IR spectrum is similar to that of monomer **117**. The mass spectrum shows a molecular ion peak at *m/z* 459 corresponding to molecular mass of **121**. One prominent peak at $[M-43]^+$ is indicative of the loss of a TIPS group in the molecule, 43 being the mass value for *i*-Pr.

Removal of the TIPS group from **120** with TBAF provided the terminal alkyne that was then coupled with *p*-iodonitrobenzene to give the D-A dimer **122** as an orange solid in 76% yield (**Eq. 2.7**). Some homocoupling product was also produced in the reaction.

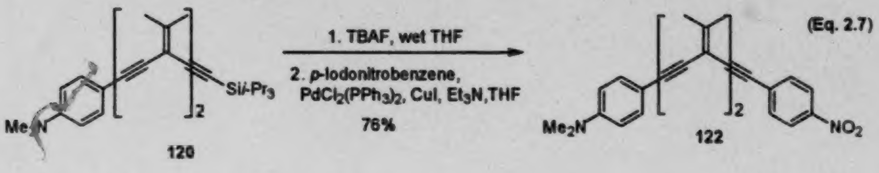

Having the spectroscopic assignments for the dimers **120** and **121** in hand, the assignments for **122** were easily performed. The aromatic proton resonances are seen at 8.16 ppm and 7.57 ppm (for the acceptor group), 7.32 ppm and 6.61 ppm (for the donor group). Two amino methyl groups, deshielded by the presence of an electronegative atom, are found at 2.95 ppm. The protons of the other four methyl groups resonate near 2 ppm. The ^{13}C NMR spectrum shows features of the spectra of dimers **120** and **121**. The IR spectrum shows the presence of triple bonds (2202 cm^{-1}), double bonds (1608 cm^{-1}) and a nitro group (1342 cm^{-1}) in the molecule. The molecular ion base peak at *m/z* 422 in the mass spectrum, corresponding to the molecular mass of **122**, indicates that the structure assignment is correct.

The UV-Vis spectra of dimers **120**, **121** and **122** do not show any observable influence from the incorporation of donor and acceptor groups to the enyne framework (**Fig. 2.6**). The absorption band of **122** looks like a combination of those of **120** and **121**. Therefore, there are no observable effects from cross-conjugation in the D-A dimer **122**, as determined by UV-Vis spectroscopy.

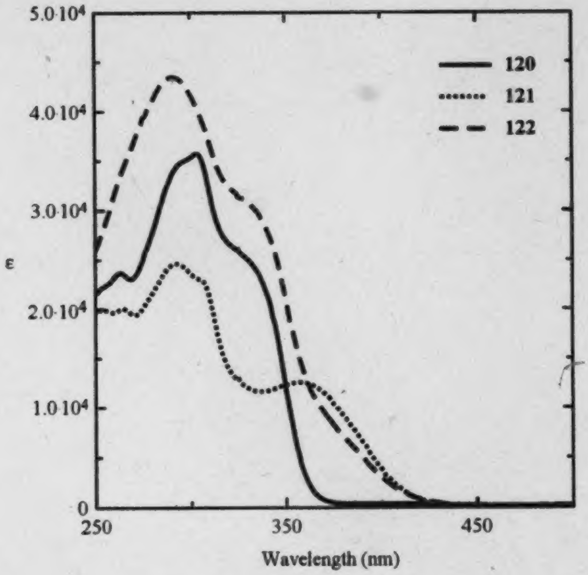

Fig. 2.6 UV-Vis absorption spectra of dimers **120-122**.

3. Trimer Synthesis

To complete this series of cross-conjugated chromophores, dimer **119** was selectively protiodesilylated and cross-coupled with vinyl triflate **114** to give the trimer **123** in 52% yield (**Eq. 2.8**).

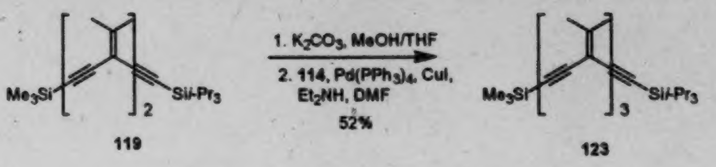

(Eq. 2.8)

As one can see, synthesis of both dimer **119** and trimer **123** has low yields. The reason is that some other secondary products were noticed in the reaction mixture. Because these byproducts were not recovered pure, it is hard to say what they are. Our guess is that the starting material decomposed during the reaction. Nonetheless, characterization of trimer **123** was based on analysis of its spectra and relative to the spectra of dimer **119**. The ^{1}H NMR spectrum shows three groups of resonances. The protons from the isopropylidene methyl groups resonate near 2 ppm as these groups are attached to sp^2 carbons. The two types of protons of the TIPS group are centered at 1 ppm. The TMS protons resonate at 0.17 ppm, as expected. The ^{13}C NMR spectrum also supports the structural assignment. Resonances from three deshielded sp^2 carbons are seen at 151-154 ppm, whereas the resonances from the three shielded sp^2 carbons are observed at 101-103 ppm. Eight sp carbon signals are seen in the range of 87-102 ppm. The six sp^3 carbons of the isopropylidene groups can be found in two groups, at 22.5 and 22.7 ppm. The TIPS group gives two signals, at 11.3 and 18.6 ppm, as found in the previous structures. The TMS group gives one signal at 0 ppm as expected. The presence of the respective functional groups for **123** is confirmed by analysis of the IR spectrum: triple bonds at 2148 cm^{-1}, double bonds at 1602 cm^{-1} and Si-C bonds at 1248 and 840 cm^{-1}. The mass spectrum shows a molecular ion base peak at *m/z* 488, corresponding to the molecular mass of **123**.

Donor-substituted trimer **124** was synthesized by desilylation of **123** followed by coupling with *p*-iodo-*N*,*N*-dimethylaniline (**Eq. 2.9**).

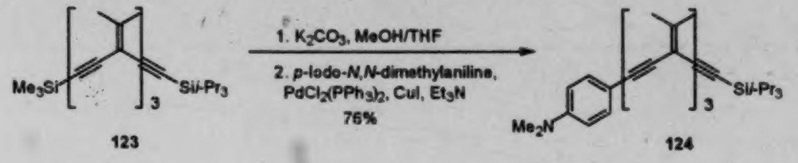
Me3Si
Si*i*-Pr3
3
123
1. K2CO3, MeOH/THF
2. *p*-Iodo-*N*,*N*-dimethylaniline,
PdCl2(PPh3)2, CuI, Et3N
76%
Me2N
Si*i*-Pr3
3
124

(Eq. 2.9)

The ^{1}H NMR spectrum of **124** is similar to the spectrum of dimer **120**, except that there are six additional isopropylidene protons resonating near 2 ppm. Also, the ^{13}C NMR spectrum reflects the additional sp, sp^2 and sp^3 carbons relative to the spectrum of **120**. The functional groups can also be confirmed in the IR spectrum: triple bonds at 2145 and 2196 cm^{-1} and double bonds/aromatic ring at 1609 and 1520 cm^{-1}. The molecular ion peak at *m/z* 535 confirms the molecular mass of **124**.

Desilylation of **123** followed by coupling of the terminal alkyne with *p*-iodonitrobenzene gave the acceptor-substituted trimer **125** in 84% yield. (**Eq. 2.10**)

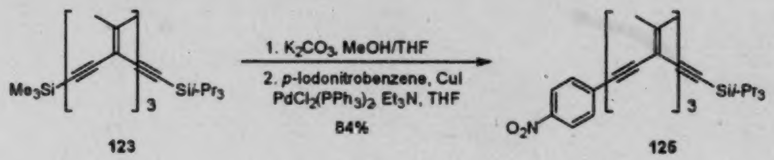
Me3Si
Si*i*-Pr3
3
123
1. K2CO3, MeOH/THF
2. *p*-Iodonitrobenzene, CuI
PdCl2(PPh3)2, Et3N, THF
84%
O2N
Si*i*-Pr3
3
125

(Eq. 2.10)

The ^{1}H and ^{13}C NMR spectra of compound **125** are similar to those of dimer **121**, with the exception that the trimer **125** has one additional triple bond and isopropylidene group, as confirmed by comparison of the spectra. The IR spectrum supports the presence of triple bonds at 2206 and 2145 cm^{-1} and double bonds/aromatic ring vibrations at 1592 and 1519 cm^{-1}. In addition, the NO_2 group gives absorption at 1342 cm^{-1}. The molecular ion peak at *m/z* 537 in the mass spectrum corresponds to the molecular mass of **125**. The base peak at *m/z* 494 is consistent with the fragment for [M - *i*-Pr]$^+$.

The last compound in this series of cross-conjugated chromophores is the donor-acceptor trimer **126**, which was synthesized by desilylation of donor **124** and cross-coupling of the terminal alkyne with *p*-iodonitrobenzene (**Eq. 2.11**).

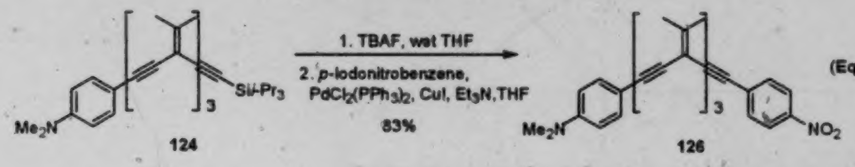

(Eq. 2.11)

Characterization of trimer **126** was accomplished by analysis of its spectra and with respect to the spectra of analogous D-A compounds **118** and **122**. The ^{1}H NMR spectrum shows the resonances of the isopropylidene methyl protons centered at 2 ppm and the *N*-methyl protons at 2.9 ppm. The aromatic protons appear as two sets of doublets and they resonate at the same chemical shift as in compounds **124** and **125**. The ^{13}C NMR spectrum shows five deshielded carbon atoms. Three of these result from the olefinic carbons bound to geminal methyl groups, the olefinic carbon closer to the acceptor moiety having a resonance at 155.7 ppm, similar to **125**. The same observation is made for the olefinic carbon nearer the donor moiety: it has almost the same chemical shift (151.7 ppm) as in **124** (151.5 ppm). The third olefinic carbon, equally distanced from the D and A groups, has an intermediate chemical shift of 152.9 ppm, which is close to its chemical shift in the D-substituted trimer **124** (152.4 ppm). The other two deshielded carbon atoms are aromatic, and they have chemical shifts similar to those as found for **124** and **125**: 150.0 ppm for the carbon bearing the dimethylamino group and 146.8 ppm for the carbon bearing the nitro group. Eight acetylenic carbon atoms resonate at 92 – 84 ppm. All the isopropylidene methyl and amino-methyl carbons resonate at 22 and 40 ppm, respectively. The functional groups of **126** can be seen in the IR spectrum: ethynyl bonds absorbing at 2201 cm^{-1}, double bonds/aromatic ring at 1611 and 1521 cm^{-1}and the nitro group at 1344 cm^{-1}. The mass spectrum shows a molecular ion base peak at *m/z* 500, which corresponds to the molecular mass of **126**, supporting the structure assignment.

As observed for dimers **120 – 122,** the UV-Vis spectra of trimers **124, 125** and **126,** do not show any observable influence from the incorporation of donor and acceptor groups to the enyne framework (**Fig. 2.7**). The spectrum of **126** is essentially a composite of the constituent parts, acceptor **124** and donor **125**.

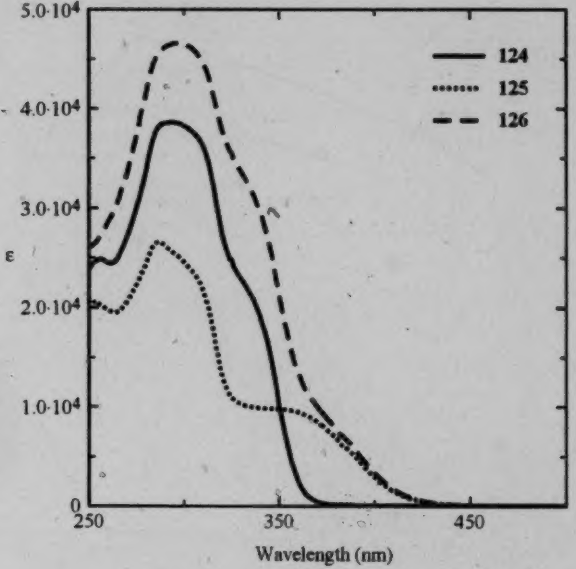

Fig. 2.7 UV-Vis absorption spectra of trimers **124 – 126**.

In summary of the electronic characteristics of the isopropylidene series of D-A *iso*-PDAs, we can say that the most obvious electronic changes are observed within the series of monomers **116 – 118a**. In the absence of cross-conjugated D–A interactions across the alkylidene spacer, one expects the spectrum of a D–A-substituted oligomer to merely be a composite of its parts, *i.e.* the D-substituted and A-substituted-oligomer. This is true for the dimer and trimer, but not for the monomer series. The change in the spectrum of **118a**, versus **116** and **117**, is found in the lower energy region, which extends out beyond 450 nm for **118a (Figure 2.5)**. The end absorption energies for all derivatives **120 - 122** and **124 - 126** are virtually identical at ca. 420 nm. The major change in the electronic absorption spectra for dimer and trimer series (**120 - 122** and **124 - 126**, respectively) is the additional bands observed at ca. 300 nm that result from the linearly conjugated ene-yne-ene segment present in each of these chromophores. For dimers **120 - 122**, two absorption bands are clearly evident corresponding to the cisoid and transoid orientation of the olefins about the central carbon-carbon triple bond. In the case of the trimer series, the increased number of rotameric conformations ultimately results in broadening of these two bands into one observable absorption.

B. Cyclohexylidene Series

Because the monomer series (**116-118**) gave the most significant electronic results, series of similar monomers, each having different pendant substitution (cyclohexylidene and diphenylvinylidene), were synthesized. Coupling of vinyl triflate **127**[62] with triisopropylsilyl acetylene afforded the diprotected monomer **128** in a good yield, (**Eq.**

2.12), and the product was easily purified by flash chromatography. A secondary product was obtained and was identified by ^{1}H NMR as being the homocoupled product of triisopropylsilyl acetylene, bis(triisopropylsilyl) butadiyne.

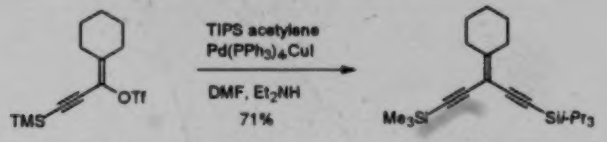

127 **128**

(Eq. 2.12)

Identification of compound **128** was based on its spectroscopic characteristics. The ^{1}H NMR spectrum confirms the presence of the TIPS and TMS moieties, with signals at 1.07 and 0.17 ppm. The cyclohexyl protons are found in two groups centered at 2.48 and 1.56 ppm, with four protons at 2.48 ppm deshielded due to their proximity to the double bond. The ^{13}C NMR spectrum shows resonances for all the carbon atoms from the molecule. As seen in the previous structures, one sp^2 carbon signal is shifted downfield as a result of the two cyclohexylidene and alkyne groups, appearing at 162.4 ppm. The sp^3 carbon atoms of the cyclohexylidene ring are not chemical shift equivalent and their electron environment is influenced by the non-equivalent alkynyl units. The IR spectrum confirms the functional groups present in the molecule. The carbon-carbon triple and double bonds are absorbing at 2150 and 1463 cm^{-1}, respectively. The Si-Me bonds give two absorbtion: one at 1249 cm^{-1}, and the other one at 843 cm^{-1}. The mass spectrum shows a molecular ion peak at *m/z* 372, corresponding to the molecular mass of **128**. The base peak is present at *m/z* 329, as a result of [M - *i*-Pr]$^+$.

Desilylation of **128** with K_2CO_3 in THF and MeOH followed by coupling of the terminal, unstable, alkyne with *p*-iodo-*N*,*N*-dimethylaniline gave the donor-substituted monomer **129**. (**Eq. 2.13**) The product was easily purified by flash chromatography. Some homocoupling of the terminal acetylene also occurred, accounting for the relatively low yield obtained (63%).

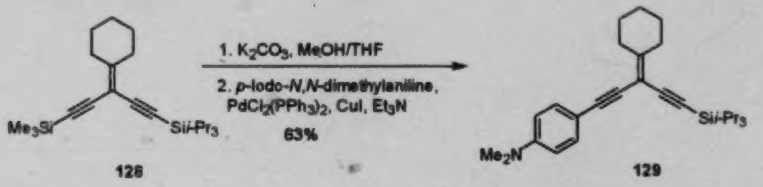

(Eq. 2.13)

Confirmation of the structure of donor-substituted monomer **129** was based on analysis of the spectroscopic data and comparison to previous donor-substituted oligomers. The ^1H NMR spectrum shows the aromatic protons as two doublets at 7.3 and 6.61 ppm, the *ortho* protons being shielded by the electron-donating effect of the NMe_2 substitution. The electronegative N atom deshields the two *N*-methyl groups and they are seen at 2.95 ppm. The protons of the cyclohexylidene and TIPS groups have the same chemical shift as found in the starting material. The ^{13}C NMR spectrum shows two deshielded sp^2 carbons: 159.7 ppm for the olefinic carbon bearing the two sp^3 carbons and 150 ppm for the aryl carbon next to N. A comparison of the chemical shift of C(11) (**Fig. 2.8**) of **129** (159.7 ppm) with that of C6 (**Fig. 2.1**) in **116** (152.8 ppm) shows a rather large dependence of this chemical shift as a result of the alkylidene substituents. The *N*-methyl group carbons resonate at 40.3 ppm. The IR spectrum confirms the presence of acetylenic bonds (2198 and 2143 cm^{-1}) and double bonds/aromatic ring (1609 and 1520 cm^{-1}). A base molecular ion peak at *m/z* 419 confirms that **129** has $C_{28}H_{41}NSi$ formula. The X-Ray structural analysis shows that the structure of **129** is very close to the structure of **116**, conformer A: the bond lengths are quite similar (**Fig. 2.8**), and the dihedral angle between the backbone and the aryl ring is 67.65°, close to 71.56° as found in **116**. The bond angle C(12)-C(11)-C(16) is 115.2°. The deviation from the standard 120° suggests a small tendency toward sp^3 hybridization due to electron delocalization. All the other C-C-C bond angles in the ring are between 110.3° and 111.8°.

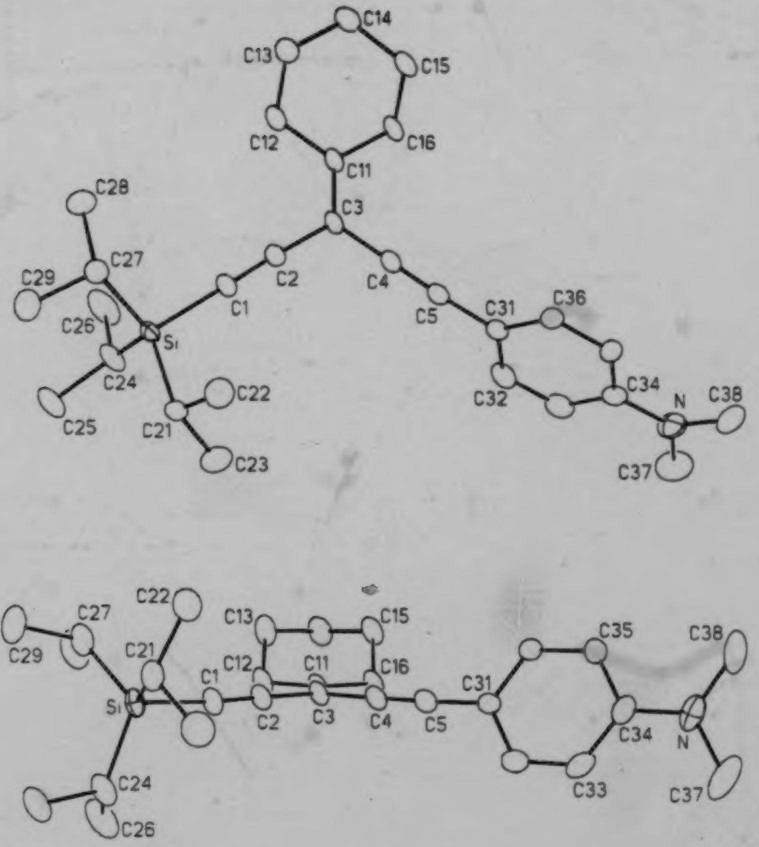
C14
C13
C15
C12
C16
C11
C28
C3
C27
C29
C2
C4
C1
C36
C26
Si
C5
C31
C24
C22
C34
N
C38
C32
C25
C21
C23
C37
C22
C27
C13
C15
C29
C21
C35
C38
C12
C11
C16
C1
C31
Si
C2
C3
C4
C5
C34
N
C24
C33
C37
C26

Fig. 2.8 ORTEP drawing (20% probability level) of **129**. Selected bond lengths (Å) and angles (°): N-C(34) 1.371(4), C(31)-C(5) 1.440(4), C(5)-C(4) 1.194(4), C(4)-C(3) 1.439(4), C(3)-C(11) 1.359(3), C(2)-C(1) 1.203(3); C(34)-N-C(37) 120.9(3), C(36)-C(31)-C(5) 121.7(3), C(2)-C(3)-C(4) 115.6(3), C(12)-C(11)-C(16) 115.2(2), Si-C(1)-C(2) 176.4(3), C(1)-Si-C(24) 107.15(13).

TIPS removal from **129** with TBAF provided the terminal alkyne that was then coupled with *p*-iodonitrobenzene to give the D-A monomer **130** in a good yield as a red solid.

(Eq. 2.14)

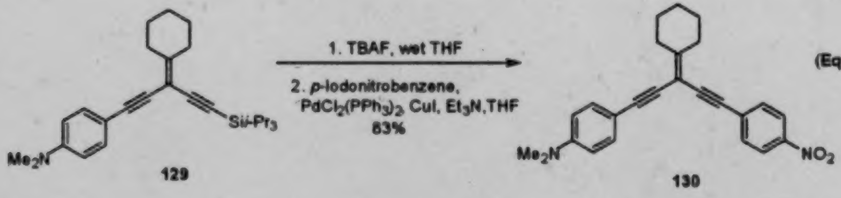

(Eq. 2.14)

The structural assignment of this donor-acceptor-substituted monomer was easily made by comparing its spectra with those of the starting material. The ^{1}H NMR spectrum shows the aromatic protons of *p*-disubstituted aryl groups as two sets of doublets. Those from the acceptor moiety are deshielded and resonate at 8.15 and 7.58 ppm. All the other resonances are similar to those of the starting material, compound **129**. The carbon resonances from the nitrobenzene moiety can be seen in the ^{13}C NMR spectrum. Two signals for the two identical C-H carbons are present at 132.1 and 123.5 ppm. The aromatic carbon bound to NO_2 is very deshielded, resonating at 146.7 ppm. The aryl carbon bound to acetylene is slightly deshielded, and it resonates at 130.7 ppm. The IR spectrum shows the functional groups present in the molecule: triple bonds (2197 cm^{-1}), double bond/benzene (1607 cm^{-1}and 1518 cm^{-1}), NO_2 group (1341 cm^{-1}). The mass spectrum shows a molecular ion base peak at *m/z* 384 giving the molecular formula of **130**: $C_{25}H_{24}O_2N_2$.

A comparison of the UV spectra of **129** and **130** shows that a bathochromic shift occurred by addition of the acceptor moiety to the donor-substituted monomer **129**. Analysis of the spectrum of D-A-substituted compound **130** shows that it extends out beyond 450 nm, whereas the spectrum of **129** is limited to less than 400 nm (**Fig. 2.9**). In the absence of the acceptor-substituted monomer, it is hard to make an affirmation about this red shift. Because the absorption spectrum of **130** extends nearly 100 nm to lower energy than that of **129**, this could be taken as a possible indication of a cross-conjugated D-A interaction.

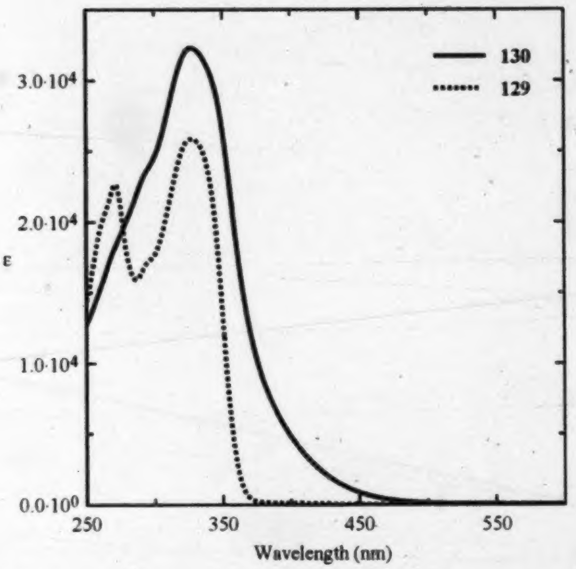

Fig. 2.9 UV-Vis absorption spectra of monomers **129** and **130**.

C. Diphenyl Series

The synthesis of the final series of monomers was intended to start from the differentially protected monomer **132**. Synthetic attempts toward triflate **131**, with TMS substitution, were not satisfactory because of the very long reaction time (4 days) and low yield (less than 10 %) when lutidine or/and DMAP were used. A slightly better yield (35%) was obtained when 2,6-di-*t*-butyl-4-methylpyridine and DMAP were used. Although this synthesis has been reported in the literature to proceed in reasonable yields (64%),[58] in our hands it was frustratingly unreliable **(Scheme 2.2)**. Cross-coupling of triflate **131** with TIPS acetylene afforded monomer **132** in 72% yield.

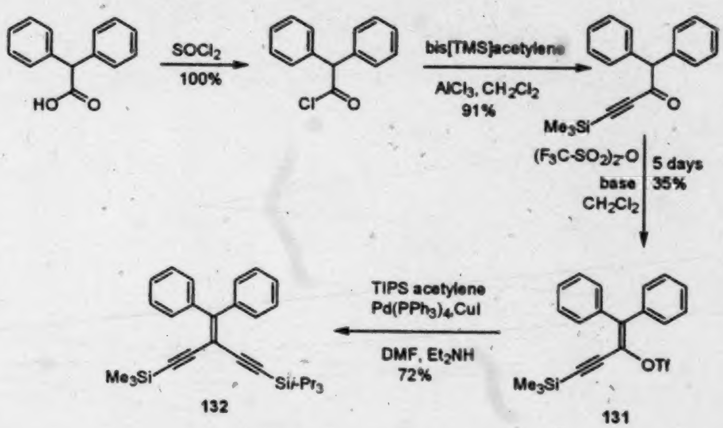
SOCl$_2$
100%
HO
O
Cl
O
bis[TMS]acetylene
AlCl$_3$, CH$_2$Cl$_2$
91%
Me$_3$Si
O
(F$_3$C-SO$_2$)$_2$-O
base
CH$_2$Cl$_2$
5 days
35%
TIPS acetylene
Pd(PPh$_3$)$_4$CuI
DMF, Et$_2$NH
72%
Me$_3$Si
Sii-Pr$_3$
132
Me$_3$Si
OTf
131

Scheme 2.2 Synthetic route toward the TMS protected starting material.[58]

As a result of a very low overall yield for synthesis of **132**, compound **135**, the TES-substituted analogue of **132**, was considered. Ketone **133**, obtained from the appropriate acyl chloride and bis(triethylsilyl)acetylene, was transformed into the 1-(triethylsilylethynyl)-vinyl triflate **134** during 2 days, in 47% yield, using 2,6-di-*t*-butyl-4-methylpyridine as the base.[58] Cross-coupling of **134** with triisopropylsilyl acetylene[54a] gave the diprotected monomer **135** as a possible basis of this series **(Scheme 2.3)**.

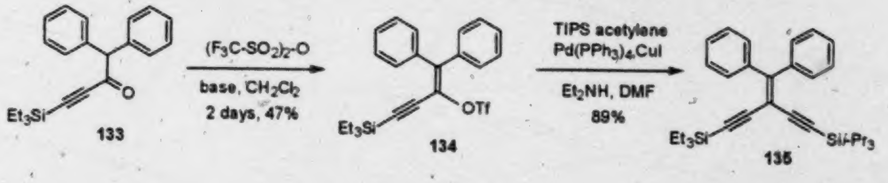
Et$_3$Si
O
133
(F$_3$C-SO$_2$)$_2$-O
base, CH$_2$Cl$_2$
2 days, 47%
Et$_3$Si
OTf
134
TIPS acetylene
Pd(PPh$_3$)$_4$CuI
Et$_2$NH, DMF
89%
Et$_3$Si
Sii-Pr$_3$
135

Scheme 2.3 The synthetic route toward the diprotected monomer **135**.

Protiodesilylation of **135** with K_2CO_3 in wet MeOH/THF (5:1) effected removal of the triethylsilyl (TES) moiety while leaving the more robust triisopropylsilyl protecting group intact (**Eq. 2.15**). This monodesilylated derivative was carried on directly, following work-up, to a Pd-catalyzed cross-coupling reaction with *p*-iodo-*N*,*N*-dimethylaniline. The product could not be purified by column chromatography, however, because it eluted together with *p*-iodo-*N*,*N*-dimethylaniline from the column. Therefore, an alternative approach was designed.

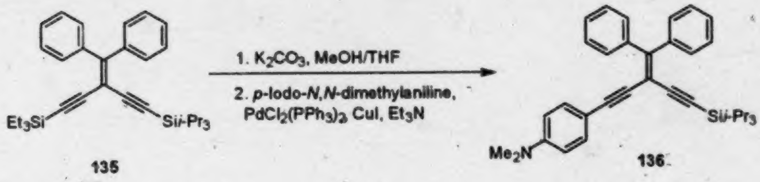
Et3Si
Si*i*-Pr3
135
1. K2CO3, MeOH/THF
2. *p*-Iodo-*N*,*N*-dimethylaniline,
PdCl2(PPh3)2, CuI, Et3N
Me2N
Si*i*-Pr3
136

(Eq. 2.15)

p-Disubstituted benzene **137**[63] was desilylated with K_2CO_3 in wet MeOH/THF (1:1) and the terminal alkyne was cross-coupled with vinyl triflate **134** to give the donor-substituted monomer **138** in a low yield (45%) (**Eq. 2.16**). Three other byproducts were observed based on TLC analysis, which accounts for the low yield, although they were not isolated.

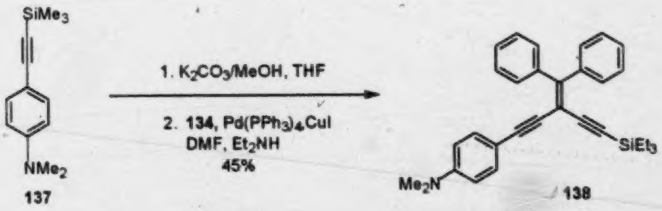
SiMe3
NMe2
137
1. K2CO3/MeOH, THF
2. 134, Pd(PPh3)4,CuI
DMF, Et2NH
45%
Me2N
SiEt3
138

(Eq. 2.16)

The structure of the donor-substituted monomer **138** was confirmed by analysis of its spectroscopic characteristics. The ^{1}H NMR spectrum shows two multiplets for the two vinylidene phenyl groups. The four protons adjacent to the double bond are somewhat deshielded, and they resonate at 7.48 ppm. The other six protons appear as a multiplet centered at 7.3 ppm. The aromatic protons from the donor moiety are shown as two doublets, at the same frequency as observed for analoguous donor-substituted compounds. The electronegative nitrogen atom deshields the two *N*-methyl groups, giving a singlet at 2.95 ppm. The three ethyl groups give a triplet and a quartet at 0.92 and 0.55 ppm, respectively. The ^{13}C NMR spectrum also supports the structural assignment. The eight unique carbons of the two pendant phenyl groups are observed in the range of 128–141 ppm. The carbon atoms bound directly to the olefin are deshielded, and they appear as two signals at 140.5 and 140.6 ppm. The carbon atoms in the *ortho* position appear as two singlets at 127 ppm, the two in the *para* position are observed as two singlets at 128 ppm. The remaining carbons (*meta*) resonate as two singlets at 130 ppm. The ethyl carbons are present upfield at 7.4 ppm (methylene) and 4.3 ppm (methyl). As seen before, the chemical shift of C(6) (**Fig. 2.1**) in **116** and C(11) (**Fig. 2.8**) in **129** are 152.8 and 159.7 ppm, respectively. The same olefinic carbon has a chemical shift of 154.4 ppm in **138**. Therefore, the methyl and the phenyl groups have similar deshielding effects in vinyl compounds. This conclusion is in agreement with data published by Pretsch *et al.*[61] All the other carbons have the same resonance frequency as the previous donor-substituted compounds. The functional groups present in **138** can be confirmed by the IR spectrum. The triple bonds absorb at 2187 and 2148 cm^{-1}. The double bonds of the aromatic rings show one strong absorption at 1608 cm^{-1} and a medium one at 1519 cm^{-1}. The mass spectrum also supports this structural assignment, with a molecular ion base peak at *m/z* 461, the molecular mass of **138**.

The acceptor-substituted monomer **139** was synthesized starting from the TMS and TIPS diprotected monomer **132**, which was available from our investigations toward optimizing the procedure for vinyl triflate **131**. Desilylation of **132** with K_2CO_3 in THF and MeOH followed by coupling of the terminal, unstable alkyne with *p*-iodonitrobenzene gave the acceptor-substituted monomer **139** in 73% yield. **(eq. 2.17)**

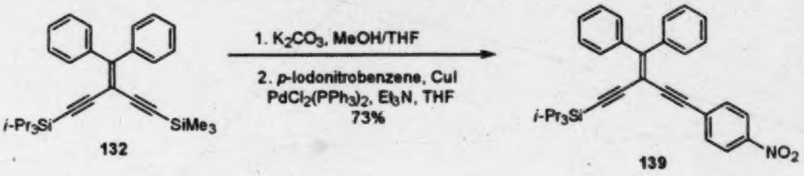

(Eq. 2.17)

The assignment of the acceptor-substituted monomer **139** was done by analysis and comparison of its spectral data with those of **138** and other acceptor-substituted compounds. Because of the multitude of aromatic protons in the molecule, only the two most deshielded protons (*ortho* to the NO_2 group) from the acceptor moiety can be clearly seen in the ^1H NMR spectrum. The remaining aryl protons have similar chemical shifts and give a multiplet in the range of 7.5-7.3 ppm. This multiplet is actually made from two multiplets, one of them showing the four protons from the phenyl groups closer to the double bond. The other multiplet is made from eight proton resonances: six from the phenyl groups and two from the acceptor moiety. The ^{13}C NMR spectrum is similar to the spectrum of the donor-substituted monomer **138**. A comparison of the chemical shift of the vinylidene carbon in **117** (157.2 ppm) and **139** (158.2 ppm) gives the same conclusion as for the donor-substituted monomers: methyl and phenyl groups have similar deshielding effects on olefinic carbons. The IR spectrum shows two weak absorptions for the acetylenic bonds at 2194 and 2147 cm^{-1}, and two medium intensity absorptions for the aromatic rings at 1593 and 1519 cm^{-1}. The nitro group shows a very strong absorption at 1341 cm^{-1}. A molecular ion base peak at *m/z* 505 in the mass spectrum confirms that the monomer **139** has the molecular formula: $C_{33}H_{35}NO_2Si$, and a strong peak at *m/z* 462 is also seen for the [M - i-Pr]$^+$ fragment.

The donor-acceptor-substituted monomer **140** was synthesized in a good yield by desilylation of **138** with TBAF and cross-coupling of the terminal alkyne with *p*-iodonitrobenzene (**Eq. 2.18**).

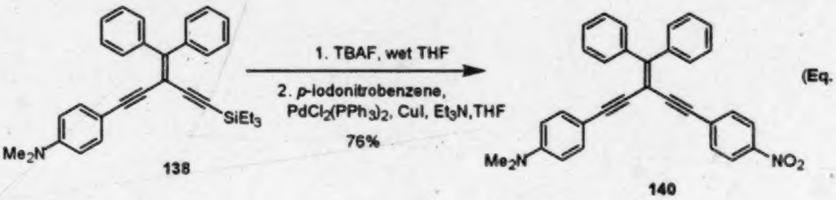

(Eq. 2.18)

The low field sectors of the ^{1}H NMR and ^{13}C NMR spectra for **140** look like a combination of the spectra of **138** and **139**. The chemical shift for the vinylidene carbon in **140** (156 ppm) is basically similar to that of **139** (158.2 ppm). Therefore, not much change is seen by incorporation of the donor group. The IR spectrum shows a broad, medium intensity signal at 2184 cm^{-1} (acetylenic bonds), two strong signals at 1607 and 1516 cm^{-1} (aromatic rings), and a very strong signal at 1340 cm^{-1} (nitro group). The mass spectrum of **140** gives a molecular ion base peak at *m/z* 468, consistent with the molecular formula $C_{32}H_{24}N_2O_2$.

The UV-Vis spectra of **138**, **139** and **140** show that a red shift occurs in λ_{max} when both the donor and the acceptor are incorporated in the molecule. The lower energy region of the spectrum for **140** shows an absorption that extends out beyond 500 nm, whereas the absorption of D/A-substituted monomers **138** and **139** are limited to higher energy (**Fig. 2.10**).

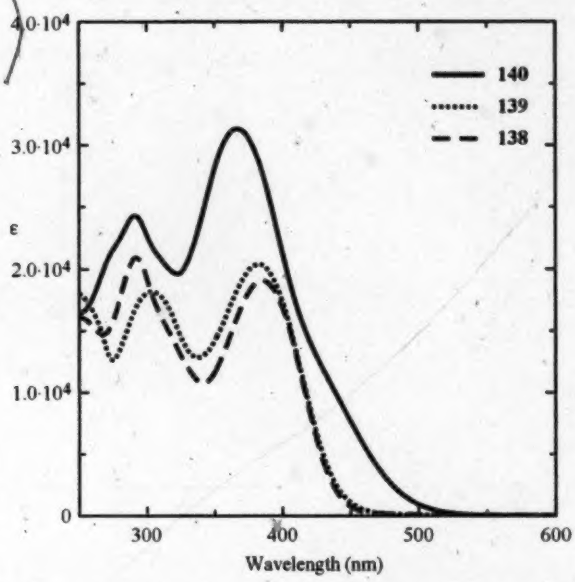

Fig. 2.10 UV-Vis absorption spectra of monomers **138**, **139**, and **140**.

This can be taken as an evidence of cross-conjugation between the donor and acceptor moieties through the intervening π-electron system.

An interesting comparison is afforded through consideration of the influence of vinylidene donor-acceptor substitution. The monomers **118a**, **130** and **140** have different substituents: dimethyl, cyclohexyl, and diphenyl, respectively. As expected, the lower energy limit of the spectra extends to about the same wavelength for **118a** and **130**, whereas it is considered red-shifted for **140**. This is understandable because the alkyl groups do not take part in the conjugation whereas the phenyl groups do take part, resulting in a red shift. **(Fig. 2.11)**

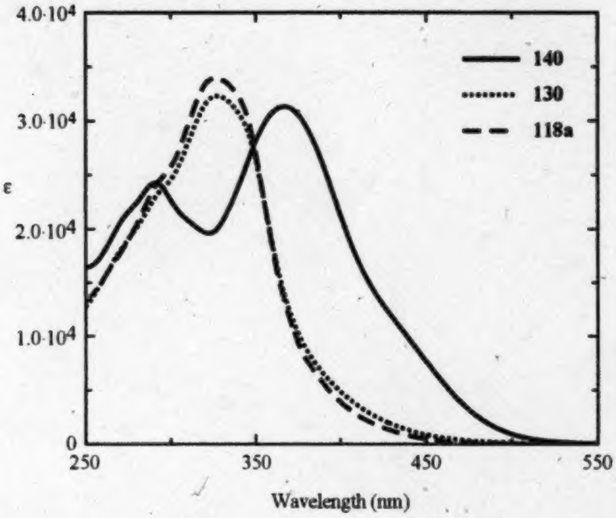

Fig. 2.11 UV-Vis absorption spectra comparing the effect of vinylidene substitution.

D. Stability

A very important characteristic of the conjugated compounds is their stability. Thermally, donor-acceptor oligomers **118a**, **122**, **126**, **130** and **140** show reasonable stability despite their potentially reactive enyne framework. Melting points for all derivatives are found in **Table 1**, as are decomposition points for D-A derivatives **118a**, **122** and **126** as determined by differential scanning calorimetry.

Table 1 Selected Physical Data for D/A *iso*-PDAs.

Compound	% yield	λ_{max} (ε)[a]	M. P. (°C)[b]
116	63	327 (22 000)	45-46
117	82	351 (15 600)	70-72
118a	70	328 (33 900)	159-162
			227 (dec.)[c]
120	56	325 (sh, 26 100)	68-69
		303 (35 700)	
		295 (sh, 34 800)	
121	92	358 (12 500)	58-60
		303 (sh, 23 100)	
		293 (24 600)	
122	76	325 (sh, 31 300)	154-156
		291 (43 500)	217 (dec.)[c]
124	76	325 (sh, 24 800)	111-113
		295 (38 600)	
125	84	352 (9 800)	77-79
		307 (sh, 22 900)	
		287 (26 600)	
126	83	372 (sh, 9600)	147 (dec.)[c]
		325 (sh, 35 500)	
		297 (46 600)	
129	63	328 (25 900)	50-57
130	83	327 (32 300)	113-115
138	45	292 (20 900)	N.A.
		385 (19 100)	
139	73	304 (18 200)	62-65
		382 (20 400)	
140	76	291 (24 300)	108-110
		367 (31 300)	

[a]In CHCl$_3$, ε in L mol^{-1} cm^{-1}. [b]Uncorrected. [c]Decomposition, by DSC.

E. Solvent Dependency

Monomers **116** and **118a** were chosen for studying the solvent effects on λ_{max}. It is known that more polar solvents can stabilize the excited state of donor-acceptor chromophores, lowering the energy of transition. Therefore a bathochromic (red) shift for

λ_{max} should be observed when more polar solvents are used.[54,11a] The UV-Vis spectra of compound **116** as measured in hexane, diethyl ether, chloroform, THF and acetonitrile are presented in **Fig. 2.12**.

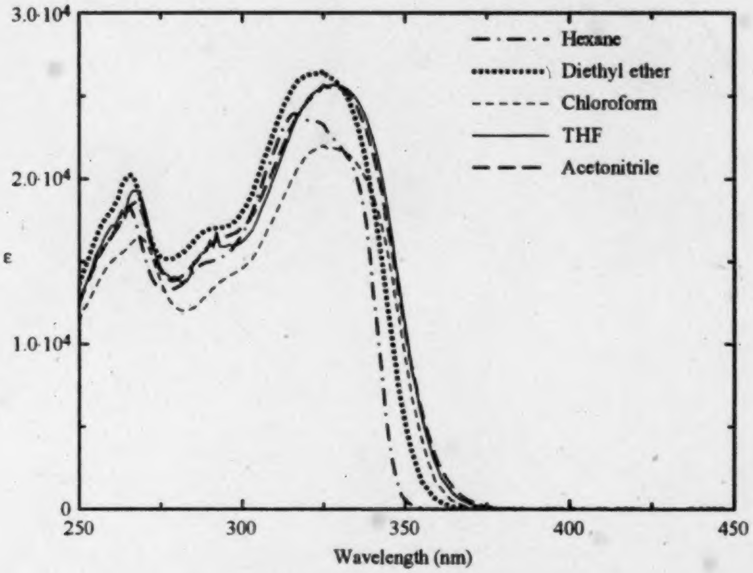

Fig. 2.12 UV-Vis spectra of donor-substituted monomer **116** in various solvents.

As can be seen in **Table 2** there is a slight relationship between λ_{max} and the solvent used. A positive solvatochromism is noticed for the less polar solvents: hexane, diethyl ether and tetrahydrofuran. A further increase in the solvent polarity did not shift the maximum wavelength. More important is the HOMO-LUMO gap, which can be approximated by the cut-off energy of the spectra.[54b] The cut-off is the wavelength read at the intersection point of the tangent to the lowest-energy absorption band and the *x* axis. As can be seen from **Table 2** a bathochromic shift is generally observed when more polar solvents were used. THF is the only solvent making an exception. This red shift suggests a slight donor-acceptor interaction for chromophore **116**.

Table 2 Absorption Characteristics of monomer **116**.

Solvent	λ_{max} (nm)	ε_{max}	Cut-off (nm)
Hexane	316	23900	347
Diethyl ether	324	26400	353
THF	327	25700	358.5
Chloroform	327	22000	357.8
Acetonitrile	327	25600	359.5

The UV-Vis spectra of donor-acceptor monomer **118a** as a function of solvent are somewhat different. As it can be seen in **Fig. 2.13**, excluding diethyl ether, ε_{max} is larger for more polar solvents.

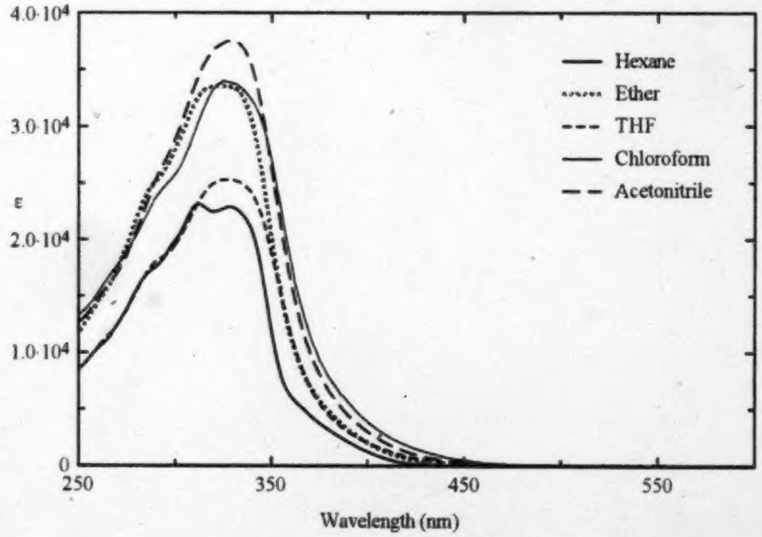

Fig. 2.13 UV-Vis spectra of donor-acceptor-substituted monomer **118a** in various solvents.

Although λ_{max} is about the same for all solvents (excluding the absorption in diethyl ether), a batochromic shift can be seen in the expansion of the spectra. The cut-off for each spectrum is posted in **Table 3**. A positive solvatochromism is noticed for monomer **118a** with one exception: the cut-off for the UV spectrum in acetonitrile is a little lower than the one for the spectrum done in chloroform.

Table 3 Absorption Characteristics of monomer **118a**.

Solvent	λ_{max} (nm)	ε_{max}	Cut-off (nm)
Hexane	328	22900	362
Diethyl ether	323	33600	368
THF	327	25300	377
Chloroform	328	33900	380
Acetonitrile	329	37500	377

Inversion of solvatochromism has been observed for some D-A chromophores.[14] Positive solvatochromism followed by negative solvatochromism was displayed by molecules having a large ground-state polarization. Although the neutral form of these molecules predominates in apolar solvents, an increase in the solvent polarity could induce an enhanced contribution of charge-separated resonance structures in the ground state. At this point, it appears that a slight positive solvatochromism is observed for **118a**.

III. CONCLUSION

The history of organic nonlinear optical materials is quite new compared to the more traditional inorganic nonlinear optical materials. Organic materials are increasingly being recognized as the materials of the future because their molecular nature, combined with the versatility of synthetic chemistry, can be used to alter and optimize structure to maximize nonlinear responses and other properties. At this time these materials are not widely used because of their environmental stability and low transparency. A few possibilities to improve the transparency have been discovered, based on a decrease in the electronic conjugation. Cross-conjugated chromophores were found to display good transparency.

The iterative synthesis of a new class of cross-conjugated *iso*-polydiacetylenes (*iso*-PDAs) oligomers was achieved. Palladium-catalyzed coupling reactions between vinyl triflates and terminal alkynes gave monomer **115**, dimer **119** and trimer **123**. Selectively end-capping of these oligomers with *p-N,N*-dimethylaniline (donor) and/or *p*-nitrobenzene (acceptor) gave donor, acceptor and donor-acceptor cross-conjugated compounds. Structure-property relationships for these compounds have been analyzed for cross-conjugated π-electronic communication as a result of contributions from donor, acceptor or donor-acceptor functionalization. The influence of the conjugation path length on the conjugation was studied by comparing the UV-Vis spectra of monomers, donors, and acceptor. Preliminary analysis of electronic absorption spectra indicated that D/A interactions were likely present in the smallest of these chromophores (monomer **118a**, **130**, **140**). Analogous D/A communication was, however, not observed for the longer oligomers **122** and **126**. The substitution effect was also studied. D-A monomers **130** and **140**, having different vinylidene substitution were synthesized. The absorption spectrum of monomer **130** was similar to that of monomer **118a**. Therefore, the cyclohexyl ring did not change dramatically the donor-acceptor interaction when it replaced the two methyl groups in **118a**. On the other hand a large red-shift was observed when the two methyl groups were replaced by two phenyl rings in **140**.

In the search for materials with better electronic and photonic properties, the synthesis and studies of structure-property relationships for new oligomers and polymers have been highly demanding over the past years. By the development of synthetic methodologies and analysis technologies, intense study will be carried out, even at the molecular level, so that we can totally understand structure-property relationships for organic materials. Therefore, the field of organic nonlinear optics offers many exciting opportunities for both fundamental research and technological application. The involvement of a variety of scientific and engineering disciplines including chemistry, polymer science, physics, optics and device engineering in both academia and industry will be essential to address the challenges that lie before this field. We hope that our research will contribute in some way to the progress in this frontier area of science and technology.

IV. EXPERIMENTAL SECTION

General. Reagents were purchased reagent grade from commercial suppliers and used without further purification. 4-Iodo-*N,N*-dimethylaniline, was made as previously reported.[59] Compounds **114**,[58]**115**,[54] **127**,[62] **131**,[58] **137**[63] were prepared as previously reported. Compound **134** was synthesized using an analogous method to that described by Stang.[58] An analogous method to that described by Zhao[54] was used to synthesize the diprotected monomers **132** and **135**.[64] Anh. $MgSO_4$ was used as the drying agent after aqueous work-up. Evaporation and concentration *in vacuo* was done at H_2O-aspirator pressure. All reactions were performed in standard, dry glassware under an inert atmosphere of N_2. A positive pressure of N_2 was essential to the success of all Pd-catalyzed reactions. Degassing of solvents was accomplished by vigorously bubbling N_2 through the solution for at least 45 min. Column chromatography: *silica gel-60* (230-400 mesh) from *General Intermediates of Canada*, silica gel H 5-40 μm from *Fluka Chemika*. Thin Layer Chromatography (TLC): plastic sheets coated with silica gel-60 F_{254} with the fluorescent indicator UV_{254} from Macherey-Nagel and aluminium sheets coated with silica gel-60 F_{254} from E. Merck; visualization by UV light or $KMnO_4$ stain. M.p.: *Gallenkamp* apparatus; uncorrected. DSC: *Pyris 1 Differential Thermal Analyzer*. UV-VIS Spectra: *Varian Cary 400* at rt; λ_{max} in nm (ε in L $M^{-1}cm^{-1}$). IR spectra (cm^{-1}): *Nicolet Magna-IR 750* (neat) or *Nic-Plan IR Microscope* (solids). ^1H- and ^{13}C-NMR: *Varian Gemini-300* and *Bruker AM-200, Bruker AM-300* or *Bruker AM-400* instruments, at rt in $CDCl_3$ (solvent peaks: 7.24 ppm for ^1H and 77.0 ppm for ^{13}C as reference) or C_6D_6 (solvent peak: 128.0 ppm for ^{13}C as reference). EI MS (*m/z*): *Kratos MS50* instrument. X-ray crystallographic analyses were done on a Siemens P4/RA X-ray diffractometer. Elemental analyses were effected by

Spectral Services at the University of Alberta. For simplicity, the coupling constants of the aryl protons for the *p-N,N*-dimethylaminophenyl and *p*-nitrophenyl moieties have been reported as pseudo first-order, even though they are second-order spin systems.

3-(*para-N,N*-Dimethylaminophenyl)ethynyl-4-methyl-1-triisopropylsilylpent-3-en-1-yne **116**

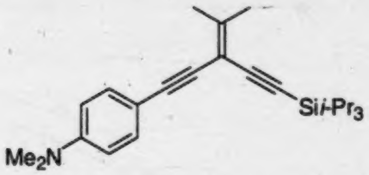

A mixture of 115 (325 mg, 0.979 mmol) and K_2CO_3 (50 mg, 0.36 mmol) in wet THF (5 mL) and MeOH (25 mL) was stirred for 4 h. Et_2O and H_2O were added, the organic phase separated, washed with saturated aq. NH_4Cl, saturated aq. NaCl, dried ($MgSO_4$) and reduced to 5 mL. Et_3N (50 mL) was added, and the solution was degassed for 2 h. *p*-Iodo-*N,N*-dimethylaniline (250 mg, 1.0120 mmol), $PdCl_2(PPh_3)_2$ (59 mg, 0.083 mmol) and CuI (31 mg, 0.16 mmol) were sequentially added. The mixture was stirred at rt for 20 h. Solvent removal and purification by column chromatography (silica gel-H, hexane/CH_2Cl_2 3:1) afforded **116** (229 mg, 63%) as a pale yellow solid. Mp 45-46 °C. R_f = 0.31 (hexane/CH_2Cl_2 2:1). UV-Vis ($CHCl_3$) λ (ε) 268 (16500), 302 (sh, 15000) 327 (22000) nm; IR (neat) 2942, 2865, 2202, 2150, 1607, 1520, 1365, 809 cm^{-1}; ^{1}H NMR (300 MHz, $CDCl_3$) δ 7.31 (d, *J* = 9.0 Hz, 2H), 6.61 (d, *J* = 9.0 Hz, 2H), 2.95 (s, 6H), 2.063 (s, 3H), 2.059 (s, 3H), 1.09 (s, 21H); ^{13}C NMR (75.5 MHz, $CDCl_3$) δ 152.8, 150.0, 132.5, 111.9, 110.7, 104.2, 102.5, 92.3, 92.0, 84.5, 40.3, 22.8, 22.7, 18.8, 11.4; EIMS *m/z* 379 (M^+, 100); HRMS calcd. for $C_{25}H_{37}NSi$ 379.2695, found 379.2699. X-Ray.

4-Methyl-3-(*para*-nitrophenyl)ethynyl-1-triisopropylsilyl-pent-3-en-1-yne

117

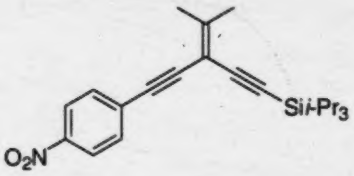

A mixture of **115** (256 mg, 0.770 mmol) and K_2CO_3 (58 mg, 0.42 mmol) in wet THF (5 mL) and MeOH (25 mL) was stirred for 4 h. Et_2O and H_2O were added, the organic phase separated, washed with saturated aq. NH_4Cl, saturated aq. NaCl, dried ($MgSO_4$) and reduced to 5 mL. Et_3N (50 mL) was added, and the solution was degassed for 1.5 h. *p*-Iodonitrobenzene (187 mg, 0.751 mmol), $PdCl_2(PPh_3)_2$ (21 mg, 0.03 mmol) and CuI (6 mg, 0.03 mmol) were sequentially added. The mixture was stirred at rt for 19 h. Solvent removal and purification by column chromatography (silica gel, hexane/CH_2Cl_2 3:1) afforded **117** (240 mg, 82%) as a bright yellow solid. Mp 70-72 °C. $R_f = 0.32$ (hexane/CH_2Cl_2 3:1). UV-Vis ($CHCl_3$) λ (ε) 268 (16200), 351 (15600) nm; IR (CH_2Cl_2, cast) 2942, 2865, 2206, 2148, 1592, 1520, 1343, 854 cm^{-1}; ^1H NMR (300 MHz, $CDCl_3$) δ 8.16 (d, $J = 8.8$ Hz, 2H), 7.54 (d, $J = 8.8$ Hz, 2H), 2.11 (s, 3H), 2.10 (s, 3H), 1.10 (s, 21H); ^{13}C NMR (75.5 MHz, $CDCl_3$) δ 157.2, 146.9, 132.0, 130.6, 123.6, 102.8, 101.7, 93.6, 92.1, 89.5, 23.1, 23.0, 18.7, 11.4; EIMS *m/z* 381.2 (M^+, 27), 338.2 ($[M - i\text{-}Pr]^+$, 100); HRMS calcd. for $C_{23}H_{31}N_2O_2Si$ 381.2124, found

381.2115. Anal. calcd. for $C_{23}H_{31}N_2O_2Si$: C, 72.39; H, 8.19; N, 3.67. Found: C, 72.20; H, 8.20; N, 3.63.

3-(*para*-*N*,*N*-Dimethylaminophenyl)ethynyl-4-methyl-1-(*para*-nitrophenyl)pent-3-en-1-yne **118a**

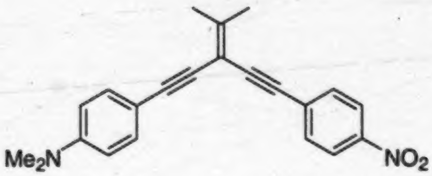

A solution of **116** (70 mg, 0.18 mmol) and Bu_4NF (0.7 mL, 1 M in THF) in wet THF (20 mL) was stirred at rt for 1 h. Et_2O and H_2O were added, the organic phase separated, washed with saturated aq. NH_4Cl, saturated aq. NaCl, dried ($MgSO_4$), reduced to 5 mL and added to Et_3N (20 mL) and THF (20 mL). The solution was degassed for 1.5 h, *p*-iodonitrobenzene (48 mg, 0.19 mmol), $PdCl_2(PPh_3)_2$ (5 mg, 0.007 mmol) and CuI (3 mg, 0.02 mmol) were added, and the mixture was stirred at rt for 12 h. Solvent removal and purification by column chromatography (silica gel-H, hexane/CH_2Cl_2 1:1) afforded **118a** (44 mg, 70%) as an orange solid and **118b** (4 mg, 10%) as an yellow solid. Mp 159-162 °C. $R_f = 0.45$ (hexane/ethyl acetate 3:1). UV-Vis ($CHCl_3$) λ (ε) 302 (sh, 26300), 328 (33900) nm; IR (CH_2Cl_2, cast) 2903, 2198, 1607, 1518, 1341, 854 cm^{-1}; ^1H NMR (300 MHz, $CDCl_3$) δ 8.16 (d, $J = 9.0$ Hz, 2H), 7.59 (d, $J = 9.0$ Hz, 2H), 7.35 (d, $J = 8.9$ Hz, 2H), 6.63 (d, $J = 8.9$ Hz, 2H), 2.97 (s, 6H), 2.143 (s, 3H), 2.137 (s, 3H); ^{13}C NMR (75.5 MHz, $CDCl_3$) δ 154.9, 150.2, 146.8, 132.6, 132.1, 130.7, 123.6, 111.9, 110.0, 101.5, 93.1, 92.6, 89.2, 83.6, 40.3, 23.03, 23.01; EIMS *m/z* 344 (M^+, 100); HRMS calcd. for $C_{22}H_{20}N_2O_2$ 344.1525, found 344.1522.

1,10-bis(*para*-*N*,*N*-dimethylaminophenyl-3,8-diisopropylidene-1,4,6,9-decatetrayne 118b

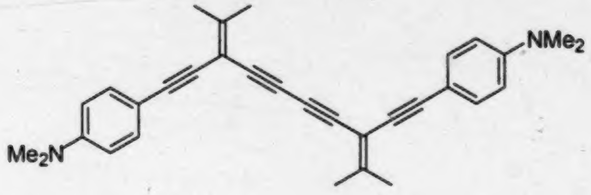

118b

Mp 185 °C (dec.). R_f = 0.11 (hexane/CH_2Cl_2 2:1). UV-Vis ($CHCl_3$) λ (ε) 296 (44900), 311 (47700), 328 (46000) nm; IR (μscope) 2904, 2202, 2133, 1609, 1585, 1521, 1363 cm^{-1}; ^1H NMR (300 MHz, $CDCl_3$) δ 7.32 (d, *J* = 9.0 Hz, 4H), 6.61 (d, *J* = 9.0 Hz, 4H), 2.95 (s, 12H), 2.086 (s, 6H), 2.084 (s, 6H); ^{13}C NMR (75.5 MHz, $CDCl_3$) δ 155.9, 150.1, 132.6, 111.9, 110.2, 101.4, 93.1, 83.4, 79.4, 75.7, 40.3, 23.0 (2C); EIMS *m/z* 444 (M^+, 100); HRMS calcd. for $C_{25}H_{37}NSi$ 444.2566, found 444.2559.

2,7-Dimethyl-6-trimethylsilylethynyl-3-triisopropylsilylethynyl-2,6-octadien-4-yne 119

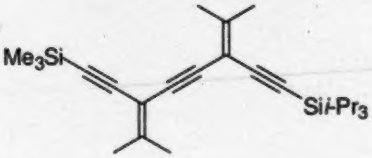

A mixture of **115** (151 mg, 0.455 mmol) and K_2CO_3 (30 mg, 0.22 mmol) in wet THF (5 mL) and MeOH (15 mL) was stirred for 2 h. Et_2O and H_2O were added, the organic phase separated, washed with saturated aq. NH_4Cl, saturated aq. NaCl, dried ($MgSO_4$), reduced to *ca.* 5 mL, and added to a degassed solution of **114** (109 mg, 0.365 mmol) in DMF (10 mL). $Pd(PPh_3)_4$ (21 mg, 0.018 mmol) and Et_2NH (3 mL) were sequentially added, the solution stirred for 5 min, CuI (10 mg, 0.052 mmol) was added and the solution stirred at rt for 2 h. Et_2O and H_2O were added, the organic phase separated, washed with saturated aq. NH_4Cl, saturated aq. NaCl and dried ($MgSO_4$). Purification by column chromatography (silica gel, hexane/CH_2Cl_2 1:1) afforded **119** (118 mg, 63%) as a yellow oil. $R_f = 0.43$ (hexane/CH_2Cl_2 4:1). IR (CH_2Cl_2, cast) 2942, 2149, 1463, 842 cm^{-1}; ^{1}H NMR (300 MHz, $CDCl_3$) δ 2.04 (s, 3H), 2.02 (s, 3H), 2.01 (s, 3H), 1.99 (s, 3H), 1.07 (s, 21H), 0.17 (s, 9H); ^{13}C NMR (50.5 MHz, $CDCl_3$) δ 154.4, 153.7, 103.6, 102.1, 101.8 (2C), 95.7, 92.2, 88.7, 88.2, 22.7 (2C), 22.5 (2C), 18.6, 11.3, -0.05; EIMS *m/z* 410 (M^+, 100); HRMS calcd. for $C_{26}H_{42}Si_2$ 410.2825, found 410.2823. Anal. calcd. for $C_{26}H_{42}Si_2$: C, 76.02; H, 10.31. Found: C, 76.12; H, 10.58.

6-(*para*-Dimethylaminophenyl)ethynyl-2,7-dimethyl-3-triisopropylsilylethynyl-2,6-octadien-4-yne 120

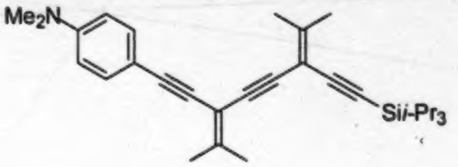

To a solution of **119** (152 mg, 0.370 mmol) in wet THF (3 mL) and MeOH (15 mL) was added K_2CO_3 (27 mg, 0.19 mmol) and the mixture stirred for 5 h. Et_2O and H_2O were added, the organic phase separated, washed with saturated aq. NH_4Cl, saturated aq. NaCl, dried ($MgSO_4$), reduced to *ca.* 5 mL, and added to a degassed solution of *p*-iodo-*N*,*N*-dimethylaniline (106 mg, 0.482 mmol) in Et_3N (40 mL). $PdCl_2(PPh_3)_2$ (27 mg, 0.038 mmol) and CuI (14 mg, 0.073 mmol) were added, and the mixture was stirred at rt for 14 h. Solvent removal and purification by column chromatography (silica gel, hexane/CH_2Cl_2 5:2) afforded **120** (96 mg, 56%) as a pale yellow solid. Mp 68-69 °C. R_f = 0.46 (hexane/CH_2Cl_2 1:1). UV-Vis λ (ε) ($CHCl_3$) 263 (23800), 295 (sh, 34800), 303 (35700), 325 (sh, 26100) nm; IR (neat) 2942, 2864, 2201, 2142, 1881, 1612, 1523, 1462, 1224, 882, 815 cm^{-1}; ^{1}H NMR (300 MHz, $CDCl_3$) δ 7.30 (d, *J* = 9.0 Hz, 2H), 6.61 (d, *J* = 9.0 Hz, 2H), 2.95 (s, 6H), 2.08 (s, 3H), 2.05 (s, 3H), 2.04 (s, 6H), 1.08 (s, 21H); ^{13}C NMR (75.5 MHz, $CDCl_3$) δ 153.6, 151.5, 150.0, 132.5, 111.9, 110.7, 103.9, 102.3, 102.0, 92.1, 92.0, 89.0, 88.2, 84.4, 40.3, 22.8, 22.7 (2C), 22.6, 18.7, 11.4; EIMS *m/z* 457 (M^+, 100); HRMS calcd. for $C_{31}H_{43}NSi$ 457.3165, found 457.3164. Anal. calcd. for $C_{31}H_{43}NSi$: C, 81.34; H, 9.47; N, 3.06. Found: C, 80.95; H, 9.59; N, 3.03.

2,7-Dimethyl-6-(*para*-nitrophenyl)ethynyl-3-triisopropylsilylethynyl-2,6-octadien-4-yne 121

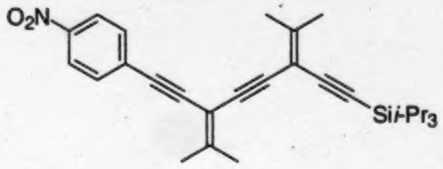

A mixture of **119** (113 mg, 0.276 mmol) and K_2CO_3 (17 mg, 0.12 mmol) in wet THF (1.5 mL) and MeOH (7.5 mL) was stirred at rt for 5 h. Et_2O and H_2O were added, the organic phase separated, washed with saturated aq. NH_4Cl, saturated aq. NaCl, dried ($MgSO_4$), and reduced to 5 mL. The solution was diluted with Et_3N (50 mL) and degassed for 1.5 h. *p*-Iodonitrobenzene (60 mg, 0.24 mmol), $PdCl_2(PPh_3)_2$ (16 mg, 0.023 mmol), and CuI (7 mg, 0.037 mmol) were added and the mixture was stirred at rt for 14 h. Solvent removal and purification by column chromatography (silica gel, hexane/CH_2Cl_2 3:2) afforded **121** (117 mg, 92%) as a bright yellow solid. Mp 58-60 °C. R_f = 0.23 (hexane/CH_2Cl_2 3:2). UV-Vis ($CHCl_3$) λ (ε) 264 (20000), 293 (24600), 303 (sh, 23100), 358 (12500) nm; IR (CH_2Cl_2, cast) 2942, 2209, 2146, 1592, 1520, 1342 cm^{-1}; ^1H NMR (300 MHz, $CDCl_3$) δ 8.16 (d, *J* = 9.0 Hz, 2H), 7.54 (d, *J* = 9.0 Hz, 2H), 2.12 (3H), 2.09 (3H), 2.06 (3H), 2.04 (3H), 1.07 (21H); ^{13}C NMR (75.5 MHz, $CDCl_3$) δ 155.8, 154.3, 146.9, 132.0, 130.6, 123.6, 103.5, 102.0, 101.3, 92.5, 92.1, 89.3, 89.2, 87.7, 23.0, 22.9, 22.8, 22.7, 18.7, 11.4; EIMS *m/z* 459 (M^+, 52), 416 ($[M - i\text{-}Pr]^+$, 100); HRMS calcd. for $C_{29}H_{37}NO_2Si$ 459.2594, found 459.2591. Anal. calcd. for $C_{29}H_{37}NO_2Si$: C, 75.77; H, 8.11; N, 3.05. Found: C, 75.46; H, 8.21; N, 2.97.

3-(*para*-Dimethylaminophenyl)etynyl-2,7-dimethyl-6-(*para*-nitrophenyl)ethynyl-2,6-octadien-4-yne 122

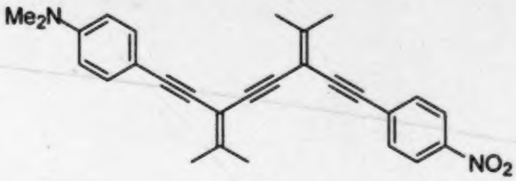

A solution of **120** (66 mg, 0.15 mmol) and Bu_4NF (0.3 mL, 1.0 M in THF) in wet THF (25 mL) was stirred at rt for 15 min. Et_2O and H_2O were added, the organic phase was separated, washed with saturated aq. NH_4Cl, saturated aq. NaCl, dried ($MgSO_4$), reduced to 5 mL and added to a mixture of Et_3N (20 mL) and THF (20 mL). The solution was degassed for 1.5 h, *p*-iodonitrobenzene (37 mg, 0.15 mmol), $PdCl_2(PPh_3)_2$ (5 mg, 0.007 mmol) and CuI (4 mg, 0.02 mmol) were added, and the mixture was stirred at rt for 6 h. Solvent removal and purification by column chromatography (silica gel, hexane/CH_2Cl_2 1:1) afforded **122** (33 mg, 76%) as an orange solid. Mp 154-156 °C. $R_f = 0.37$ (hexane/CH_2Cl_2 1:2). UV-Vis ($CHCl_3$) λ (ε) 291 (43500), 325 (sh, 31300) nm; IR ($CHCl_3$, cast) 2924, 2202, 1608, 1519, 1342 cm^{-1}; ^{1}H NMR (300 MHz, $CDCl_3$) δ 8.16 (d, $J = 9.0$ Hz, 2H), 7.57 (d, $J = 9.0$ Hz, 2H), 7.32 (d, $J = 8.9$ Hz, 2H), 6.61 (d, $J = 8.9$ Hz, 2H), 2.95 (s, 6 H), 2.12 (s, 6H), 2.10 (s, 3H), 2.08 (s, 3H); ^{13}C NMR (75.5 MHz, C_6D_6) δ 155.4, 151.9, 150.3, 147.1, 133.0, 132.0, 130.0, 123.4, 112.2, 111.0, 103.0, 102.3, 93.6, 92.2, 90.5, 90.0, 87.9, 85.1, 39.6, 22.8, 22.7 (3C); EIMS *m/z* 422 (M^+, 100); HRMS calcd. for $C_{28}H_{26}N_2O_2$ 422.1994, found 422.1987.

2,10-Dimethyl-6-isopropylidene-9-trimethylsilylethynyl-3-triisopropylsilylethynyl-2,9-undecadiene-4,7-diyne **123**

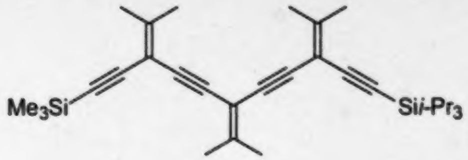

A mixture of **119** (274 mg, 0.67 mmol) and K_2CO_3 (28 mg, 0.20 mmol) in wet THF (10 mL) and MeOH (10 mL) was stirred for 3 h. Et_2O and H_2O were added, the organic phase separated, washed with saturated aq. NH_4Cl, saturated aq. NaCl, dried ($MgSO_4$), reduced to *ca.* 5 mL, added to a degassed solution of **114** (193 mg, 0.643 mmol) in DMF (30 mL), and degassed for 0.5 h. $Pd(PPh_3)_4$ (37 mg, 0.03) and Et_2NH (5 mL) were sequentially added, the solution stirred for 5 min, CuI (17 mg, 0.09 mmol) was added, and the solution stirred at rt for 15 h. Et_2O and H_2O were added, the organic phase separated, washed with saturated aq. NH_4Cl, saturated aq. NaCl and dried ($MgSO_4$). Elution on a silica gel column with hexane afforded **123** (171 mg , 52%) as a yellow solid; Mp 48-50 °C. $R_f = 0.6$ (hexane/CH_2Cl_2 5:1). UV-Vis λ (ε) ($CHCl_3$) 255 (25600), 284 (27600) nm; IR (neat) 2946, 2148, 1602, 840 cm^{-1}; ^1H NMR (300 MHz, $CDCl_3$) δ 2.04 (s, 3H), 2.03 (s, 3H), 2.02 (s, 6H), 2.01 (s, 3H), 1.99 (s, 3H), 1.07 (s, 3H), 1.06 (s, 18H), 0.17 (s, 9H); ^{13}C NMR (50.5 MHz, $CDCl_3$) δ 154.4, 153.8, 152.7, 103.6, 102.1, 101.8, 101.7, 95.7 (2C), 92.1, 88.6, 88.5, 88.3, 87.9, 22.7 (3C), 22.5 (3C), 18.7, 11.3, -0.04; EIMS *m/z* 488 (M^+, 100); HRMS calcd. for $C_{32}H_{48}Si_2$ 488.3295, found 488.3292. Anal. calcd. for $C_{32}H_{48}Si_2$: C, 78.62; H, 9.90. Found: C, 78.27, H, 10.09.

9-(*para*-Dimethylaminophenyl)etynyl-2,10-dimethyl-6-isopropylidene-3-triisopropylsilylethynyl-2,9-undecadiene-4,7-diyne 124

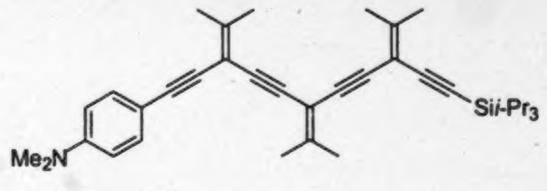

A mixture of **123** (115 mg, 0.236 mmol) and K_2CO_3 (25 mg, 0.18 mmol) in wet THF (2 mL) and MeOH (10 mL) was stirred for 4.5 h. Et_2O and H_2O were added, the organic phase separated, washed with saturated aq. NH_4Cl, saturated aq. NaCl, dried ($MgSO_4$) and reduced to *ca*. 5 mL. Et_3N (15 mL) was added and the solution was degassed for 1.5 h. *p*-Iodo-*N,N*-dimethylaniline (58 mg, 0.23 mmol), $PdCl_2(PPh_3)_2$ (15 mg, 0.021 mmol) and CuI (7 mg, 0.04 mmol) were sequentially added. The mixture was stirred at rt for 16 h. Solvent removal and purification by column chromatography (silica gel, hexane/CH_2Cl_2 4:1) afforded **124** (96 mg, 76%) as a pale yellow solid. Mp 111-113 °C. R_f = 0.44 (hexane/ethyl acetate 5:1). UV-Vis ($CHCl_3$) λ (ε) 295 (38600), 325 (sh, 24800) nm; IR ($CHCl_3$, cast) 2940, 2196, 2145, 1609, 1520, 1347 cm^{-1}; ^1H NMR (300 MHz, $CDCl_3$) δ 7.30 (d, *J* = 8.9 Hz, 2H), 6.61 (d, *J* = 8.9 Hz, 2H), 2.95 (s, 6H), 2.08 (s, 3H), 2.06 (s, 3H), 2.05 (s, 6H), 2.03 (s, 3H), 2.02 (s, 3H), 1.07 (s, 21H); ^{13}C NMR (75.5 MHz, $CDCl_3$) δ 153.8, 152.5, 151.5, 150.0, 132.5, 111.9, 110.7, 103.8, 102.2, 102.0, 101.9, 92.2, 92.0, 88.7, 88.7, 88.3, 88.1, 84.5, 40.3, 22.8 (2C), 22.7, 22.65 (2C), 22.60, 18.7, 11.4; EIMS *m/z* 535 (M^+, 100); HRMS calcd. for $C_{37}H_{49}NSi$ 535.3634, found 535.3616. Anal. calcd. for $C_{37}H_{49}NSi$: C, 82.93; H, 9.22; N, 2.61. Found C, 82.44; H, 9.32; N, 2.54.

2,10-Dimethyl-9-(*para*-nitrophenyl)ethynyl-6-isopropylidene-3-triisopropylsilylethynyl-2,9-undecadiene-4,7-diyne 125

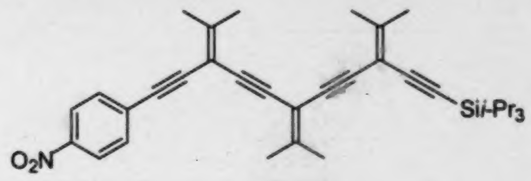

A mixture of **123** (14 mg, 0.029 mmol) and K_2CO_3 (3 mg, 0.02 mmol) in wet THF (0.5 mL) and MeOH (1.5 mL) was stirred at rt for 4 h. Et_2O and H_2O were added, the organic phase separated, washed with saturated NH_4Cl, saturated NaCl, dried ($MgSO_4$) and reduced to 5 mL. The solution was diluted with Et_3N (10 mL) and degassed for 1.5 h. *p*-Iodonitrobenzene (7 mg, 0.03 mmol), $PdCl_2(PPh_3)_2$ (2 mg, 0.002 mmol), and CuI (1 mg, 0.004 mmol) were added and the mixture was stirred at rt, under nitrogen, for 15 h. Solvent removal and purification by column chromatography (silica gel, hexane/CH_2Cl_2 1:2) afforded **125** (13 mg, 84%) as a bright yellow solid. Mp 77-79 °C. $R_f = 0.27$ (hexane/CH_2Cl_2 2:1). UV-Vis ($CHCl_3$) λ (ε) 287 (26600), 307 (sh, 22900), 352 (9800) nm; IR (CH_2Cl_2, cast) 2941, 2206, 2145, 1592, 1519, 1342 cm^{-1}; ^1H NMR (300 MHz, $CDCl_3$) δ 8.16 (d, $J = 9.0$ Hz, 2H), 7.55 (d, $J = 9.0$ Hz, 2H), 2.12 (s, 3H), 2.09 (s, 3H), 2.06 (s, 3H), 2.05 (s, 6H), 2.02 (s, 3H), 1.06 (s, 21H); ^{13}C NMR (100.5 MHz, $CDCl_3$, APT) δ 155.8, 153.9, 153.2, 146.8, 132.0, 130.6, 123.6, 103.6, 102.1, 101.6, 101.2, 92.3, 92.1, 89.2, 89.1, 88.5, 88.3, 87.3, 23.0, 22.9, 22.8 (2C), 22.6 (2C), 18.6, 11.3; EIMS *m/z* 537 (M^+, 81), 494 ([M - *i*-Pr]$^+$, 100); HRMS calcd. for $C_{35}H_{43}O_2NSi$ 537.3063, found 537.3062. Anal. calcd. for $C_{35}H_{43}O_2NSi$: C, 78.16; H, 8.06; N, 2.60. Found: C, 77.48; H, 7.91; N, 1.57.

9-(*para*-Dimethylaminophenyl)etynyl-2,10-dimethyl-3-(*para*-nitrophenyl)ethynyl-6-isopropylidene-2,9-undecadiene-4,7-diyne 126

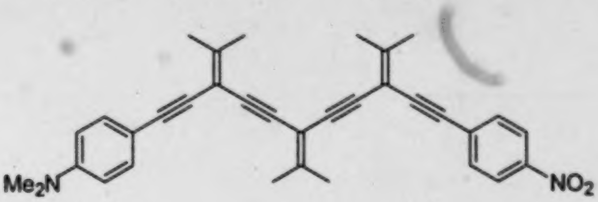

A solution of **124** (22 mg, 0.04 mmol) and Bu_4NF (0.2 mL, 1 M in THF) in wet THF (10 mL) was stirred at rt, for 45 min. Et_2O and H_2O were added, the organic phase was separated, washed with saturated aq. NH_4Cl, saturated aq. NaCl, dried ($MgSO_4$), reduced to 5 mL and added to Et_3N (10 mL) and THF (10 mL). The solution was degassed for 1.5 h, *p*-iodonitrobenzene (10 mg, 0.04 mmol), $PdCl_2(PPh_3)_2$ (4 mg, 0.005 mmol) and CuI (1 mg, 0.006 mmol) were added, and the mixture was stirred at rt for 19 h. Solvent removal and purification by column chromatography (silica gel, hexane/CH_2Cl_2 1:1) afforded **126** (17 mg, 83%) as an orange solid. Mp 147 °C (dec.). R_f = 0.24 (hexane/CH_2Cl_2 1:1). UV-Vis ($CHCl_3$) λ (ε) 297 (46600), 325 (sh, 35500), 372 (sh, 9600) nm; IR (film) 2906, 2201, 1611, 1521, 1344 cm^{-1}; ^1H NMR (300 MHz, $CDCl_3$) δ 8.10 (d, *J* = 9.0 Hz, 2H), 7.53 (d, *J* = 9.0 Hz, 2H), 7.30 (d, *J* = 8.8 Hz, 2H), 6.59 (d, *J* = 8.8 Hz, 2H), 2.95 (s, 6H), 2.12 (s, 3H), 2.11 (s, 3H), 2.08 (s, 6H), 2.07 (s, 3H), 2.06 (s, 3H); ^{13}C NMR (75.5, $CDCl_3$) δ 155.7, 152.9, 151.6, 150.0, 146.9, 132.5, 132.0, 130.6, 123.6, 111.9, 110.7, 102.1, 101.8, 101.4, 92.23, 92.18, 89.4 (2C), 89.0, 87.9, 87.4, 84.4, 40.2, 23.0 (2C), 22.85 (2C), 22.76, 22.73; EIMS *m/z* 500 (M^+, 100); HRMS calcd. for $C_{34}H_{32}O_2N_2$ 500.2464, found 500.2458. Anal. calcd. for $C_{34}H_{32}O_2N_2$: C, 81.36; H, 7.02; N, 5.42. Found: C, 81.39; H, 7.07; N, 5.23.

3-Cyclohexylidene-1-trimethylsilyl-5-triisopropylsilyl-1,4-pentadiyne

128

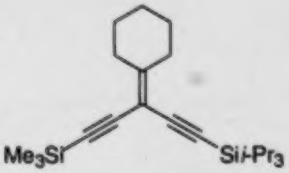

To a degassed solution of triflate **127** (218 mg, 0.641 mmol) in DMF (50 mL), was added TIPS acetylene (159 mg, 0.872 mmol), $Pd(PPh_3)_4$ (41 mg, 0.035 mmol) and Et_2NH (3 mL). The mixture was stirred for 5 min. under nitrogen, at rt and CuI (25 mg, 0.13 mmol) was added. The solution was stirred under nitrogen, at rt, for 2 h. Et_2O and H_2O were added, the organic phase was separated, washed with saturated aq. NH_4Cl, saturated aq. NaCl and dried over $MgSO_4$. Solvent removal and purification by column chromatography (silica gel, hexane/CH_2Cl_2 8:1) afforded **128** (170 mg, 71%) as a yellow oil. R_f = 0.58 (hexane/CH_2Cl_2 5:1). IR ($CHCl_3$, cast) 2940, 2864, 2150, 1463, 1249, 843 cm^{-1}; ^1H NMR (300 MHz, $CDCl_3$) δ 2.48 (m, 4H), 1.56 (m, 6H), 1.07 (s, 21H), 0.17 (s, 9H); ^{13}C NMR (75.5 MHz, $CDCl_3$) δ 162.4, 103.3, 101.6, 98.9, 96.1, 92.8, 32.9, 32.8, 27.6, 27.5, 26.2, 18.7, 11.4, 0.02; EIMS m/z 372 (M^+, 100); HRMS calcd. for $C_{23}H_{40}Si_2$ 372.2669, found 372.2669.

5-(*para*-Dimethylaminophenyl)-3-cyclohexylidene-1-triisopropylsilyl-1,4-pentadiyne 129

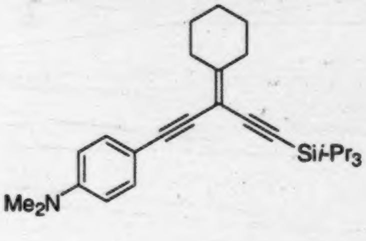

A mixture of **128** (123 mg, 0.330 mmol) and K_2CO_3 (20 mg, 0.15 mmol) in wet THF (2 mL) and MeOH (10 mL) was stirred at room temperature for 1.5 h. Et_2O and H_2O were added, the organic phase separated, washed with saturated aq. NH_4Cl, saturated aq. NaCl, dried ($MgSO_4$) and reduced to *ca.* 3 mL. Et_3N (30 mL) was added and the solution was degassed for 1.5 h. *p*-Iodo-*N,N*-dimethylaniline (74 mg, 0.34 mmol), $PdCl_2(PPh_3)_2$ (22 mg, 0.032 mmol) and CuI (12 mg, 0.065 mmol) were sequentially added. The mixture was stirred at rt, under nitrogen, for 18 h. Solvent removal and purification by column chromatography (silica gel, hexane/ CH_2Cl_2 8:1) afforded **129** (87 mg, 63%) as a yellow solid. Mp 50-57 °C. $R_f = 0.19$ (hexane/CH_2Cl_2 5:1). UV-Vis ($CHCl_3$) λ (ε) 271 (22600), 299 (sh, 17500), 328 (25900) nm; IR (CH_2Cl_2, cast) 2939, 2863, 2198, 2143, 1609, 1520 cm^{-1} ; ^1H NMR (300 MHz, $CDCl_3$) δ 7.30 (d, J = 8.8 Hz, 2H), 6.61 (d, J = 8.8 Hz, 2H), 2.95 (s, 6H), 2.54 (m, 4H), 1.58 (m, 6H), 1.08 (s, 21 H); ^{13}C NMR (75.5 MHz, $CDCl_3$) δ 159.7, 150.0, 132.5, 111.9, 110.8, 104.0, 99.1, 92.2, 91.9, 84.2, 40.3, 33.0, 32.8, 27.7, 27.6, 26.3, 18.7, 11.4; EIMS 419 (M^+, 100); HRMS calcd. for $C_{28}H_{41}NSi$ 419.3008, found 419.3006.

5-(*para*-dimethylaminophenyl)-3-cyclohexylidene-1-(*para*-nitrophenyl)-1,4-pentadiyne 130

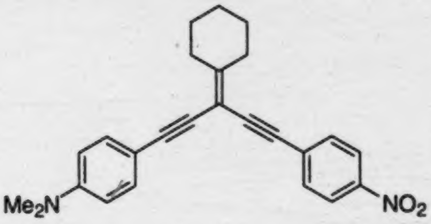

A solution of **129** (79 mg, 0.19 mmol) and Bu_4NF (0.7 mL, 1 M in THF) in wet THF (40 mL) was stirred at rt for 0.5 h. Et_2O and H_2O were added, the organic phase separated, washed with saturated aq. NH_4Cl, saturated aq. NaCl, dried ($MgSO_4$), reduced to *ca.* 5 mL and added to a mixture of Et_3N (20 mL) and THF (20 mL). The solution was degassed for 1.5 h, *p*-iodonitrobenzene (56 mg, 0.23 mmol), $PdCl_2(PPh_3)_2$ (9 mg, 0.01 mmol) and CuI (4 mg, 0.02 mmol) were added, and the mixture was stirred at rt, under nitrogen, for 18 h. Solvent removal and purification by column chromatography (silica gel, hexane/ethyl acetate 10:1) afforded **130** (62 mg, 83%) as a red solid. Mp 113-115 °C. $R_f = 0.29$ (hexane/CH_2Cl_2 5:1). UV-Vis ($CHCl_3$) λ (ε) 292 (sh, 23200), 327 (32300) nm; IR (CH_2Cl_2, cast) 2928, 2854, 2197, 1607, 1518, 1341, 854 cm^{-1}; ^1H NMR (300 MHz, $CDCl_3$) δ 8.15 (d, $J = 9.0$ Hz, 2H), 7.58 (d, $J = 9.0$ Hz, 2H), 7.34 (d, $J = 9.0$ Hz, 2H), 6.61 (d, $J = 9.0$ Hz, 2H), 2.95 (s, 6H), 2.60 (m, 4H), 1.63 (m, 6H); ^{13}C NMR (75.5 MHz, $CDCl_3$) δ 161.9, 150.1, 146.7, 132.6, 132.1, 130.7, 123.5, 111.8, 110.0, 98.1, 92.8, 92.4, 89.0, 83.2, 40.2, 33.1, 33.0, 27.9, 27.7, 26.2; EIMS 384 (M^+, 100); HRMS calcd. for $C_{25}H_{24}N_2O_2$ 384.1827, found 384.1827. Anal. calcd. for $C_{25}H_{24}N_2O_2$: C, 78.10; H, 6.29; N, 7.29. Found: C, 77.31; H, 6.56; N, 6.82.

5-(*para*-Dimethylaminophenyl)-3-diphenylvinylidene-1-triethylsilyl-pent-1,4-diyne 138

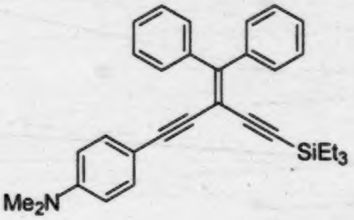

A mixture of **137** (100 mg, 0.460 mmol) and K_2CO_3 (20 mg, 0.15 mmol) in wet THF (10 mL) and MeOH (10 mL) was stirred at room temperature for 4 h. Et_2O and H_2O were added, the organic phase separated, washed with saturated aq. NH_4Cl, saturated aq. NaCl, dried ($MgSO_4$) reduced to *ca.* 3 mL, added to a degassed solution of **134** (180 mg, 0.386 mmol) in DMF (125 mL), and degassed for 0.5 h. $Pd(PPh_3)_4$ (24 mg, 0.021 mmol) and Et_2NH (3 mL) were sequentially added, the solution stirred for 5 min, CuI (13 mg, 0.071 mmol) was added, and the solution stirred at rt for 17 h. Et_2O and H_2O were added, the organic phase separated, washed with saturated aq. NH_4Cl, saturated aq. NaCl and dried ($MgSO_4$). Solvent removal and purification by column chromatography (silica gel, ethyl acetate/hexanes 1:6 followed by CH_2Cl_2/hexanes 1:3) afforded **138** (80 mg, 45%) as a yellow semisolid. $R_f = 0.3$ (hexane/CH_2Cl_2 2:1). UV-Vis ($CHCl_3$) λ (ε) 292 (20900), 385 (19100) nm; IR (CH_2Cl_2, cast) 2954, 2924, 2187, 1608, 1519, 1362, 729 cm^{-1}; ^1H NMR (300 MHz, $CDCl_3$) δ 7.49 (m, 4H), 7.30 (m, 6H), 7.16 (d, J = 9.0 Hz, 2H), 6.58 (d, J = 9.0 Hz, 2H), 2.95 (s, 6H), 0.92 (t, J = 8.0, 9H), 0.55 (q, J = 8.0, 6H); ^{13}C NMR (75.5

MHz, $CDCl_3$) δ 154.4, 150.0, 140.7, 140.5, 132.6, 130.43, 130.39, 128.1, 128.0, 127.51, 127.48, 111.7, 110.2, 104.9, 102.8, 95.0, 93.4, 87.2, 40.2, 7.4, 4.3; EIMS 461 (M^+, 100); HRMS calcd. for $C_{32}H_{35}NSi$ 461.2545, found 461.2545.

3-diphenylvinylidene-5-(*para*-nitrophenyl)-1-triisopropylsilyl-pent-1,4-diyne 139

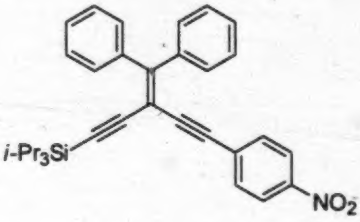

A solution of **132** (41 mg, 0.090 mmol) and K_2CO_3 (6 mg, 0.04 mmol) in wet THF (0.5 mL) and MeOH (3 mL) was stirred for 9 days. Et_2O and H_2O were added, the organic phase separated, washed with saturated aq. NH_4Cl, saturated aq. NaCl, dried ($MgSO_4$) and reduced to *ca.* 2 mL. Et_3N (5 mL) was added, and the solution was degassed for 1.5 h. *p*-Iodo-nitrobenzene (25 mg, 0.10 mmol), $PdCl_2(PPh_3)_2$ (4 mg, 0.005 mmol) and CuI (2 mg, 0.01 mmol) were sequentially added. The mixture was stirred at rt, under nitrogen, for 24 h. Solvent removal and purification by column chromatography (silica gel H, hexane/CH_2Cl_2 3:1) afforded **139** (33 mg, 73%) as a yellow solid. Mp 62-65 °C. $R_f = 0.32$ (hexane/CH_2Cl_2 2:1). UV-Vis ($CHCl_3$) λ (ε) 304 (18200), 382 (20400) nm; IR ($CHCl_3$, cast) 2941, 2864, 2194, 2147, 1593, 1519, 1342, 853 cm^{-1}; ^1H NMR (300 MHz, $CDCl_3$) δ 8.11 (d, $J = 8.8$ Hz, 2H), 7.5-7.29 (m, 12H), 1.03 (s, 21H); ^{13}C NMR (75.5 MHz, $CDCl_3$) δ 158.2, 146.9, 140.3, 139.8, 132.0, 130.4 (2C), 128.92, 128.89, 127.84, 127.82, 123.6, 104.3, 101.7, 95.8, 94.8, 89.6, 18.7, 11.4 (one carbon not observed); EIMS 505 (M^+, 100); HRMS calcd. for $C_{33}H_{35}NO_2Si$ 505.2437, found 505.2444.

5-(*para*-Dimethylaminophenyl)-3-diphenylvinylidene-1-(*para*-nitrophenyl)pent-1,4-diyne 140

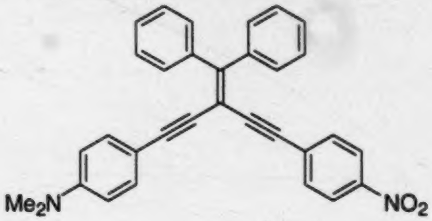

A solution of **138** (65 mg, 0.14 mmol) and Bu_4NF (0.3 mL, 1 M in THF) in wet THF (20 mL) was stirred at rt for 0.5 h. Et_2O and H_2O were added, the organic phase separated, washed with saturated aq. NH_4Cl, saturated aq. NaCl, dried ($MgSO_4$), reduced to 3 mL and added to Et_3N (20 mL) and THF (20 mL). The solution was degassed for 2 h, *p*-iodonitrobenzene (42 mg, 0.17 mmol), $PdCl_2(PPh_3)_2$ (6 mg, 0.008 mmol) and CuI (4 mg, 0.02 mmol) were added, and the mixture was stirred at rt, under nitrogen for 17 h. Solvent removal and purification by column chromatography (silica gel-H, hexane/ CH_2Cl_2 3:1) afforded **140** (50 mg, 76%) as a red solid. Mp 108-110°C. $R_f = 0.56$ (hexane/CH_2Cl_2 1:2). UV-Vis ($CHCl_3$) λ (ε) 272 (sh, 21000), 291 (24300), 367 (31300) nm; IR (CH_2Cl_2, cast) 2925, 2185, 1607, 1516, 1340, 853 cm^{-1}; ^1H NMR (300 MHz, $CDCl_3$) δ 8.16 (d, $J = 9.0$ Hz, 2H), 7.61 (m, 2H), 7.53 (m, 2H), 7.42 (m, 10H), 7.27 (d, $J = 8.8$ Hz, 2H), 6.67 (d, $J = 8.8$ MHz, 2H), 3.02 (s, 6H); ^{13}C NMR (75.5 MHz, $CDCl_3$, APT) δ 156.0, 150.2, 146.8, 140.7, 140.2, 132.7, 132.0, 130.6 (2C), 130.3, 128.7, 128.6, 127.8, 127.7, 123.5, 111.9, 102.0, 94.9, 94.1, 89.4, 86.3, 40.2 (one carbon not observed); EIMS 468 (M^+, 100); HRMS calcd. for $C_{32}H_{24}N_2O_2$ 468.1838, found 468.1833.

V. REFERENCES

(1) (a) Bosshard, C.; Sutter, K.; Prêtre, P.; Hulliger, J.; Flörsheimer, M.; Kaatz, P.; Günter, P. *Organic Nonlinear Optical Materials*; Gordon and Breach: Basel, **1995**. (b) Nalwa, H. S.; Miyata, S. *Nonlinear Optics of Organic Molecules and Polymers*; CRC Press: Boca Raton, FL, **1997**. (c) Skotheim, T. A.; Elsenbaumer, R. L.; Reynolds, J. R. *Handbook of Conducting Polymers*; 2nd ed.; Marcel Dekker, Inc.: New York, **1997**. (d) Agrawal, G. P.; Boyd, R. W. *Contemporary Nonlinear Optics*; Academic Press, Inc.: San Diego, CA, **1992**. (e) Wegner, G.; Müllen, K. *Electronic Materials – the Oligomer Approach*; Wiley-VCH: Weinheim, **1998**.

(2) Prasad, P. N.; Williams, D. J. *Introduction to Nonlinear Optical Effects in Molecules and Polymers*; John Wiley & Sons, Inc.: New York, **1991**.

(3) Cassidy, C.; Halbout, J. M.; Donaldson, W.; Tang, C. L. *Opt. Commun.* **1979**, *29*, 243.

(4) Oudar, J. L.; Chemla, D. S. *J. Chem. Phys.* **1977**, *66*, 2664.

(5) (a) Hutchings, M. G.; Ferguson, I.; McGeein, D. J.; Morley, J. O.; Zyss, J.; Ledoux, I. *J. Chem. Soc., Perkin Trans. 2* **1995**, 171. (b) Steybe, F.; Effenberger, F.; Gubler, U.; Bosshard, C.; Günter, P. *Tetrahedron* **1998**, *54*, 8469. (c) Marder, S. R.; Gorman, C. B.; Meyers, F.; Perry, J. W.; Bourhill, G.; Brédas, J.-L.; Pierce, B. M. *Science (Washington, D.C.)* **1994**, *265*, 632. (d) Alain, V.; Rédoglia, S.; Blanchard-Desce, M.; Lebus, S.; Lukaszuk, K.; Wortmann, R.; Gubler, U.; Bosshard, C.; Günter, P. *Chem. Phys.* **1999**, *245*, 51. (e) Cheng, L.-T.; Tam, W.;

Marder, S. R.; Stiegman, A. E.; Rikken, G.; Spangler, C. W. *J. Phys. Chem.* **1991**, *95*, 10643. (f) Moylan, C. R.; Twieg, R. J.; Lee, V. Y.; Swanson, S. A.; Betterton, K. M.; Miller, R. D. *J. Am. Chem. Soc.* **1993**, *115*, 12599. (g) Brédas, J.-L. *Conjugated Oligomers, Polymers, and Dendrimers: From Polyacetylene to DNA*: De Boeck & Larcier, Brussels, **1999**; Chapter 15, page 425. (h) Mladenova, M.; Ventelon, L.; Blanchard-Desce, M. *Tetrahedron Lett.* **1999**, *40*, 6923.

(6) Krausz, F.; Wintner, E.; Leising, G. *Phys. Rev. B* **1989**, *39*, 3701.

(7) (a) Painelli, A. *Chem. Phys.* **1999**, *245*, 185. (b) Tretiak, S.; Chernyak, V.; Mukamel S. *Chem. Phys Lett.* **1998**, *287*, 75.

(8) (a) Alain, V.; Thouin, L.; Blanchard-Desce, M.; Gubler, U.; Bosshard, C.; Günter, P.; Muller, J.; Fort, A.; Barzoukas, M. *Adv. Mat.* **1999**, *11*, 1210. (b) Plaza, P.; Laage, D.; Martin, M. M.; Alain, V.; Blanchard-Desce, M.; Thompson, W. H.; Hynes, J. T. *J. Phys. Chem. A* **2000**, *104*, 2396.

(9) Marder, S. R.; Cheng, L.-T.; Tiemann, B. G.; Friedli, A. C.; Blanchard-Desce, M.; Perry, J. W.; Skindhoj, J. *Science* (Washington, D.C.) **1994**, *263*, 511.

(10) (a) Hendrickx, E.; Clays, K.; Persoons, A.; Dehu, C.; Brédas, J.-L. *J. Am. Chem. Soc.* **1995**, *117*, 3547. (b) Barzoukas, M.; Blanchard-Desce, M.; Josse, D.; Lehn, J.-M.; Zyss, J. *Chem. Phys.* **1989**, *133*, 323.

(11) a) Eckert, K.; Schröder, A.; Hartmann, H. *Eur. J. Org. Chem.* **2000**, 1327. b) Müller, T.; Robert, J. P.; Schmälzlin, E.; Bräuchle, C.; Meerholz, K. *Org. Lett.* **2000**, *2*, 2419. c) Cai, C.; Liakatas, I.; Wong, M.-S.; Bösch, M.; Bosshard, C.; Günter, P.; Concilio, S.; Tirelli, N.; Suter, U. *Org. Lett.* **1999**, *1*, 1847. d) Rajca, A.; Wang, H.; Pink, M.; Rajca, S. *Angew. Chem. Int. Ed.* **2000**, *39*, 4481. e) Van

Keuren, E.; Wakebe, T.; Andreaus, R.; Möhwald, H.; Schrof, W.; Belov, V.; Matsuda, H.; Rangel-Rojo, R. *Appl. Phys. Lett.* **1999**, *75*, 3312. f) Keshari, V.; Wijekoon, W. M. K. P.; Prasad, P. N.; Karna, S. P. *J. Phys. Chem.* **1995**, *99*, 9045. g) Adant, C.; Brédas, J.-L.; Dupuis, M. *J. Phys. Chem. A* **1997**, *101*, 3025. h) Yamaguchi, S.; Tamao, K. *J. Chem. Soc., Dalton Trans.* **1998**, 3693. i) Nerenz, H.; Meier, M.; Grahn, W.; Reisner, A.; Schmälzlin, E.; Stadler, S.; Meerholz, K.; Bräuchle, C.; Jones, P. *J. Chem., Perkin Trans. 2* **1998**, 437.

(12) Morley, J. *J. Chem. Soc., Faraday Trans.* **1991**, *87*, 3009.

(13) Kirsch, G.; Prim, D.; Leising, F.; Mignani, G. *J. Heterocyclic Chem.* **1994**, *31*, 1005.

(14) Kim, O.-K.; Fort, A.; Barzoukas, M.; Blanchard-Desce, M.; Lehn, J.-M. *J. Mater. Chem.* **1999**, *9*, 2227.

(15) Marder, S. R.; Perry, J.; Tiemann, B.; Gorman, C.; Gilmour, S.; Biddle, S.; Bourhill, G. *J. Am. Chem. Soc.* **1993**, *115*, 2524.

(16) Blanchard-Desce, M.; Alain, V.; Bedworth, P.; Marder, S. R.; Fort, A.; Runser, C.; Barzoukas, M.; Lebus, S.; Wortmann, R. *Chem. Eur. J.* **1997**, *3*, 1091.

(17) Albert, I. D. L.; Marks, T. J.; Ratner, M. A. *J. Am. Chem. Soc.* **1977**, *119*, 6575.

(18) (a) Breitung, E. M.; Shu, C.-F.; McMahon, R. J. *J. Am. Chem. Soc.* **2000**, *122*, 1154. (b) Wang,Y.-K.; Shu, C.-F.; Breitung, E. M.; McMahon, R. J. *J. Mater. Chem.* **1999**, *9*, 1449.

(19) van Walree, C. A.; Franssen, O.; Marsman, A. W.; Flipse, M. C.; Jenneskens, L. W. *J. Chem. Soc., Perkin Trans. 2* **1997**, 803.

(20) Cheng, L.-T.; Tam, W.; Stevenson, S. H.; Meredith, G. R.; Rikken, G.; Marder, S. R. *J. Phys. Chem.* **1991**, *95*, 10631.

(21) (a) Stiegman, A. E.; Miskowski, V. M.; Perry, J. W.; Coulter, D. R. *J. Am. Chem. Soc.* **1987**, *109*, 5884. (b) Graham, E. M.; Miskowski, V. M.; Perry, J. W.; Coulter D. R.; Stiegman, A. E.; Schaefer, W. P.; Marsh, R. E. *J. Am. Chem. Soc.* **1989**, *111*, 8771. (c) Stiegman, A. E.; Graham, E.; Perry, K. J.; Khundkar, L. R.; Cheng, L.-T.; Perry, J. W. *J. Am. Chem. Soc.* **1991**, *113*, 7658.

(22) Wong, M. S.; Nicoud, J.-F. *Tetrahedron Lett.* **1994**, *35*, 6113.

(23) Schreiber, M.; Anthony, J.; Diederich, F.; Spahr, M. E.; Nesper, R.; Hubrich, M.; Bommeli, F.; Degiorgi, L.; Wachter, P.; Kaatz, P.; Bosshard, C.; Günter, P.; Colussi, M.; Suter, U. W.; Boudon, C.; Gisselbrecht, J.-P.; Gross, M. *Adv. Mater.* **1994**, *6*, 786.

(24) a) Martin, R. E.; Bartek, J.; Diederich, F.; Tykwinski, R. R.; Meister, E. C.; Hilger, A.; Lüthi, H. P *J. Chem. Soc., Perkin Trans. 2* **1998**, 233. b) Tykwinski, R. R.; Diederich, F. *Liebigs. Ann.* **1997**, 649.

(25) Martin, R. E.; Gubler, U.; Boundon, C.; Bosshard, C.; Gisselbrecht, J.-P.; Günter, P.; Gross, M.; Diederich, F. *Chem. Eur. J.* **2000**, 4400.

(26) (a) Alain, V.; Blanchard-Desce, M.; Ledoux-Rak, I.; Zyss, J. *Chem. Commun.* **2000**, 353. (b) Endtner, J.; Effenberger, F.; Hartschuh, A.; Port, H. *J. Am. Chem. Soc.* **2000**, *122*, 3037. (c) Lambert, C.; Schmälzin, E.; Meerholz, K.; Bräuchle, C. *Chem. Eur. J.* **1998**, *4*, 512.

(27) Nicoud, J.-F.; Serbutoviez, C.; Barrans, Y.; Chasseau, D.; Gautier-Luneau, I.; Ledoux, I.; Zyss, J. *Nonlinear Opt.* **1995**, *9*, 127.

(28) Morley, J.; Docherty, V.; Pugh, D. *J. Chem. Soc., Perkin Trans. 2* **1987**, 1351.

(29) Ledoux, I.; Zyss, J.; Jutand, A.; Amatore, C. *Chem. Phys.* **1991**, *150*, 117.

(30) (a) Ledoux, I.; Zyss, J.; Siegel, J.; Brienne, J.; Lehn, J.-M. *Chem. Phys. Lett.* **1990**, *172*, 440. (b) Brédas, J.-L.; Meyers, F.; Pierce, B.; Zyss, J. *J. Am. Chem. Soc.* **1992**, *114*, 4928. (c) Zyss, J.; Ledoux, I. *Chem. Rev.* **1994**, *94*, 77.

(31) (a) Chérioux, F.; Maillotte, H.; Audebert, P.; Zyss, J. *Chem. Comm.* **1999**, 2083. (b) Wortmann, R.; Glania, C.; Krämer, P.; Matschiner, R.; Wolff, J. J.; Kraft, S.; Treptow, B.; Barbu E.; Längle, D.; Görlitz, G. *Chem. Eur. J.* **1997**, *3*, 1765. (c) Sastre, A.; Torres, T.; Diaz-Garcia, M. A.; Aguiló-López, F.; Dhenaut, C.; Brasselet, S.; Ledoux, I.; Zyss, J. *J. Am. Chem. Soc.* **1996**, *118*, 2746. (d) Di Bella, S.; Fragala, I.; Ledoux, I.; Zyss, J. *Chem. Eur. J.* **2001**, *7*, 3738. (e) Lambert, C.; Nöll, G.; Schmäzlin, E.; Meerholz, K.; Bräuchle, C. *Chem. Eur. J.* **1998**, *4*, 2129. (f) Wolff, J. J.; Siegler, F.; Matschiner, R.; Wortmann, R. *Angew. Chem. Int. Ed.* **2000**, *39*, 1436.

(32) (a) Lequan, M.; Branger, C.; Simon, J.; Thami, T.; Chauchard, E.; Persoon, A. *Adv. Mater.* **1994**, *6*, 851. (b) Blanchard-Desce, M.; Baudin, J.-B.; Ruel, O.; Jullien, L.; Brasselet, S.; Zyss, J. *Optical Materials* **1998**, *9*, 277. (c) Brasselet, S.; Cherioux, F.; Audebert, P.; Zyss, *J. Chem. Mater.* **1999**, *11*, 1915.

(33) Blanchard-Desce, M.; Baudin, J.-B.; Jullien, L.; Lorne, R.; Ruel, O.; Brasselet, S.; Zyss, J. *Opt. Mater.* **1999**, *12*, 333.

(34) (a) Morley, J.; Docherty, V.; Pugh, D. *J. Chem. Soc., Perkin Trans. 2* **1987**, 1361. (b) Ulman, A.; Willand, C.; Kohler, W.; Robello, D.; Williams, D.; Handley, L. *J. Am. Chem. Soc.* **1990**, *112*, 7083.

(35) (a) Wong, K.; Han, S.; Vardeny Z.; Shinar, J.; Pang, Y.; Ijadi-Maghsoodi, S.; Barton, T.; Grigoras, S.; Parbhoo, B. *Appl. Phys. Lett.* **1991**, *58*, 1695. (b) Moreau, C.; Serein-Spirau, F.; Létard, J.-F.; Lapouyade, R.; Jonusauskas, G.; Rullière, C. *J. Phys. Chem. B* **1998**, *102*, 1487. (c) Hissink, D.; van Hutten, P. F.; Hadziioannou, G.; van Bolhuis, F. *J. Organomet. Chem.* **1993**, *454*, 25.

(36) Zyss, J. *Molecular Nonlinear Optics: Materials, Physics, and Devices*; Academic Press, Inc.: San Diego, CA, 1994; Chapter 4.

(37) Mignani, G.; Barzoukas, M.; Zyss, J.; Soula, G.; Balegroune, F.; Grandjean, D.; Josse, D. *Organometallics* **1991**, *10*, 3661.

(38) Tsunekawa, T.; Gotho, T.; Iwamoto, M. *Chem. Phys. Lett.* **1990**, *166*, 353.

(39) (a) Maslak, P. *Adv. Mater.* **1994**, *6*, 405. (b) Maslak, P.; Chopra, A.; Moylan, C. R.; Wortmann, R.; Lebus, S.; Rheingold, A. L.; Yap, G. P. A. *J. Am. Chem. Soc.* **1996**, *118*, 1471. (c) Abe, J.; Shirai, Y.; Nemoto, N.; Nagase, Y. *J. Phys. Chem. A* **1997**, *101*, 1.

(40) Luo, Y.; Norman, P.; Ågren, H. *Chem. Phys. Lett.* **1999**, *303*, 616.

(41) Kim, S.; Lee, M.; Boo, B. *J. Chem. Phys.* **1998**, *109*, 2593.

(42) Schweig, A.; Weidner, U.; Hill, R.; Cullison, D. *J. Am. Chem. Soc.* **1973**, *95*, 5426.

(43) a) Gleiter, R.; Uschmann, J. *J. Org. Chem.* **1986**, *51*, 370. b) Dürr, H.; Gleiter, R. *Angew. Chem. Int. Ed.* **1978**, *17*, 559.

(44) Gleiter, R.; Hoffmann, H.; Irngartinger, H.; Nixdorf, M. *Chem. Ber.* **1994**, *127*, 2215.

(45) Phelan, N.; Orchin, M. *J. Chem. Educ.* **1968**, *45*, 633.

(46) Hopf, H. *Classics in Hydrocarbon Chemistry* Wiley-VCH: Weinheim, New York, **2000**; Chapter 11.

(47) Maertens, C.; Detrembleur, C.; Dubois, P.; Jérôme, R.; Boutton, C.; Persoons, A.; Kogej, T.; Brédas, J.-L. *Chem. Eur. J.* **1999**, *5*, 369.

(48) Rubin, Y.; Knoebler, C.; Diederich, F. *Angew. Chem. Int. Ed.* **1991**, *30*, 698.

(49) (a) Boldi, A. M.; Anthony, J.; Gramlich, V.; Knobler, C. B.; Boudon, C.; Gisselbrecht, J.-P.; Gross, M.; Diederich, F. *Helv. Chim. Acta* **1995**, *78*, 779. (b) Anthony, J.; Boldi, A. M.; Rubin, Y.; Hobi, M.; Gramlich, V.; Knobler, C. B.; Seiler, P.; Diederich, F. *Helv. Chim. Acta* **1995**, *78*, 13. (c) Diederich, F. *Nature* **1994**, *369*, 199. (d) Anthony, J.; Boudon, C.; Diederich, F.; Gisselbrecht, J.-P.; Gramlich, V.; Gross, M.; Hobi, M.; Seiler, P. *Angew. Chem. Int. Ed. Engl.* **1994**, *33*, 763. (e) Diederich, F. *Chem. Commun.* **2001**, *3*, 219. (f) Anthony, J.; Boldi, A. M.; Boudon, C.; Gisselbrecht, J.-P.; Gross, M.; Seiler, P.; Knobler, C. B.; Diederich, F. *Helv. Chim. Acta*, **1995**, *78*, 797.

(50) (a) Tykwinski, R. R.; Schreiber, M.; Gramlich, V.; Seiler, P.; Diederich, F. *Adv. Mater.* **1996**, *8*, 226. (b) Tykwinski, R. R.; Schreiber, M.; Carlon, R.; Diederich, F.; Gramlich, V. *Helv. Chim. Acta* **1996**, *79*, 2249.

(51) Takahashi, S.; Kuroyama, Y.; Sonogashira, K.; Hagihara, N. *Synthesis* **1980**, 627.

(52) Spreiter, R.; Bosshard, C.; Knöpfle, G.; Günter, P.; Tykwinski, R. R.; Schreiber, M.; Diederich, F. *J. Phys. Chem. B* **1998**, *102*, 29.

(53) Tykwinski, R. R.; Gubler, U.; Martin, R. E.; Diederich, F.; Bosshard, C.; Günter, P. *J. Phys. Chem. B* **1998**, *102*, 4451.

(54) (a) Zhao, Y.; Tykwinski, R. R. *J. Am. Chem. Soc.* **1999**, *121*, 458. (b) Zhao, Y.; Campbell, K.; Tykwinski, R.R. *J. Org. Chem.* **2002**, *67*, 336.

(55) Zhao, Y.; McDonald, R.; Tykwinski, R. R. *Chem. Commun.* **2000**, 77.

(56) Zhang, Y.; Jen, A. K.-Y.; Chen, T.-A.; Liu, Y.-J.; Zhang, X.-Q.; Kenney, J. T. *Proc. SPIE* **1997**, *3006*, 372.

(57) (a) Thayumanavan, S.; Mendez, J.; Marder, S. R. *J. Org. Chem.* **1999**, *64*, 4289. (b) Zhang, J. X.; Dubois, P.; Jérôme, R. *J. Chem. Soc., Perkin Trans. 2* **1997**, 1209. (c) Serbutoviez, C.; Bosshard, Ch.; Knopfle, G.; Wyss, P.; Pretre, P.; Günter, P.; Schenk, K.; Solari, E.; Chapuis, G. *Chem. Mater.* **1995**, *7*, 1198.

(58) Stang, P. J.; Fisk, T. E. *Synthesis* **1979**, 438-440.

(59) Dawson, D. J.; Frazier, J. D.; Brock, P. J.; Twieg, R. J. in *Polymers for High Technology*; ACS: Washington, D.C., **1987**; Vol. 346, page 445.

(60) Pretsch, E.; Seibl, J.; Simon, W.; Clerc. T. *Tables of Spectral Data for Structure Determination of Organic Compounds*; Springer-Verlag: Berlin, **1989**; page C90.

(61) Sorrell, T. N. *Interpreting Spectra of Organic Molecules*; University Science Books: Mill Valley, California, **1988**; page 37.

(62) Eisler, S.; Tykwinski, R.R *Angew. Chem. Int. Ed.* **1999**, *38*, 1941.

(63) Leonard, K.; Nelen, M.; Raghu, M.; Detty, M. R. *J. Heterocycl. Chem.* **1999**, *36*, 707.

(64) Zhao, Y.; Tykwinski, R.R., unpublished results.

VI. APPENDIX

1. Selected Crystallographic Data For Monomers 116, 117 and 129

A. Selected X-Ray Crystallographic data for 3-(*para-N,N*-dimethylaminophenyl)ethynyl-4-methyl-1-triisopropylsilyl-pent-3-en-1-yne 116

Table 4 Crystallographic Experimental Details

A. Crystal Data	
formula	$C_{25}H_{37}NSi$
formula weight	379.65
crystal dimensions (mm)	0.42 × 0.22 × 0.18
crystal system	triclinic
space group	$P\bar{1}$ (No. 2)
unit cell parameters[a]	
a (Å)	8.8003 (6)
b (Å)	13.6654 (10)
c (Å)	20.8790 (14)
α (deg)	90.7840 (10)
β (deg)	94.8880 (10)
γ (deg)	93.1440 (10)
V (Å^3)	2497.6 (3)
Z	4
ρ_{calcd} (g cm^{-3})	1.010
μ (mm^{-1})	0.103
B. Data Collection and Refinement Conditions	
diffractometer	Bruker P4/RA/SMART 1000 CCD[b]

radiation (λ [Å])	graphite-monochromated Mo Kα (0.71073)
temperature (°C)	22[c]
scan type	ϕ rotations (0.3°) / ω scans (0.3°) (20 s exposures)
data collection 2θ limit (deg)	51.50
total data collected	13484 ($-10 \le h \le 10$, $-16 \le k \le 16$, $-25 \le l \le 22$)
independent reflections	9449
number of observations (*NO*)	3918 ($F_o^2 \ge 2\sigma(F_o^2)$)
structure solution method	direct methods (*SHELXS–86*[d])
refinement method	full-matrix least-squares on F^2 (*SHELXL–93*[e])
absorption correction method	*SADABS*
range of transmission factors	0.9879–0.6820
data/restraints/parameters	9449 [$F_o^2 \ge -3\sigma(F_o^2)$] / 0 / 495
goodness-of-fit (S)[f]	0.840 [$F_o^2 \ge -3\sigma(F_o^2)$]
final R indices[g]	
$F_o^2 > 2\sigma(F_o^2)$	$R_1 = 0.0543$, $wR_2 = 0.1187$
all data	$R_1 = 0.1480$, $wR_2 = 0.1477$
largest difference peak and hole	0.146 and –0.181 e Å^{-3}

[a] Obtained from least-squares refinement of 4292 centered reflections.

[b] Programs for diffractometer operation, data collection, data reduction and absorption correction were those supplied by Bruker

[c] Data collection was attempted at –80 °C but at this temperature the crystal undergoes a phase change, with concomitant loss of data quality.

[d] Sheldrick, G. M. *Acta Crystallogr.* **1990**, *A46*, 467–473.

[e]Sheldrick, G. M. *SHELXL-93*. Program for crystal structure determination. University of Göttingen, Germany, 1993. Refinement on F_o^2 for all reflections (all of these having $F_o^2 \geq -3\sigma(F_o^2)$). Weighted R-factors wR_2 and all goodnesses of fit S are based on F_o^2; conventional R-factors R_1 are based on F_o, with F_o set to zero for negative F_o^2. The observed criterion of $F_o^2 > 2\sigma(F_o^2)$ is used only for calculating R_1, and is not relevant to the choice of reflections for refinement. R-factors based on F_o^2 are statistically about twice as large as those based on F_o, and R-factors based on ALL data will be even larger.

[f]$S = [\Sigma w(F_o^2 - F_c^2)^2/(n-p)]^{1/2}$ (n = number of data; p = number of parameters varied; $w = [\sigma^2(F_o^2) + (0.0600P)^2]^{-1}$ where $P = [\mathrm{Max}(F_o^2, 0) + 2F_c^2]/3$).

[g]$R_1 = \Sigma||F_o| - |F_c||/\Sigma|F_o|$; $wR_2 = [\Sigma w(F_o^2 - F_c^2)^2/\Sigma w(F_o^4)]^{1/2}$.

Table 5 Selected Interatomic Distances (Å)

(a) Molecule A			*(b) Molecule B*		
Atom1	Atom2	Distance	Atom1	Atom2	Distance
Si	C1	1.821(3)	Si	C1	1.839(3)
Si	C11	1.871(3)	Si	C11	1.866(3)
Si	C14	1.871(3)	Si	C14	1.872(3)
Si	C17	1.869(3)	Si	C17	1.877(3)
N	C24	1.367(4)	N	C24	1.370(4)
N	C27	1.444(4)	N	C24	1.439(4)
N	C28	1.431(4)	N	C28	1.452(4)
C1	C2	1.200(3)	C1	C2	1.200(3)
C2	C3	1.448(4)	C2	C3	1.440(4)
C3	C4	1.442(4)	C3	C4	1.444(4)
C3	C6	1.335(4)	C3	C6	1.339(4)
C4	C5	1.193(4)	C4	C5	1.182(4)
C5	C21	1.433(4)	C5	C21	1.434(4)

C6	C7	1.492(4)	C6	C7	1.498(4)
C6	C8	1.490(4)	C6	C8	1.488(4)
C11	C12	1.529(4)	C11	C12	1.517(4)
C11	C13	1.521(4)	C11	C13	1.514(4)
C14	C15	1.539(4)	C14	C15	1.520(4)
C14	C16	1.510(4)	C14	C16	1.523(4)
C17	C18	1.514(4)	C17	C18	1.522(4)
C17	C19	1.503(4)	C17	C19	1.497(4)
C21	C22	1.385(4)	C21	C22	1.386(4)
C21	C26	1.380(4)	C21	C26	1.374(4)
C22	C23	1.372(4)	C22	C23	1.378(4)
C23	C24	1.395(4)	C23	C24	1.384(4)
C24	C25	1.391(4)	C24	C25	1.394(4)
C25	C26	1.367(4)	C25	C26	1.365(4)

Table 6 Selected Interatomic Angles (deg)

(a) Molecule A				*(b) Molecule B*			
Atom1	Atom2	Atom3	Angle	Atom1	Atom2	Atom3	Angle
C1	Si	C11	106.64(13)	C1	Si	C11	107.95(12)
C1	Si	C14	106.96(13)	C1	Si	C14	106.04(13)
C1	Si	C17	106.91(14)	C1	Si	C17	107.18(13)
C11	Si	C14	109.80(15)	C11	Si	C14	109.47(14)
C11	Si	C17	110.35(16)	C11	Si	C17	109.68(13)
C14	Si	C17	115.70(14)	C14	Si	C17	116.14(14)
C24	N	C27	120.6(3)	C24	N	C27	121.5(3)
C24	N	C28	121.2(3)	C24	N	C28	121.0(3)
C27	N	C28	117.8(3)	C27	N	C28	117.1(3)
Si	C1	C2	177.6(3)	Si	C1	C2	175.7(3)
C1	C2	C3	178.3(3)	C1	C2	C3	178.5(3)
C2	C3	C4	114.6(3)	C2	C3	C4	116.5(3)
C2	C3	C6	122.1(3)	C2	C3	C6	121.0(3)

C4	C3	C6	123.3(3)	C4	C3	C6	122.5(3)
C3	C4	C5	178.4(4)	C3	C4	C5	179.3(3)
C4	C5	C21	178.4(3)	C4	C5	C21	177.6(3)
C3	C6	C7	121.4(3)	C3	C6	C7	122.5(3)
C3	C6	C8	121.5(3)	C3	C6	C8	122.1(3)
C7	C6	C8	117.0(3)	C7	C6	C8	115.4(3)
Si	C11	C12	112.7(2)	Si	C11	C12	113.1(2)
Si	C11	C13	111.7(2)	Si	C11	C13	113.2(2)
C12	C11	C13	109.8(3)	C12	C11	C13	109.3(2)
Si	C14	C15	113.6(2)	Si	C14	C15	114.6(2)
Si	C14	C16	115.5(2)	Si	C14	C16	115.6(2)
C15	C14	C16	111.5(3)	C15	C14	C16	110.5(3)
Si	C17	C18	114.6(2)	Si	C17	C18	114.1(2)
Si	C17	C19	115.8(2)	Si	C17	C19	115.3(2)
C18	C17	C19	111.7(3)	C18	C17	C19	111.9(2)
C5	C21	C22	120.8(3)	C5	C21	C22	122.4(3)
C5	C21	C26	122.8(3)	C5	C21	C26	121.5(3)
C22	C21	C26	116.4(3)	C22	C21	C26	116.1(3)
C21	C22	C23	121.7(3)	C21	C22	C23	121.9(3)
C22	C23	C24	121.6(3)	C22	C23	C24	121.5(3)
N	C24	C23	121.2(3)	N	C24	C23	121.9(3)
N	C24	C25	122.5(3)	N	C24	C25	121.8(3)
C23	C24	C25	116.4(3)	C23	C24	C25	116.3(3)
C24	C25	C26	121.3(3)	C24	C25	C26	121.4(3)
C21	C26	C25	122.6(3)	C21	C26	C25	122.8(3)

Table 7 Torsional Angles (deg)

(a) Molecule A

Atom1	Atom2	Atom3	Atom4	Angle
C11	Si	C1	C2	98(7)
C14	Si	C1	C2	-145(7)

(b) Molecule B

Atom1	Atom2	Atom3	Atom4	Angle
C11	Si	C1	C2	-116(3)
C14	Si	C1	C2	1(3)

C17	Si	C1	C2	-20(7)
C1	Si	C11	C12	-66.6(3)
C1	Si	C11	C13	57.5(3)
C14	Si	C11	C12	177.9(2)
C14	Si	C11	C13	-58.0(3)
C17	Si	C11	C12	49.2(3)
C17	Si	C11	C13	173.3(2)
C1	Si	C14	C15	-169.4(2)
C1	Si	C14	C16	59.9(2)
C11	Si	C14	C15	-54.1(3)
C11	Si	C14	C16	175.2(2)
C17	Si	C14	C15	71.6(3)
C17	Si	C14	C16	-59.1(3)
C1	Si	C17	C18	175.7(3)
C1	Si	C17	C19	-52.0(3)
C11	Si	C17	C18	60.1(3)
C11	Si	C17	C19	-167.6(3)
C14	Si	C17	C18	-65.3(3)
C14	Si	C17	C19	67.0(3)
C27	N	C24	C23	-1.7(4)
C27	N	C24	C25	178.6(3)
C28	N	C24	C23	-174.6(3)
C28	N	C24	C25	5.7(5)
Si	C1	C2	C3	-42(16)
C1	C2	C3	C4	-44(11)
C1	C2	C3	C6	136(10)
C2	C3	C4	C5	-79(13)
C6	C3	C4	C5	102(12)
C2	C3	C6	C7	-176.7(3)
C2	C3	C6	C8	2.0(5)
C4	C3	C6	C7	2.5(5)

C17	Si	C1	C2	126(3)
C1	Si	C11	C12	-66.1(2)
C1	Si	C11	C13	58.9(2)
C14	Si	C11	C12	178.9(2)
C14	Si	C11	C13	-56.1(2)
C17	Si	C11	C12	50.4(2)
C17	Si	C11	C13	175.4(2)
C1	Si	C14	C15	-173.3(2)
C1	Si	C14	C16	56.5(2)
C11	Si	C14	C15	-57.0(3)
C11	Si	C14	C16	172.7(2)
C17	Si	C14	C15	67.8(3)
C17	Si	C14	C16	-62.4(3)
C1	Si	C17	C18	175.3(2)
C1	Si	C17	C19	-53.1(3)
C11	Si	C17	C18	58.3(3)
C11	Si	C17	C19	-170.1(2)
C14	Si	C17	C18	-66.4(3)
C14	Si	C17	C19	65.2(3)
C27	N	C24	C23	0.6(5)
C27	N	C24	C25	-179.7(3)
C28	N	C24	C23	173.6(3)
C28	N	C24	C25	-6.8(5)
Si	C1	C2	C3	-21(14)
C1	C2	C3	C4	163(11)
C1	C2	C3	C6	-17(11)
C2	C3	C4	C5	90(29)
C6	C3	C4	C5	-90(29)
C2	C3	C6	C7	179.0(2)
C2	C3	C6	C8	-1.0(4)
C4	C3	C6	C7	-1.1(5)

C4	C3	C6	C8	-178.7(3)	C4	C3	C6	C8	178.9(3)
C3	C4	C5	C21	-99(18)	C3	C4	C5	C21	-29(34)
C4	C5	C21	C22	66(15)	C4	C5	C21	C22	129(7)
C4	C5	C21	C26	-111(15)	C4	C5	C21	C26	-50(8)
C5	C21	C22	C23	-177.8(3)	C5	C21	C22	C23	-179.2(3)
C26	C21	C22	C23	-0.1(4)	C26	C21	C22	C23	-0.5(5)
C5	C21	C26	C25	177.3(3)	C5	C21	C26	C25	178.8(3)
C22	C21	C26	C25	-0.3(5)	C22	C21	C26	C25	0.1(5)
C21	C22	C23	C24	0.6(4)	C21	C22	C23	C24	0.9(5)
C22	C23	C24	N	179.6(3)	C22	C23	C24	N	178.9(3)
C22	C23	C24	C25	-0.6(4)	C22	C23	C24	C25	-0.7(5)
N	C24	C25	C26	179.9(3)	N	C24	C25	C26	-179.4(3)
C23	C24	C25	C26	0.2(4)	C23	C24	C25	C26	0.3(4)
C24	C25	C26	C21	0.3(5)	C24	C25	C26	C21	0.0(5)

Table 8 Least-Squares Planes

(a) Molecule A

Plane	Coefficients^a				Defining Atoms with Deviations (Å)			
1	-4.593(14)	-6.20(2)	[illegible]	0.396(14)				
					C3	0.0025(10)	C6	-0.007(3)
					C7	0.0021(8)	C8	0.0021(8)
2	1.757(10)	12.430(7)	-7.61(2)	1.797(2)				
					C21	-0.001(2)	C22	-0.002(2)
					C23	0.004(2)	C24	-0.002(2)
					C25	-0.001(2)	C26	0.003(2)

Dihedral angle between planes 1 and 2: 71.56(11)°

(b) Molecule B

Plane	Coefficients^a				Defining Atoms with Deviations (Å)			
3	4.168(14)	6.53(2)	13.98(3)	8.716(3)				
					C3	0.0000(10)	C6	0.000(3)

					C7	0.0000(8)	C8	0.0000(8)
4	3.378(10)	8.576(14)	12.72(2)	8.775(5)				
					C21	0.001(2)	C22	-0.004(2)
					C23	0.004(2)	C24	-0.002(2)
					C25	-0.000(2)	C26	0.001(2)

Dihedral angle between planes 3 and 4: 10.5(2)°

[a] Coefficients are for the form $ax+by+cz = d$ where x, y and z are crystallographic coordinates.

B. Selected X-Ray Crystallographic data for 4-Methyl-3-(*para*-nitrophenyl)ethynyl-1-triisopropylsilyl-pent-3-en-1-yne 117

Table 9 Crystallographic Experimental Details

A. Crystal Data	
formula	$C_{23}H_{31}NO_2Si$
formula weight	381.58
crystal dimensions (mm)	0.45 × 0.22 × 0.18
crystal system	triclinic
space group	$P\bar{1}$ (No. 2)
unit cell parameters[a]	
a (Å)	7.7041 (5)
b (Å)	11.2582 (8)
c (Å)	13.1958 (9)
α (deg)	84.7476 (12)
β (deg)	82.7816 (16)
γ (deg)	77.0706 (12)
V (Å^3)	1104.29 (13)
Z	2
ρ_{calcd} (g cm^{-3})	1.148
μ (mm^{-1})	0.123
B. Data Collection and Refinement Conditions	
diffractometer	Bruker P4/RA/SMART 1000 CCD[b]
radiation (λ [Å])	graphite-monochromated Mo Kα (0.71073)
temperature (°C)	–80
scan type	ϕ rotations (0.3°) / ω scans (0.3°) (20 s

exposures)	
data collection 2θ limit (deg)	52.76
total data collected	5503 ($-9 \leq h \leq 7$, $-14 \leq k \leq 13$, $-11 \leq l \leq 16$)
independent reflections	4474
number of observed reflections (*NO*)	3415 [$F_o^2 \geq 2\sigma(F_o^2)$]
structure solution method	direct methods (*SHELXS–86*[c])
refinement method (*SHELXL–93*[d])	full-matrix least-squares on F^2
absorption correction method	Gaussian integration (face-indexed)
range of transmission factors	0.9789–0.9583
data/restraints/parameters	4474 [$F_o^2 \geq -3\sigma(F_o^2)$] / 0 / 246
goodness-of-fit (S)[e]	1.034 [$F_o^2 \geq -3\sigma(F_o^2)$]
final R indices[f]	
R_1 [$F_o^2 \geq 2\sigma(F_o^2)$]	0.0460
wR_2 [$F_o^2 \geq -3\sigma(F_o^2)$]	0.1272
largest difference peak and hole	0.308 and –0.271 e Å^{-3}

[a] Obtained from least-squares refinement of 4362 centered reflections.

[b] Programs for diffractometer operation, data collection, data reduction and absorption correction were those supplied by Bruker.

[c] Sheldrick, G. M. *Acta Crystallogr.* **1990,** *A46*, 467–473.

[d] Sheldrick, G. M. *SHELXL-93*. Program for crystal structure determination. University of Göttingen, Germany, 1993. Refinement on F_o^2 for all reflections (all of these having $F_o^2 \geq -3\sigma(F_o^2)$). Weighted R-factors wR_2 and all goodnesses of fit S are based on F_o^2; conventional R-factors R_1 are based on F_o, with F_o set to zero for negative F_o^2. The observed criterion of $F_o^2 > 2\sigma(F_o^2)$ is used only for calculating R_1, and is not relevant to the choice of reflections for refinement. R-factors based on F_o^2 are statistically about twice as large as those based on F_o, and R-factors based on ALL data will be even larger.

[e] $S = [\Sigma w(F_o^2 - F_c^2)^2/(n - p)]^{1/2}$ (n = number of data; p = number of parameters varied; $w = [\sigma^2(F_o^2) + (0.0685P)^2 + 0.1102P]^{-1}$ where $P = [\mathrm{Max}(F_o^2, 0) + 2F_c^2]/3$).

[f] $R_1 = \Sigma||F_o| - |F_c||/\Sigma|F_o|$; $wR_2 = [\Sigma w(F_o^2 - F_c^2)^2/\Sigma w(F_o^4)]^{1/2}$.

Table 10 Selected Interatomic Distances (Å)

Atom1	Atom2	Distance	Atom1	Atom2	Distance
Si	C1	1.8464(18)	C8	C21	1.439(2)
Si	C11	1.8864(18)	C11	C12	1.534(3)
Si	C14	1.8830(19)	C11	C13	1.538(3)

Si	C17	1.8852(17)	C14	C15	1.534(3)
O1	N	1.222(2)	C14	C16	1.529(3)
O2	N	1.231(3)	C17	C18	1.536(3)
N	C24	1.471(3)	C17	C19	1.538(3)
C1	C2	1.211(2)	C21	C22	1.401(2)
C2	C3	1.444(2)	C21	C26	1.392(3)
C3	C4	1.362(2)	C22	C23	1.380(3)
C3	C7	1.439(2)	C23	C24	1.372(3)
C4	C5	1.493(2)	C24	C25	1.387(3)
C4	C6	1.498(2)	C25	C26	1.376(3)
C7	C8	1.196(2)			

Table 11 Selected Interatomic Angles (deg)

Atom1	Atom2	Atom3	Angle	Atom1	Atom2	Atom3	Angle
C1	Si	C11	109.35(8)	Si	C11	C12	114.92(13)
C1	Si	C14	107.30(8)	Si	C11	C13	112.56(13)
C1	Si	C17	105.67(8)	C12	C11	C13	110.04(16)
C11	Si	C14	111.06(8)	Si	C14	C15	112.69(14)
C11	Si	C17	113.08(8)	Si	C14	C16	112.52(15)
C14	Si	C17	110.09(9)	C15	C14	C16	111.18(18)
O1	N	O2	123.9(2)	Si	C17	C18	112.72(13)
O1	N	C24	118.0(2)	Si	C17	C19	111.35(13)
O2	N	C24	118.05(19)	C18	C17	C19	110.39(15)
Si	C1	C2	171.88(14)	C8	C21	C22	120.84(16)
C1	C2	C3	176.82(17)	C8	C21	C26	120.14(16)
C2	C3	C4	121.28(16)	C22	C21	C26	118.99(17)
C2	C3	C7	117.80(14)	C21	C22	C23	120.29(17)
C4	C3	C7	120.92(16)	C22	C23	C24	119.04(16)
C3	C4	C5	121.67(16)	N	C24	C23	119.31(17)
C3	C4	C6	121.91(17)	N	C24	C25	118.41(19)
C5	C4	C6	116.42(15)	C23	C24	C25	122.26(18)
C3	C7	C8	177.52(19)	C24	C25	C26	118.29(18)
C7	C8	C21	176.42(19)	C21	C26	C25	121.11(17)

Table 12 Torsional Angles (deg)

Atom1	Atom2	Atom3	Atom4	Angle	Atom1	Atom2	Atom3	Atom4	Angle
C11	Si	C1	C2	138.5(11)	O2	N	C24	C25	20.0(3)
C14	Si	C1	C2	-100.9(11)	Si	C1	C2	C3	-6(4)
C17	Si	C1	C2	16.5(11)	C1	C2	C3	C4	-10(3)
C1	Si	C11	C12	-33.00(15)	C1	C2	C3	C7	170(3)
C1	Si	C11	C13	-160.02(13)	C2	C3	C4	C5	0.1(3)

C14	Si	C11	C12	-151.22(13)	C2	C3	C4	C6	-179.67(17)
C14	Si	C11	C13	81.75(15)	C7	C3	C4	C5	-179.75(17)
C17	Si	C11	C12	84.44(15)	C7	C3	C4	C6	0.5(3)
C17	Si	C11	C13	-42.58(16)	C2	C3	C7	C8	-168(4)
C1	Si	C14	C15	169.75(15)	C4	C3	C7	C8	12(5)
C1	Si	C14	C16	-63.57(17)	C3	C7	C8	C21	12(7)
C11	Si	C14	C15	-70.79(17)	C7	C8	C21	C22	145(3)
C11	Si	C14	C16	55.89(17)	C7	C8	C21	C26	-33(3)
C17	Si	C14	C15	55.23(17)	C8	C21	C22	C23	-177.87(17)
C17	Si	C14	C16	-178.09(15)	C26	C21	C22	C23	0.1(3)
C1	Si	C17	C18	61.30(15)	C8	C21	C26	C25	176.55(18)
C1	Si	C17	C19	-63.39(15)	C22	C21	C26	C25	-1.4(3)
C11	Si	C17	C18	-58.28(15)	C21	C22	C23	C24	0.8(3)
C11	Si	C17	C19	177.04(13)	C22	C23	C24	N	178.11(17)
C14	Si	C17	C18	176.85(13)	C22	C23	C24	C25	-0.3(3)
C14	Si	C17	C19	52.17(16)	N	C24	C25	C26	-179.42(18)
O1	N	C24	C23	19.5(3)	C23	C24	C25	C26	-1.0(3)
O1	N	C24	C25	-162.0(2)	C24	C25	C26	C21	1.8(3)
O2	N	C24	C23	-158.5(2)					

Table 13 Least-Squares Planes

Plane	Coefficients^a				Defining Atoms with Deviations			
(Å)^b								
1	3.757(4)	9.173(4)	7.804(8)	2.495(5)				
					C1	-0.0048(10)	C2	0.0052(14)
					C3	0.0030(15)	C4	-0.0036(8)
					C7	0.0049(15)	C8	-0.0047(10)
					Si	-0.094(2)	C5	-0.011(3)
					C6	0.001(3)		
2	3.005(6)	8.333(6)	9.474(8)	1.703(8)				
					C21	-0.0033(13)	C22	-0.0043(13)
					C23	0.0057(13)	C24	0.0004(14)
					C25	-0.0080(15)	C26	0.0095(14)
3	3.13(3)	10.372(13)	5.723(18)	4.55(5)				
					O1	O2	N	

Dihedral angle between planes 1 and 2: 10.44(10)°

Dihedral angle between planes 1 and 3: 12.6(3)°

Dihedral angle between planes 2 and 3: 20.3(2)°

[a]Coefficients are for the form $ax+by+cz = d$ where x, y and z are crystallographic coordinates.

[b]Underlined atoms were not included in the definition of the plane.

C. Selected X-Ray Crystallographic data for 5-(*para*-Dimethylaminophenyl)-3-cyclohexylidene-1-triisopropylsilyl-1,4-pentadiyne 129

Table 14 Crystallographic Experimental Details

A. Crystal Data	
formula	$C_{28}H_{41}NSi$
formula weight	419.71
crystal dimensions (mm)	0.36 × 0.31 × 0.04
crystal system	triclinic
space group	$P\bar{1}$ (No. 2)
unit cell parameters[a]	
a (Å)	9.0111 (10)
b (Å)	12.0833 (13)
c (Å)	13.6351 (15)
α (deg)	114.047 (2)
β (deg)	93.407 (2)
γ (deg)	93.899 (2)
V (Å^3)	1346.5 (3)
Z	2
ρ_{calcd} (g cm^{-3})	1.035
μ (mm^{-1})	0.101
B. Data Collection and Refinement Conditions	
diffractometer	Bruker P4/RA/SMART 1000 CCD[b]
radiation (λ [Å])	graphite-monochromated Mo Kα (0.71073)
temperature (°C)	–80
scan type	ϕ rotations (0.3°) / ω scans (0.3°) (30 s exposures)
data collection 2θ limit (deg)	52.82

total data collected	6728 ($-10 \leq h \leq 11$, $-10 \leq k \leq 15$, $-16 \leq l \leq 17$)
independent reflections	5442
number of observed reflections (*NO*)	2361 [$F_o^2 \geq 2\sigma(F_o^2)$]
structure solution method	direct methods (*SHELXS–86*[c])
refinement method	full-matrix least-squares on F^2 (*SHELXL–93*[d])
absorption correction method	Gaussian integration (face-indexed)
range of transmission factors	0.9959–0.9661
data/restraints/parameters	5442 [$F_o^2 \geq -3\sigma(F_o^2)$] / 0 / 273
goodness-of-fit (S)[e]	0.862 [$F_o^2 \geq -3\sigma(F_o^2)$]
final R indices[f]	
R_1 [$F_o^2 \geq 2\sigma(F_o^2)$]	0.0607
wR_2 [$F_o^2 \geq -3\sigma(F_o^2)$]	0.1434
largest difference peak and hole	0.180 and –0.198 e Å^{-3}

[a] Obtained from least-squares refinement of 2375 centered reflections.

[b] Programs for diffractometer operation, data collection, data reduction and absorption correction were those supplied by Bruker.

[c] Sheldrick, G. M. *Acta Crystallogr.* **1990,** *A46*, 467–473.

[d] Sheldrick, G. M. *SHELXL-93*. Program for crystal structure determination. University of Göttingen, Germany, 1993. Refinement on F_o^2 for all reflections (all of these having $F_o^2 \geq -3\sigma(F_o^2)$). Weighted R-factors wR_2 and all goodnesses of fit S are based on F_o^2; conventional R-factors R_1 are based on F_o, with F_o set to zero for negative F_o^2. The observed criterion of $F_o^2 > 2\sigma(F_o^2)$ is used only for calculating R_1, and is not relevant to the choice of reflections for refinement. R-factors based on F_o^2 are statistically about twice as large as those based on F_o, and R-factors based on ALL data will be even larger.

[e] $S = [\Sigma w(F_o^2 - F_c^2)^2/(n - p)]^{1/2}$ (n = number of data; p = number of parameters varied; $w = [\sigma^2(F_o^2) + (0.0540P)^2]^{-1}$ where $P = [\mathrm{Max}(F_o^2, 0) + 2F_c^2]/3$).

[f] $R_1 = \Sigma||F_o| - |F_c||/\Sigma|F_o|$; $wR_2 = [\Sigma w(F_o^2 - F_c^2)^2/\Sigma w(F_o^4)]^{1/2}$.

Table 15 Selected Interatomic Distances (Å)

Atom1	Atom2	Distance	Atom1	Atom2	Distance
Si	C1	1.837(3)	C13	C14	1.525(4)
Si	C21	1.874(3)	C14	C15	1.525(4)
Si	C24	1.866(3)	C15	C16	1.519(4)
Si	C27	1.879(3)	C21	C22	1.513(4)
N	C34	1.371(4)	C21	C23	1.524(4)

N	C37	1.451(4)
N	C38	1.435(4)
C1	C2	1.203(3)
C2	C3	1.449(4)
C3	C4	1.439(4)
C3	C11	1.359(3)
C4	C5	1.194(4)
C5	C31	1.440(4)
C11	C12	1.493(4)
C11	C16	1.513(3)
C12	C13	1.533(4)
C24	C25	1.535(4)
C24	C26	1.480(4)
C27	C28	1.515(4)
C27	C29	1.533(4)
C31	C32	1.395(4)
C31	C36	1.386(3)
C32	C33	1.369(4)
C33	C34	1.388(4)
C34	C35	1.397(4)
C35	C36	1.374(4)

Table 16 Selected Interatomic Angles (deg)

Atom1	Atom2	Atom3	Angle
C1	Si	C21	107.51(13)
C1	Si	C24	107.15(13)
C1	Si	C27	105.61(14)
C21	Si	C24	110.03(14)
C21	Si	C27	109.42(14)
C24	Si	C27	116.65(16)
C34	N	C37	120.7(4)
C34	N	C38	120.9(3)
C37	N	C38	118.3(3)
Si	C1	C2	176.4(3)
C1	C2	C3	177.6(3)
C2	C3	C4	115.6(2)
C2	C3	C11	121.9(3)
C4	C3	C11	122.5(2)
C3	C4	C5	179.2(3)
C4	C5	C31	176.6(3)
C3	C11	C12	123.6(2)
C3	C11	C16	121.2(3)
C12	C11	C16	115.2(2)
C11	C12	C13	111.8(2)
C12	C13	C14	111.8(3)
C13	C14	C15	110.3(2)
C14	C15	C16	111.0(3)
C11	C16	C15	110.5(3)
Si	C21	C22	112.0(2)
Si	C21	C23	112.9(2)
C22	C21	C23	109.5(3)
Si	C24	C25	114.3(2)
Si	C24	C26	117.0(3)
C25	C24	C26	111.8(3)
Si	C27	C28	116.3(3)
Si	C27	C29	114.3(2)
C28	C27	C29	111.2(3)
C5	C31	C32	121.8(3)
C5	C31	C36	121.7(3)
C32	C31	C36	116.5(3)
C31	C32	C33	121.5(3)
C32	C33	C34	121.7(3)
N	C34	C33	122.1(3)
N	C34	C35	120.7(3)
C33	C34	C35	117.2(3)
C34	C35	C36	120.5(3)
C31	C36	C35	122.5(3)

Table 17 Torsional Angles (deg)

Atom1	Atom2	Atom3	Atom4	Angle
C21	Si	C1	C2	-66(4)
C24	Si	C1	C2	176(4)
C27	Si	C1	C2	51(4)
C2	C3	C4	C5	-71(20)
C11	C3	C4	C5	109(20)
C2	C3	C11	C12	0.7(4)

C1	Si	C21	C22	56.9(2)
C1	Si	C21	C23	-67.2(3)
C24	Si	C21	C22	173.3(2)
C24	Si	C21	C23	49.1(3)
C27	Si	C21	C22	-57.3(2)
C27	Si	C21	C23	178.5(2)
C1	Si	C24	C25	174.7(2)
C1	Si	C24	C26	-51.7(3)
C21	Si	C24	C25	58.1(3)
C21	Si	C24	C26	-168.2(3)
C27	Si	C24	C25	-67.2(3)
C27	Si	C24	C26	66.4(3)
C1	Si	C27	C28	55.8(3)
C1	Si	C27	C29	-172.6(2)
C21	Si	C27	C28	171.3(2)
C21	Si	C27	C29	-57.1(3)
C24	Si	C27	C28	-63.1(3)
C24	Si	C27	C29	68.5(3)
C37	N	C34	C33	2.4(5)
C37	N	C34	C35	-177.3(3)
C38	N	C34	C33	-173.6(3)
C38	N	C34	C35	6.8(4)
Si	C1	C2	C3	106(8)
C1	C2	C3	C4	-17(7)
C1	C2	C3	C11	162(7)
C2	C3	C11	C16	-179.5(3)
C4	C3	C11	C12	-179.6(3)
C4	C3	C11	C16	0.1(4)
C3	C4	C5	C31	-94(20)
C4	C5	C31	C32	-126(5)
C4	C5	C31	C36	53(5)
C3	C11	C12	C13	130.3(3)
C16	C11	C12	C13	-49.5(3)
C3	C11	C16	C15	-127.9(3)
C12	C11	C16	C15	51.8(3)
C11	C12	C13	C14	50.9(3)
C12	C13	C14	C15	-55.9(4)
C13	C14	C15	C16	58.6(4)
C14	C15	C16	C11	-55.5(3)
C5	C31	C32	C33	176.9(3)
C36	C31	C32	C33	-2.3(4)
C5	C31	C36	C35	-177.6(2)
C32	C31	C36	C35	1.6(4)
C31	C32	C33	C34	1.0(5)
C32	C33	C34	N	-178.7(3)
C32	C33	C34	C35	1.0(4)
N	C34	C35	C36	178.0(3)
C33	C34	C35	C36	-1.7(4)
C34	C35	C36	C31	0.4(4)

Table 18 Least-Squares Planes

Plane	Coefficients[a]			(Å)[b]	Defining Atoms with Deviations			
1	-4.803(10)	-9.647(7)	3.57(3)	1.159(6)				
					C1	-0.0035(13)	C2	0.006(2)
					C3	0.0001(14)	C4	-0.007(2)
					C5	0.0038(13)		
					Si	0.097(5)		
2	-4.72(2)	-9.735(15)	3.68(5)	1.25(2)				
					C11	C12	C16	
3	1.420(9)	2.381(13)	10.666(10)	3.803(12)				
					C31	0.0128(18)	C32	-0.010(2)

C33	-0.001(2)	C34	0.011(2)
C35	-0.0086(19)	C36	-0.0033(18)

Dihedral angle between planes 1 and 2: 0.7(3)°

Dihedral angle between planes 1 and 3: 67.65(14)°

Dihedral angle between planes 2 and 3: 68.03(25)°

[a] Coefficients are for the form $ax+by+cz = d$ where x, y and z are crystallographic coordinates.

[b] Underlined atoms were not included in the definition of the plane.

2. NMR spectra

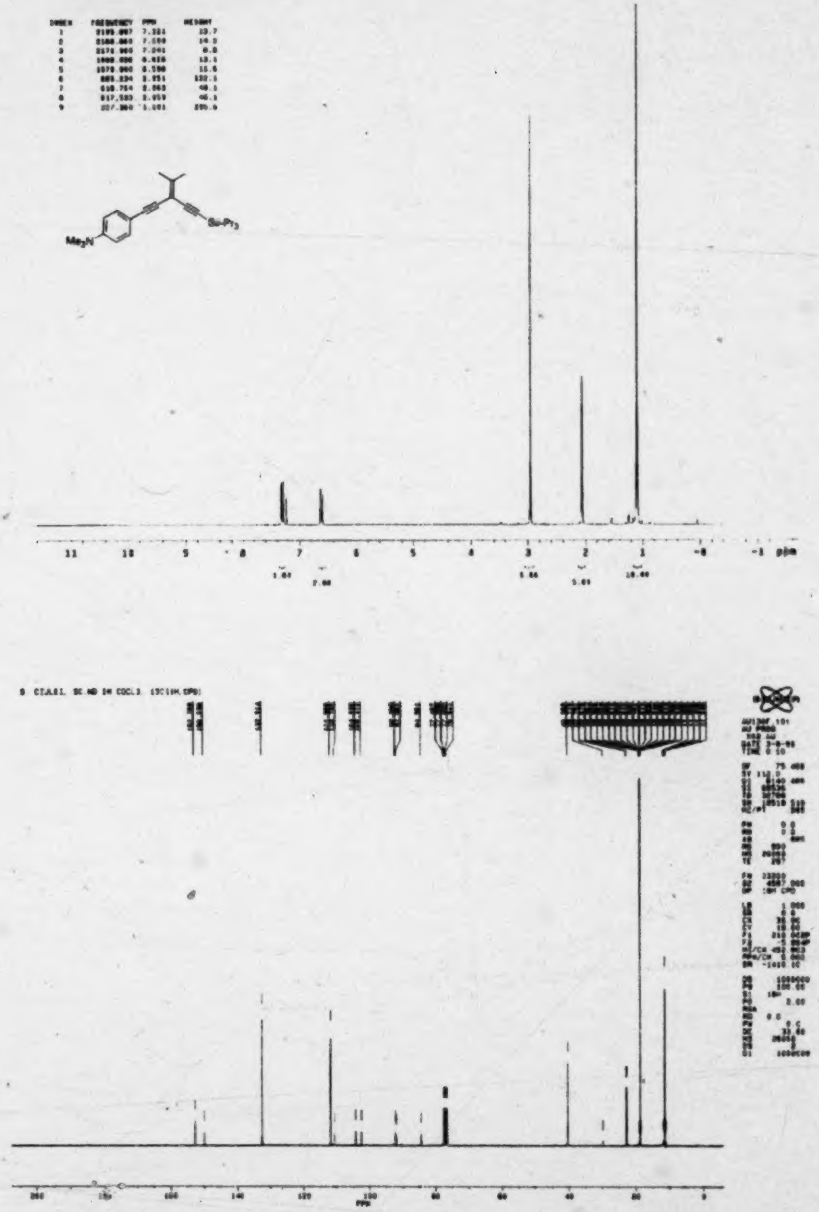

Fig. 6.1 ^{1}H and ^{13}C NMR spectra of compound **116**.

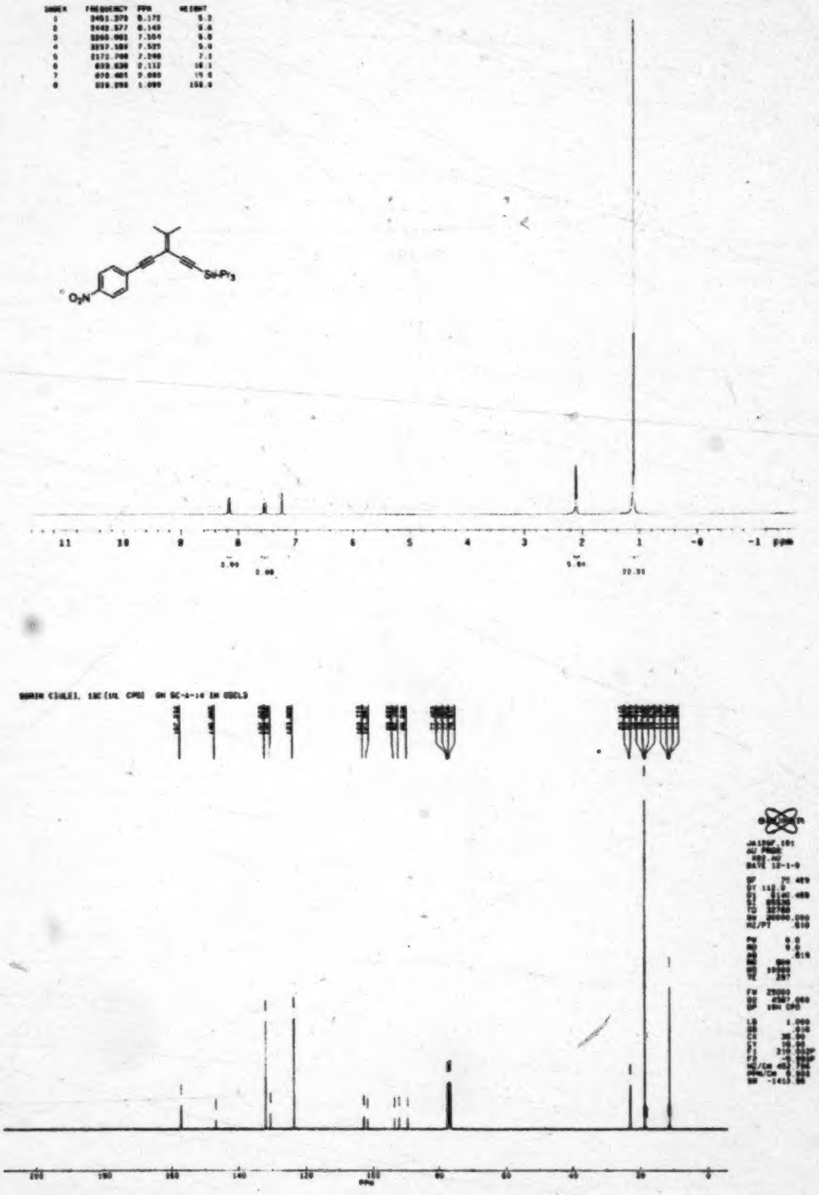

Fig. 6.2 ^{1}H and ^{13}C NMR spectra of compound **117**.

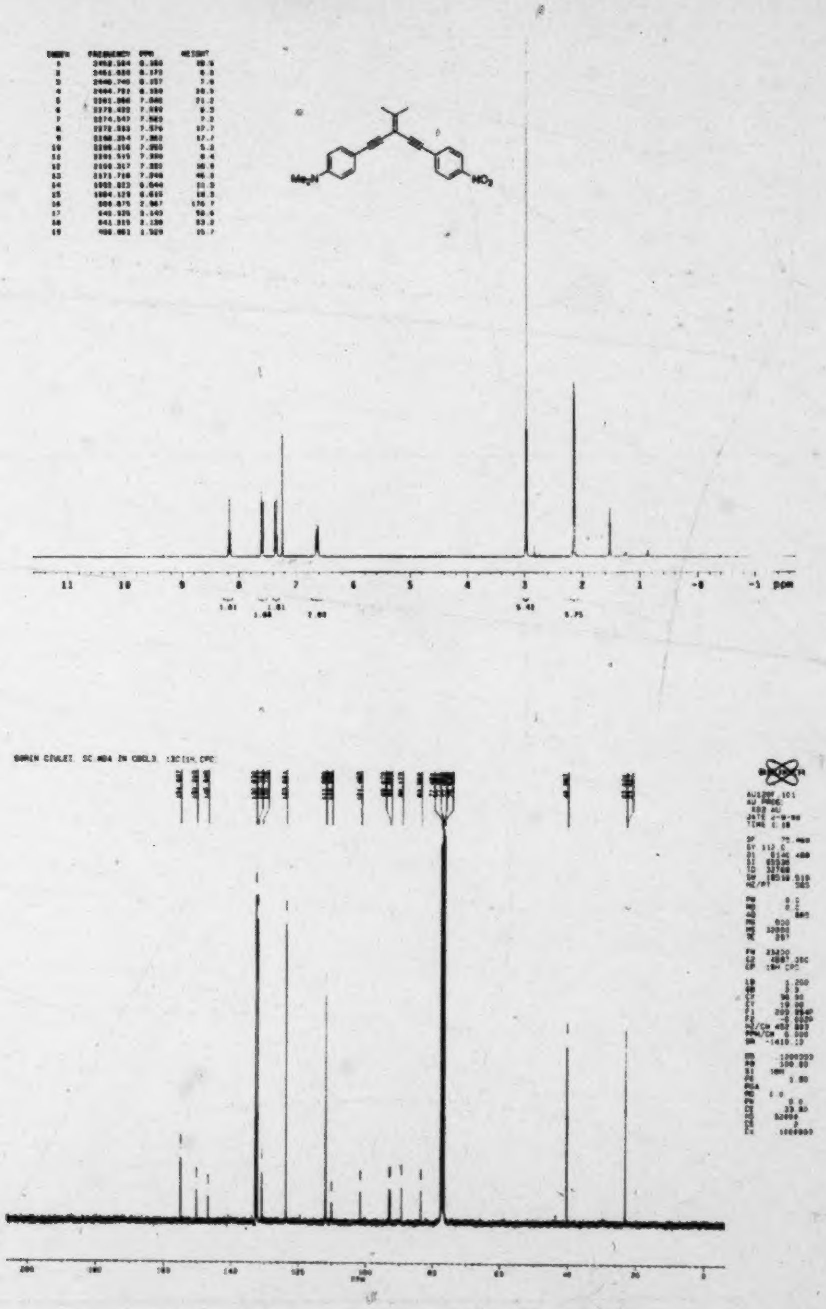

Fig. 6.3 ^{1}H and ^{13}C NMR spectra of compound **118a**.

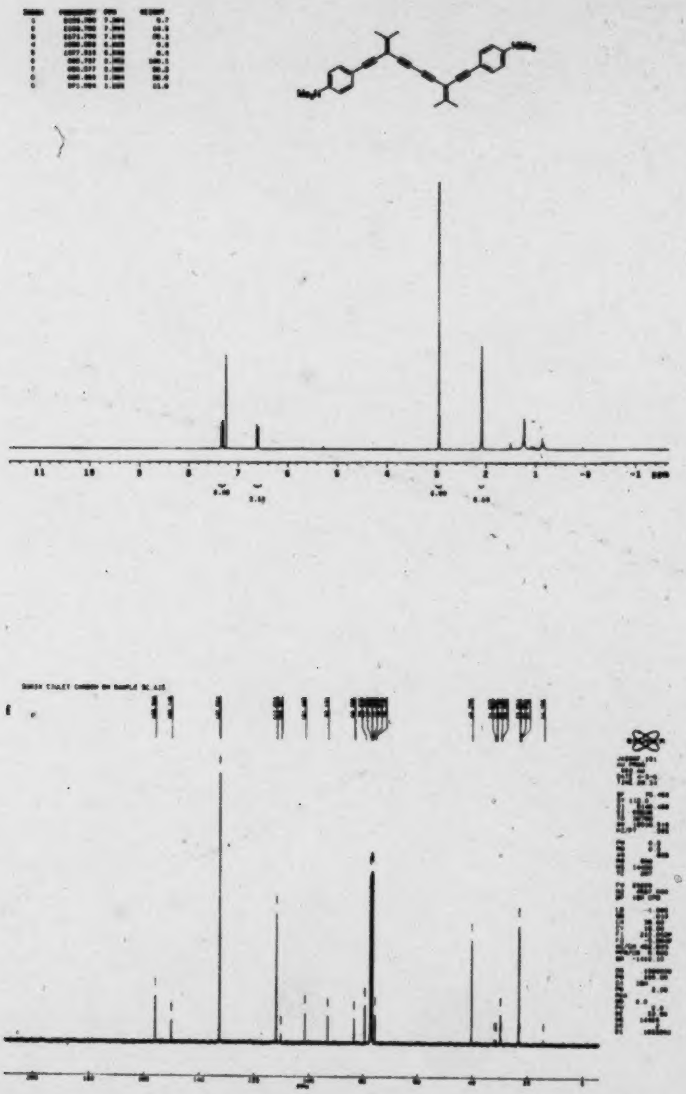

Fig. 6.4 ^{1}H and ^{13}C NMR spectra of compound **118b**.

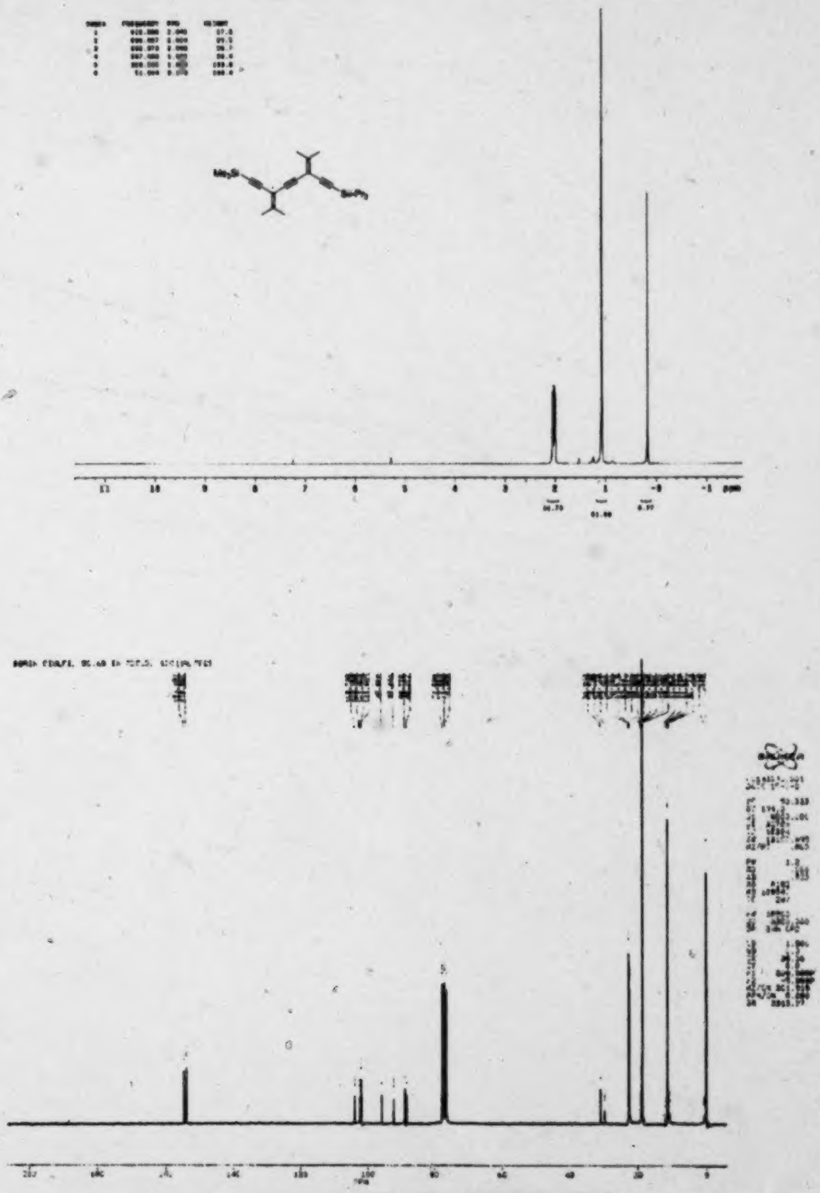

Fig. 6.5 ^{1}H and ^{13}C NMR spectra of compound **119**.

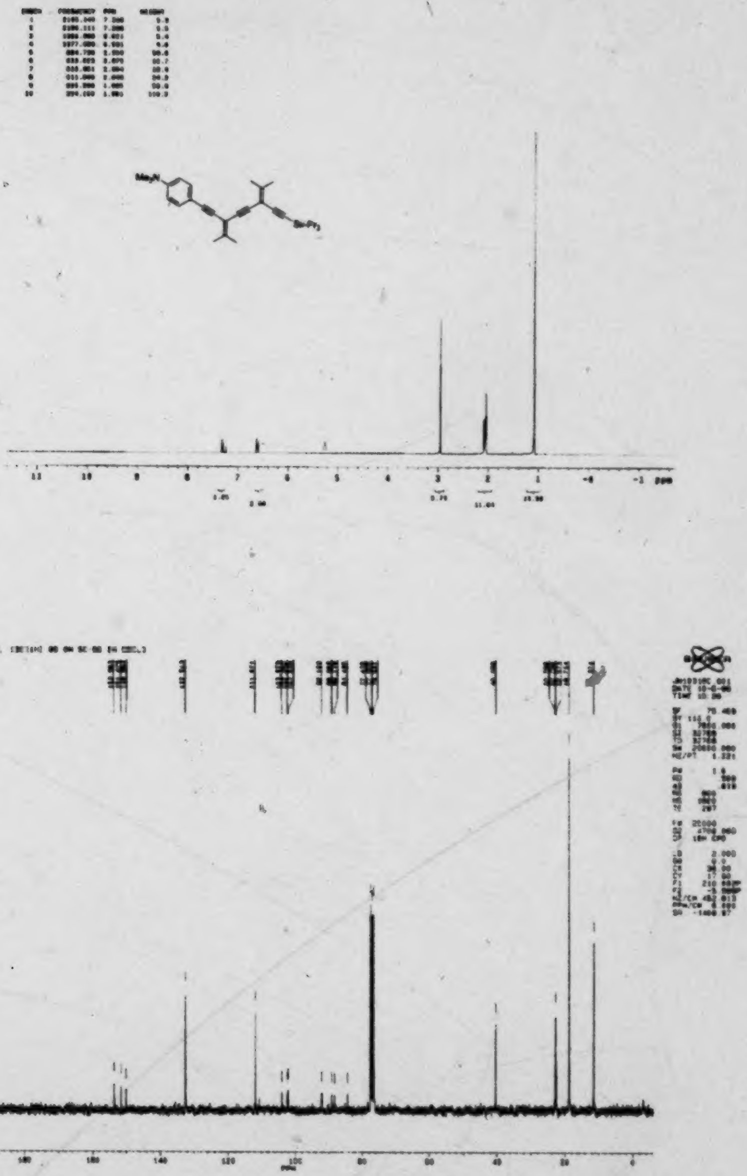

Fig. 6.6 ^{1}H and ^{13}C NMR spectra of compound **120**.

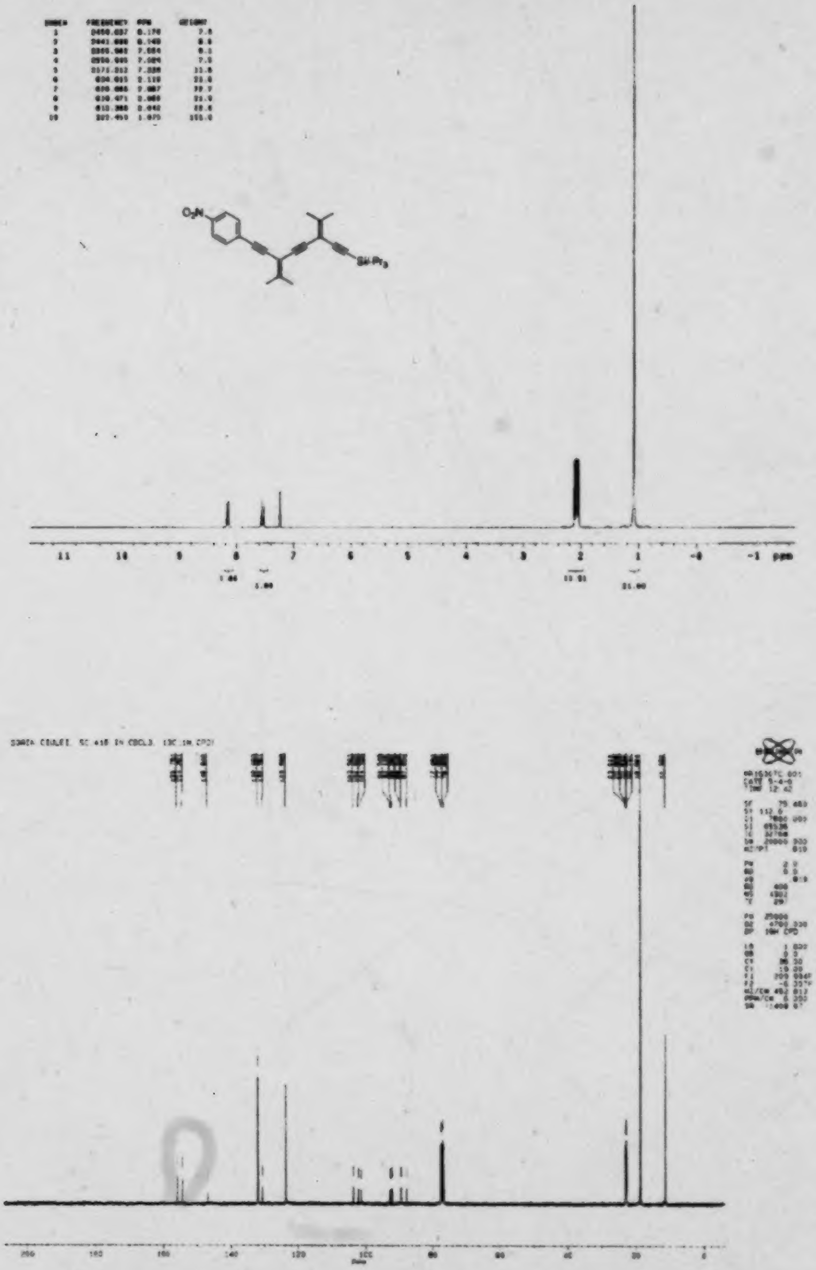

Fig. 6.7 ^{1}H and ^{13}C NMR spectra of compound **121**.

5

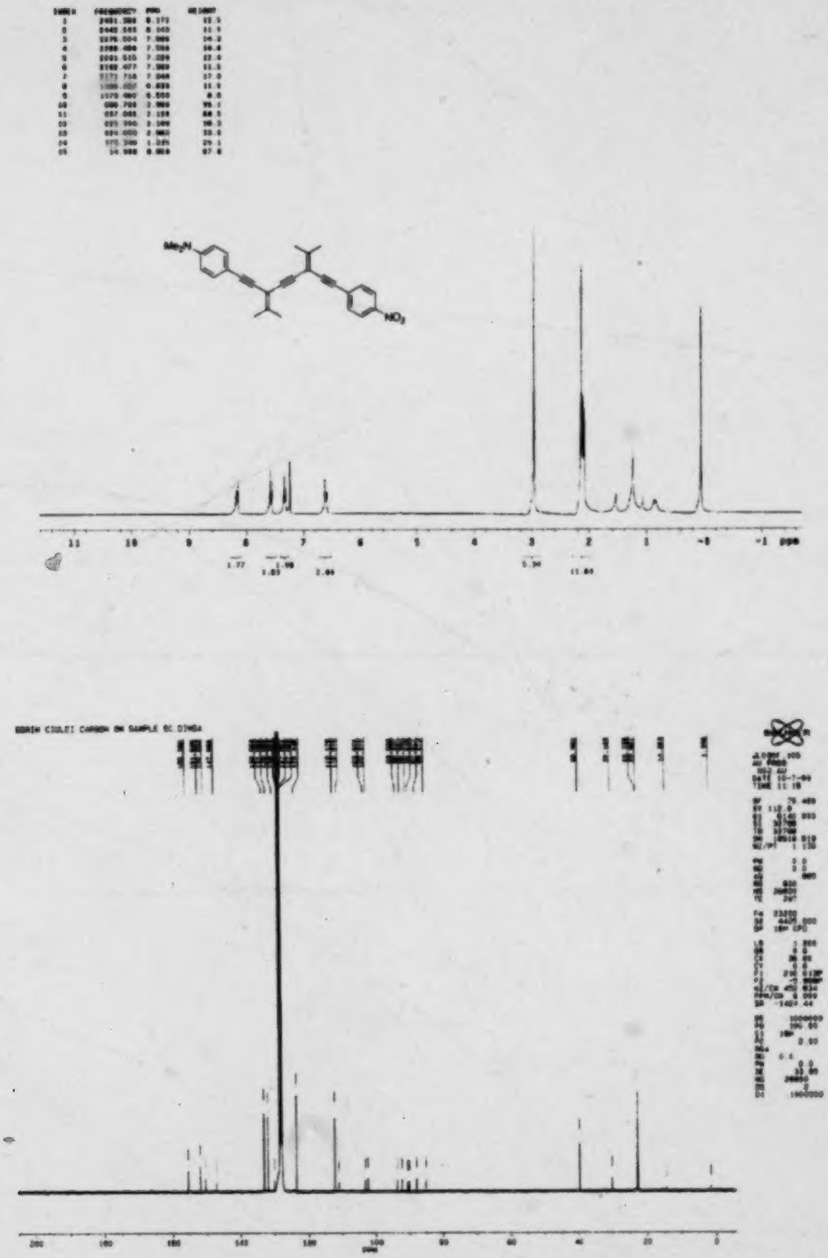

Fig. 6.8 ^{1}H and ^{13}C NMR spectra of compound **122**.

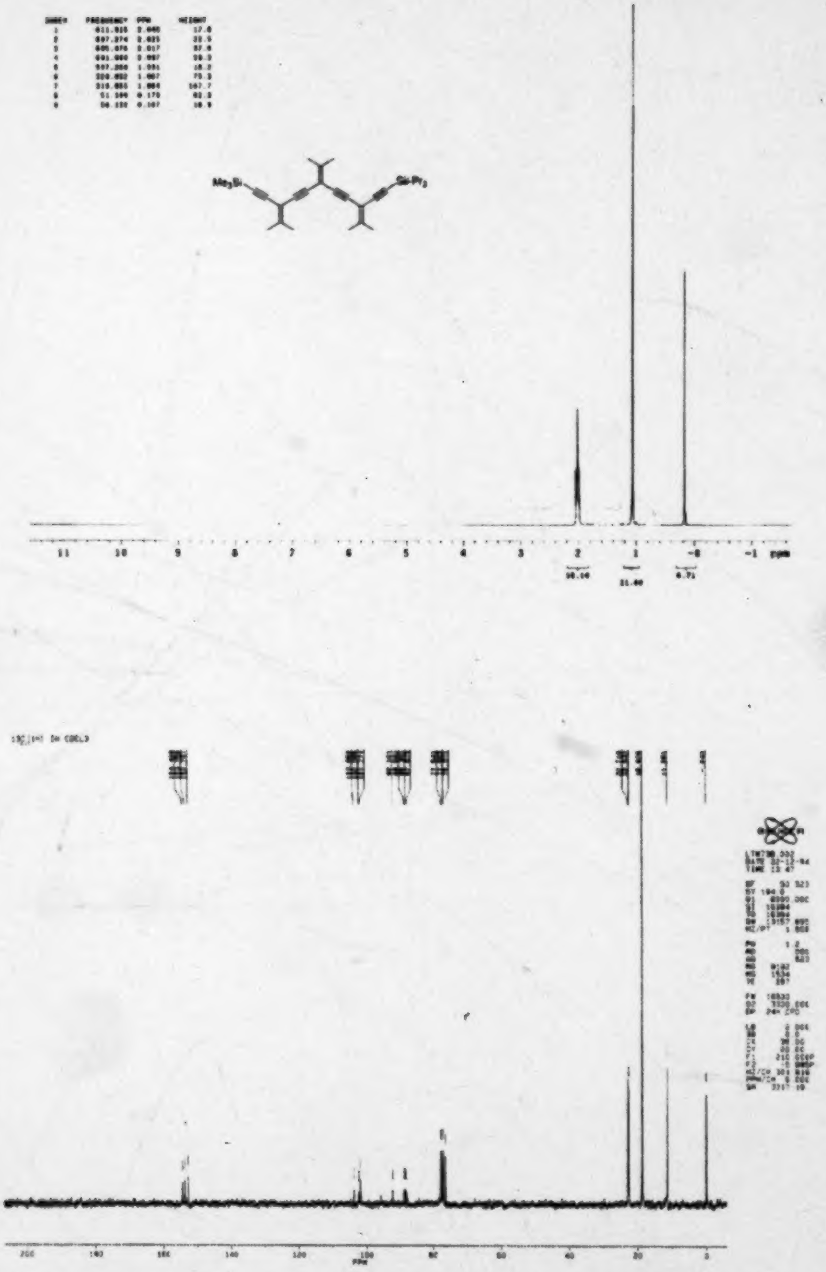

Fig. 6.9 ^{1}H and ^{13}C NMR spectra of compound **123**.

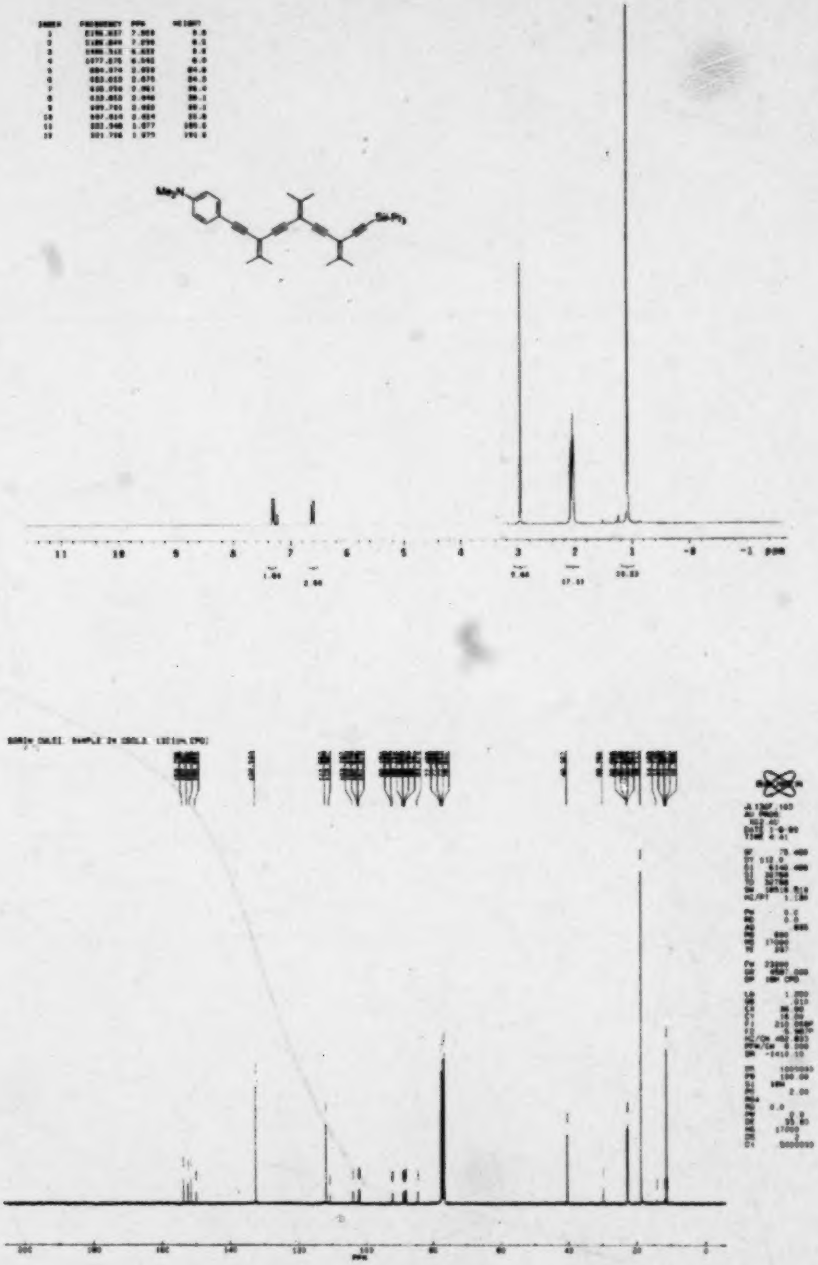

Fig. 6.10 ^{1}H and ^{13}C NMR spectra of compound **124**.

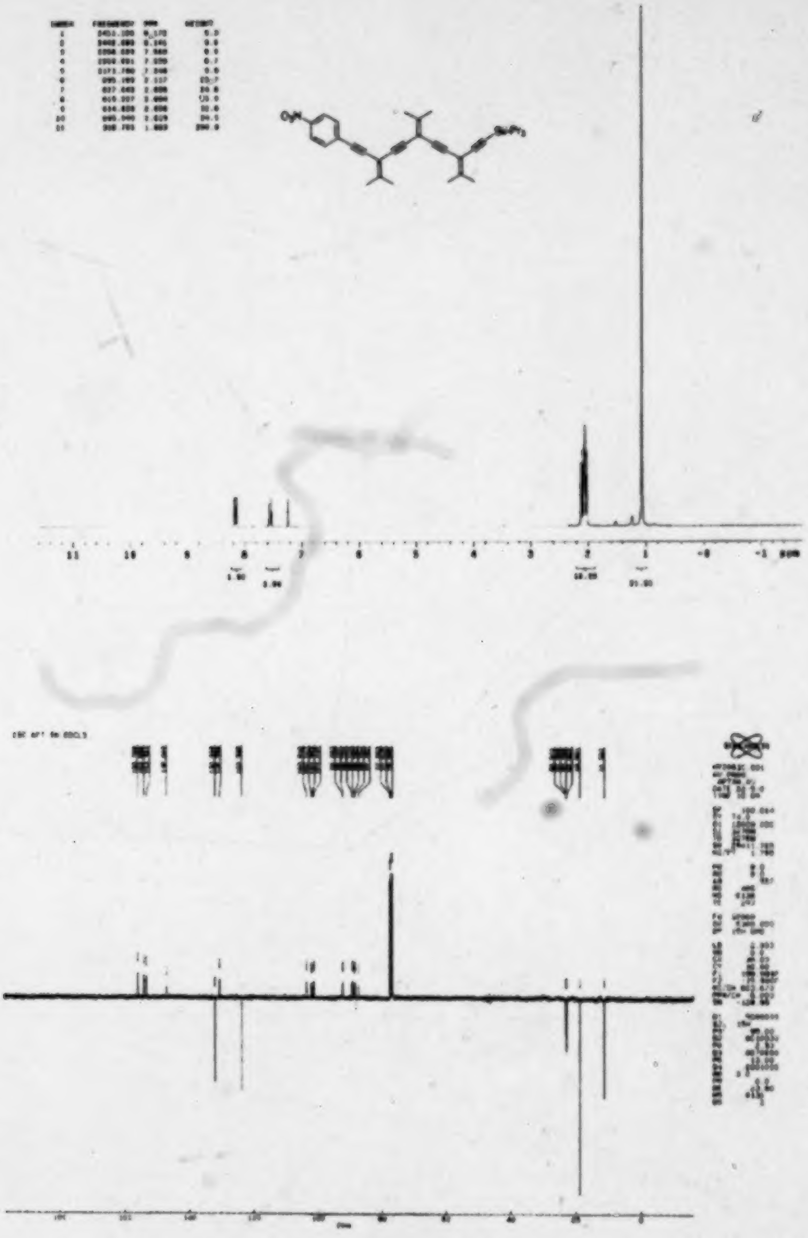

Fig. 6.11 ¹H and ¹³C NMR spectra of compound **125**.

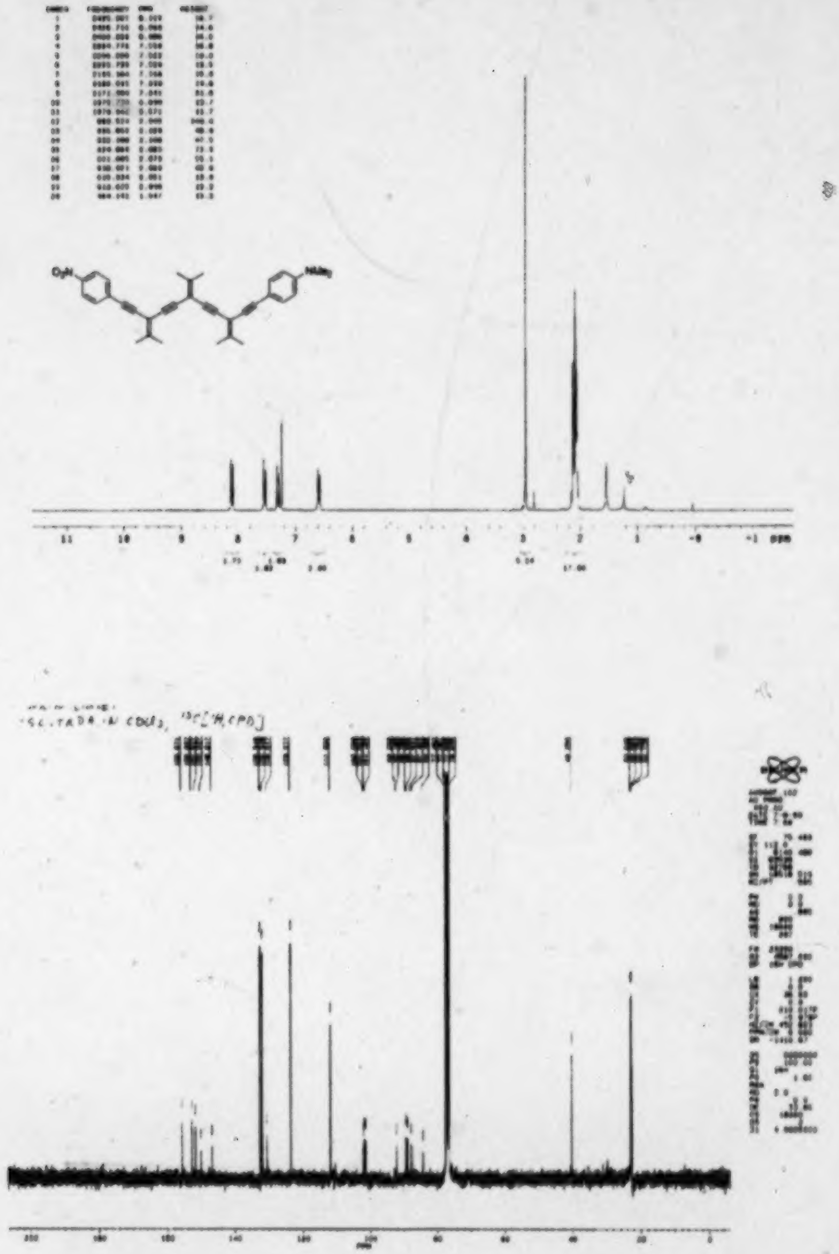

Fig. 6.12 ^{1}H and ^{13}C NMR spectra of compound **126**.

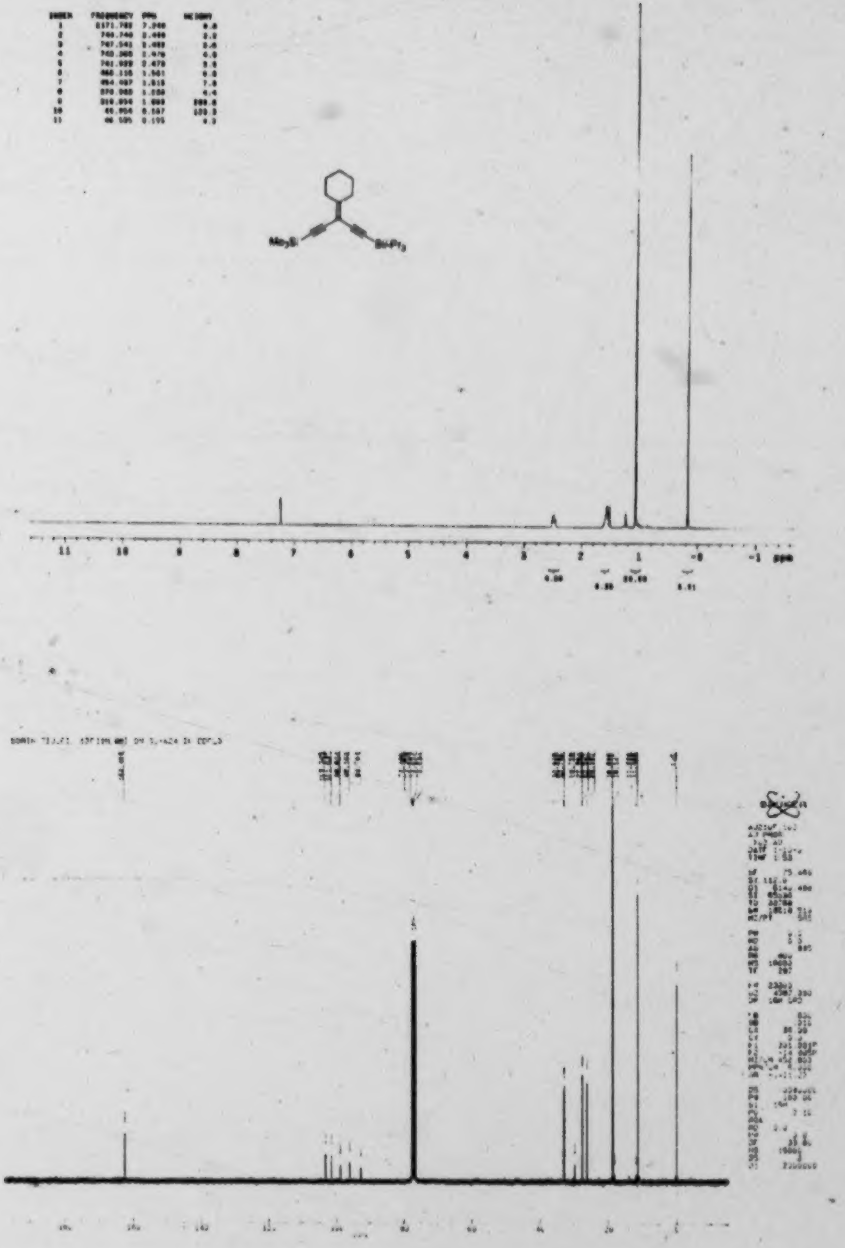

Fig. 6.13 ^{1}H and ^{13}C NMR spectra of compound **128**.

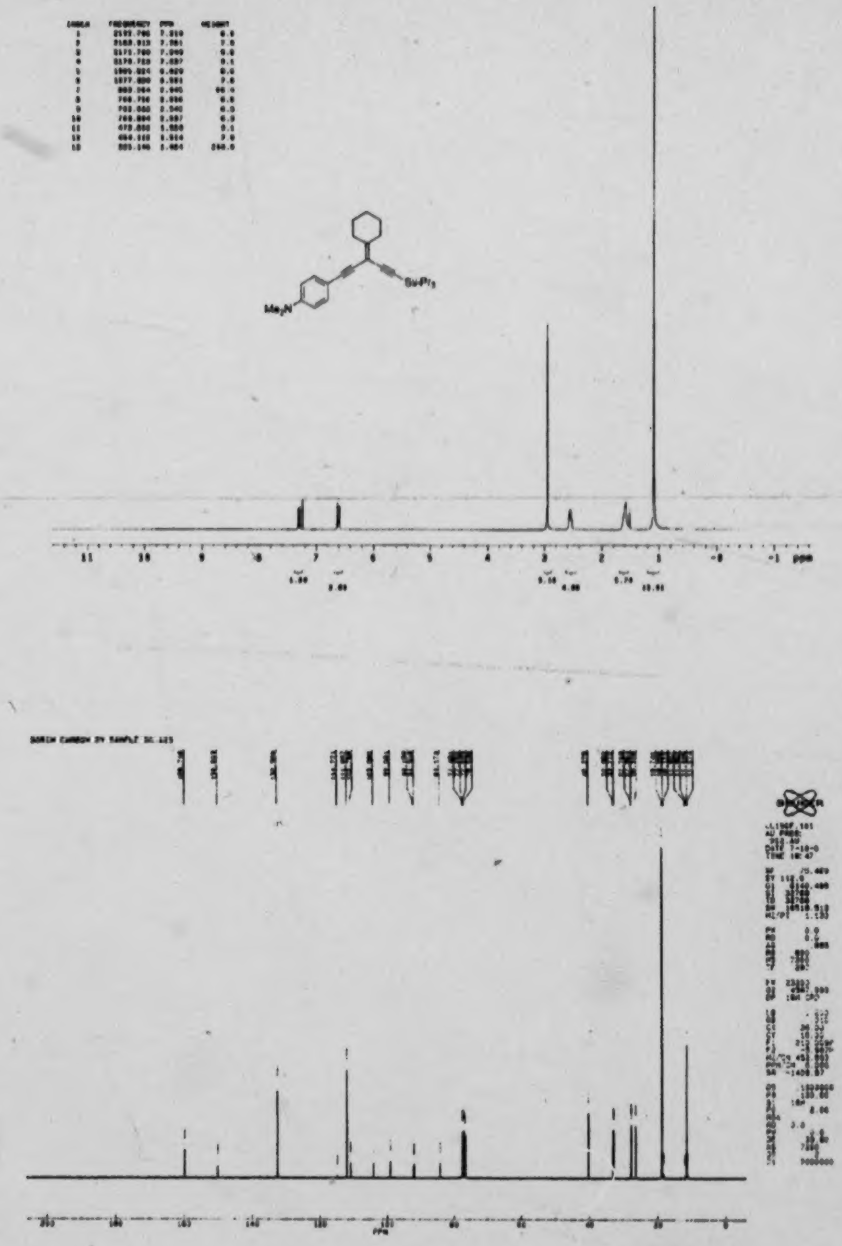

Fig. 6.14 ¹H and ¹³C NMR spectra of compound **129**.

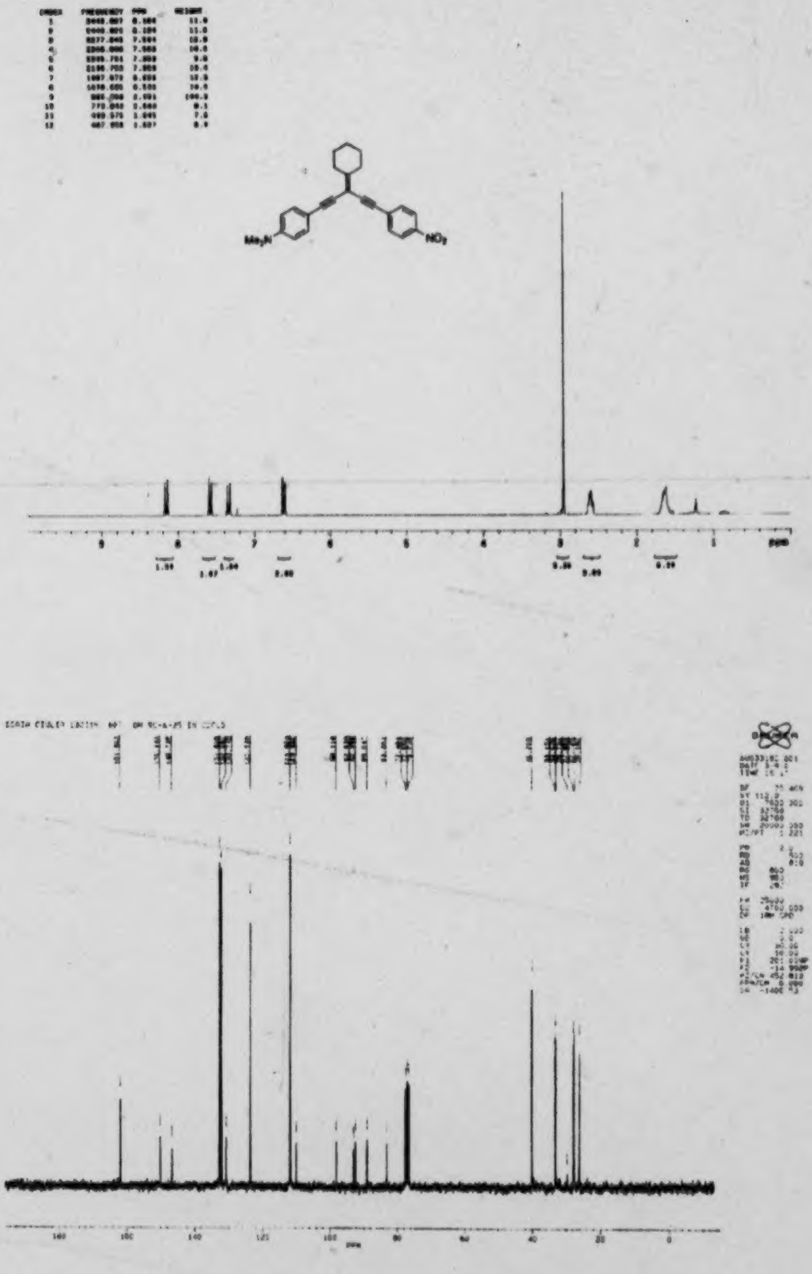

Fig. 6.15 ^{1}H and ^{13}C NMR spectra of compound **130**.

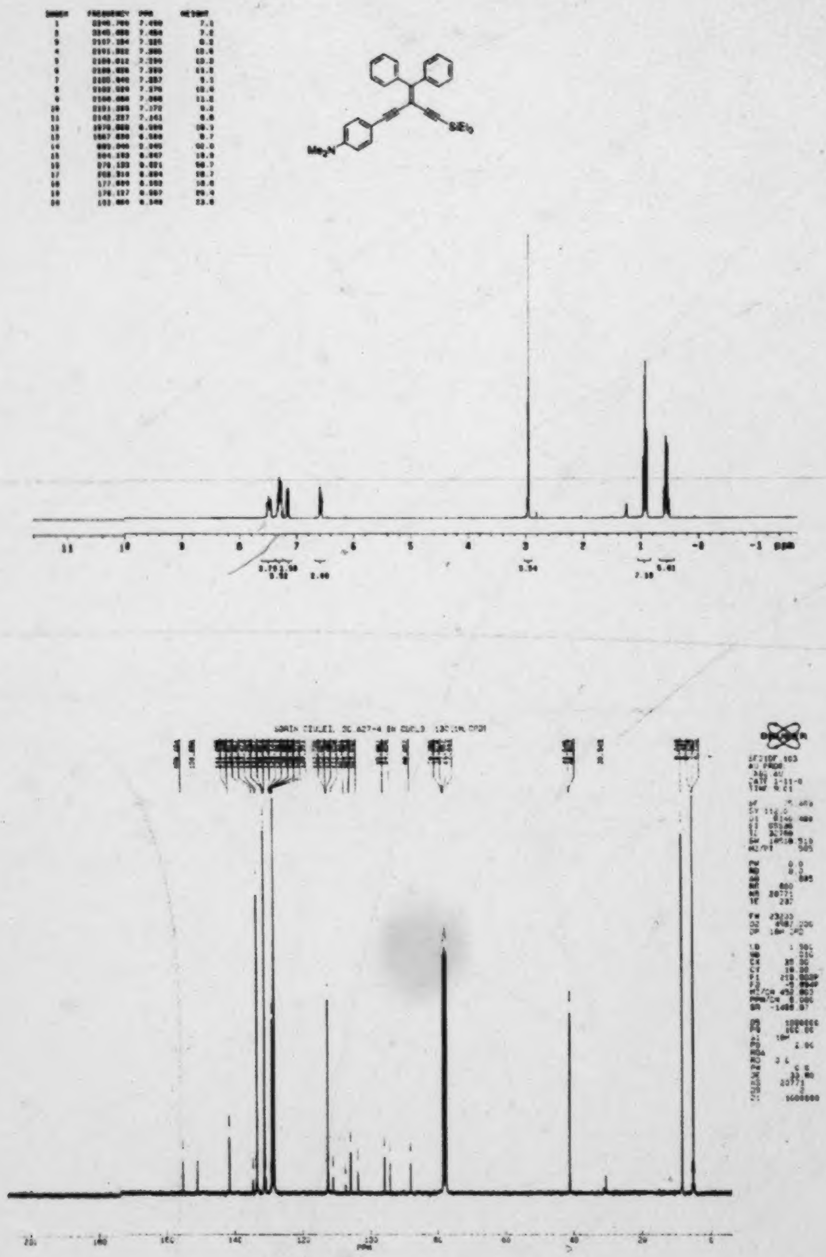

Fig. 6.16 ^{1}H and ^{13}C NMR spectra of compound **138**.

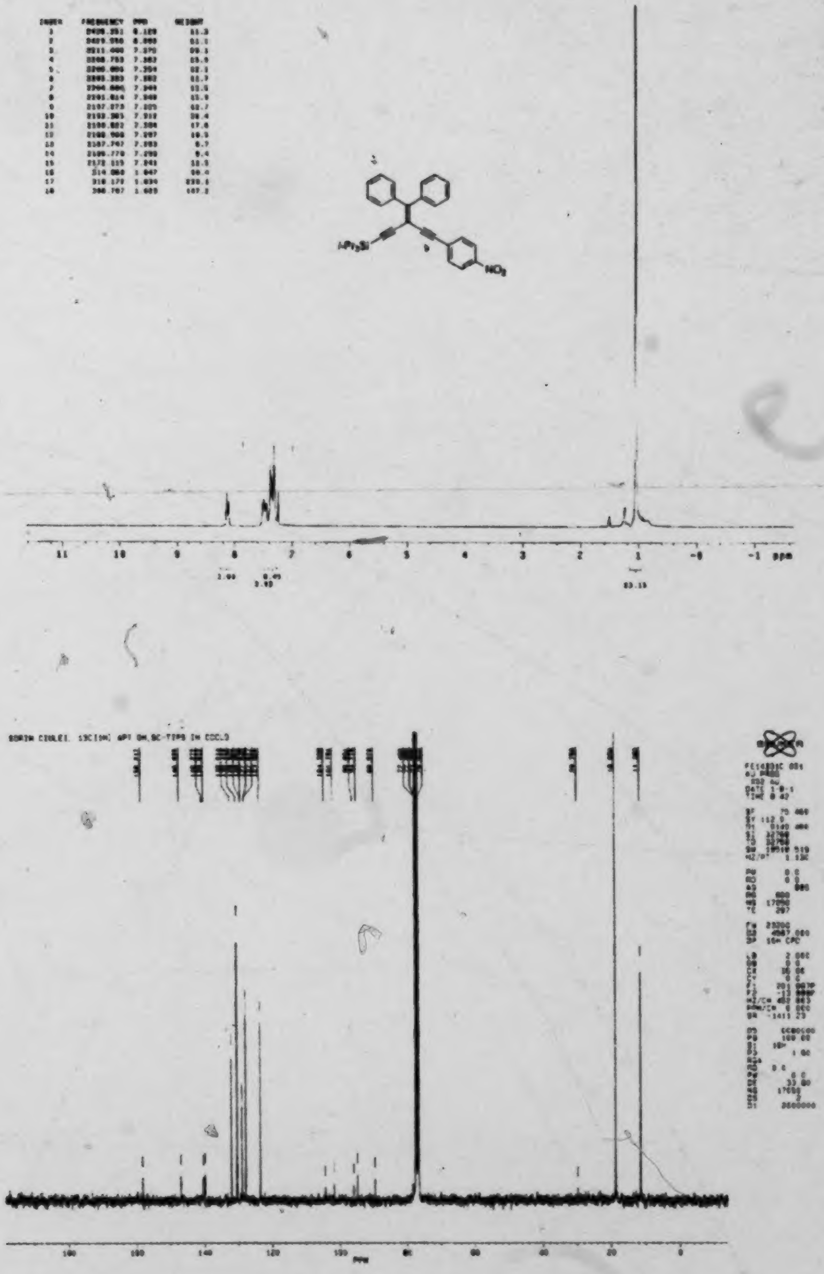

Fig. 6.17 ^{1}H and ^{13}C NMR spectra of compound **139**.

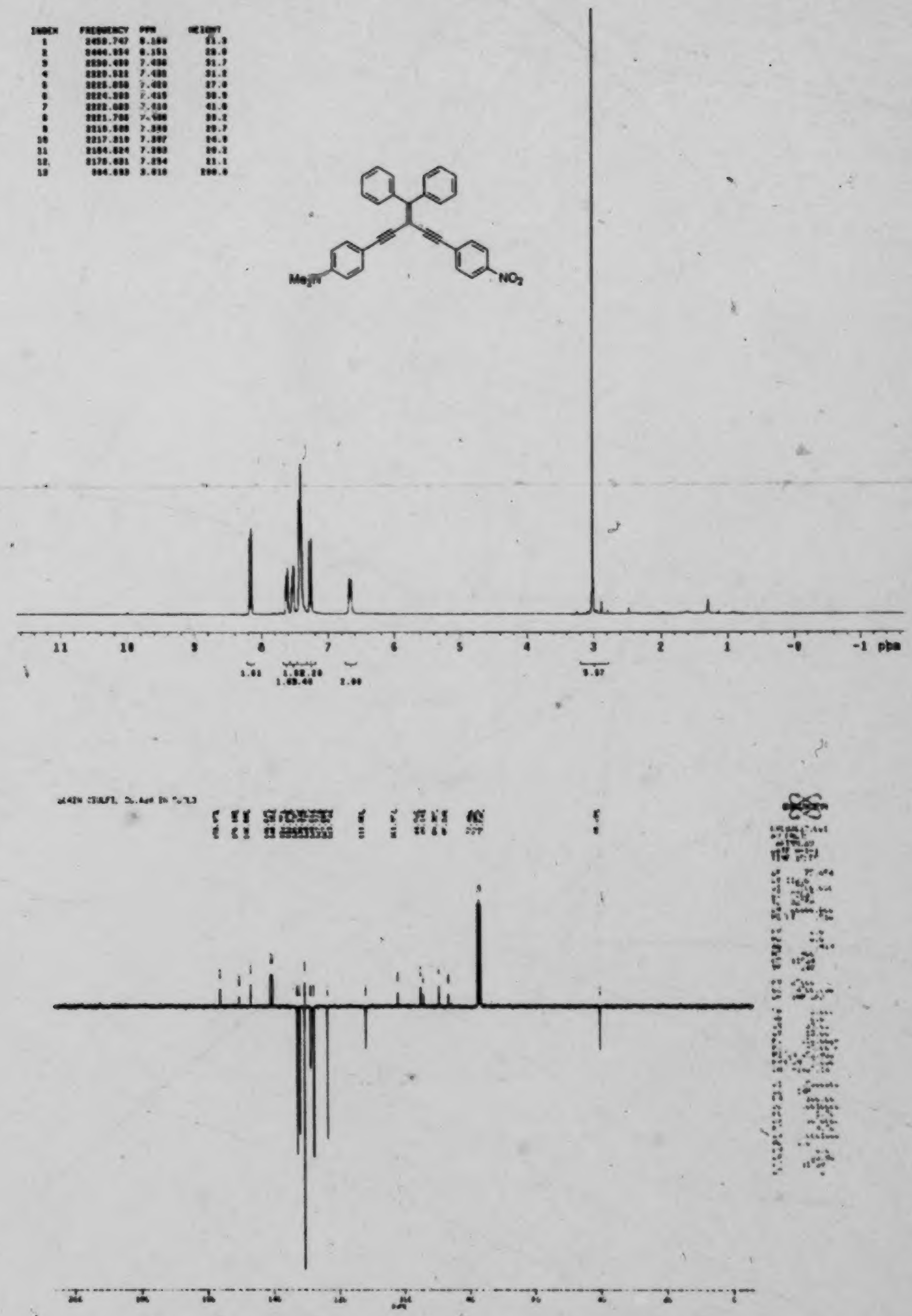

Fig. 6.18 ^{1}H and ^{13}C NMR spectra of compound **140**.